Poster Jamboree

European Conference on Few-Body Problems in Physics

Ground Rules

- 3 minute presentations
- Community wide vote for best poster (top 3) and best presentation
- Save questions for the poster session

https://tinyurl.com/EFBPoster

Nuclear structure corrections in muonic atoms

Simone Salvatore Li Muli

Sonia Bacca

Image credit: Oak Ridge National Laboratory, US department of energy;
Conceptual art by LeJean Hardin and Andy Sproles

Muonic atoms

Hydrogen-like systems

Ordinary atoms

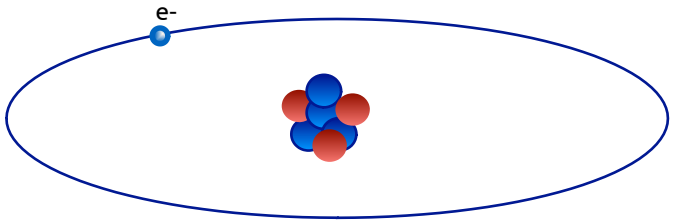

Muonic atoms

The muon is more sensitive to the nucleus

Excellent precision probe for the nucleus

Experimental program at **PSI** of the **CREMA** collaboration

Muonic Hydrogen
- Pohl et al., Nature (2010)
- Antognini et al., Science (2013)

Muonic Deuterium
- Pohl et al., Science (2016)

Muonic Helium isotopes
- Krauth et al., Nature (2021)
- Schuhmann et al., Arxiv (2023)

A matter of precision

$$\delta_{\mathrm{LS}} = \delta_{\mathrm{QED+NR}} + \delta_{\mathrm{FS}}^{(4)} \times r_c^2 + \delta_{\mathrm{TPE}}^{(5)} + \delta_{\mathrm{3PE}}^{(6)} + \dots$$

Measured Calculated Extracted

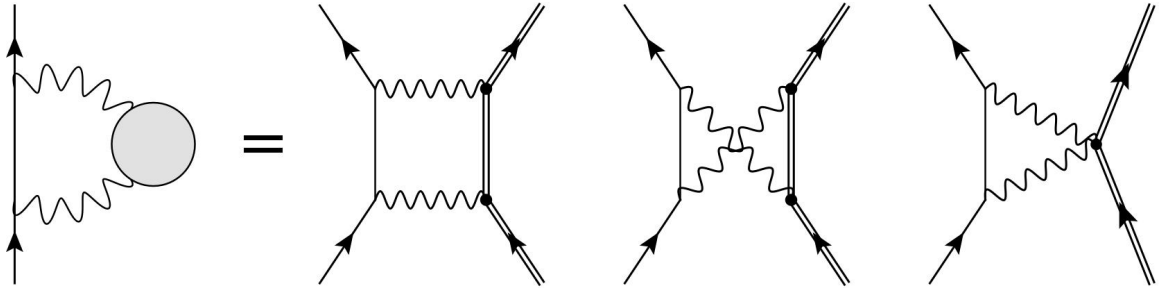

NS corrections in muonic Helium

S.S.LM, et al. In preparation for 2023

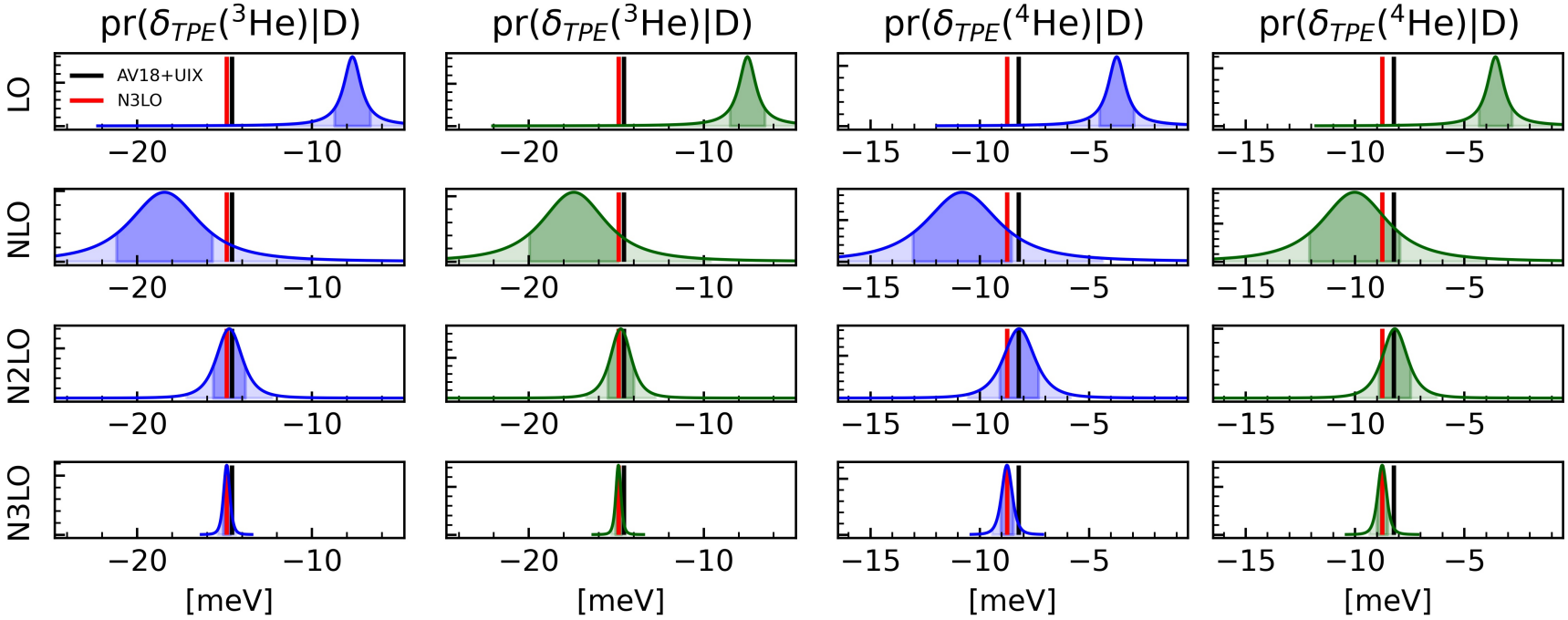

C. Ji, et al. J. Phys. G: Nucl. Part. Phys. 45 (2018)

Difference in charge radii

S.S.LM, et al. In preparation for 2023

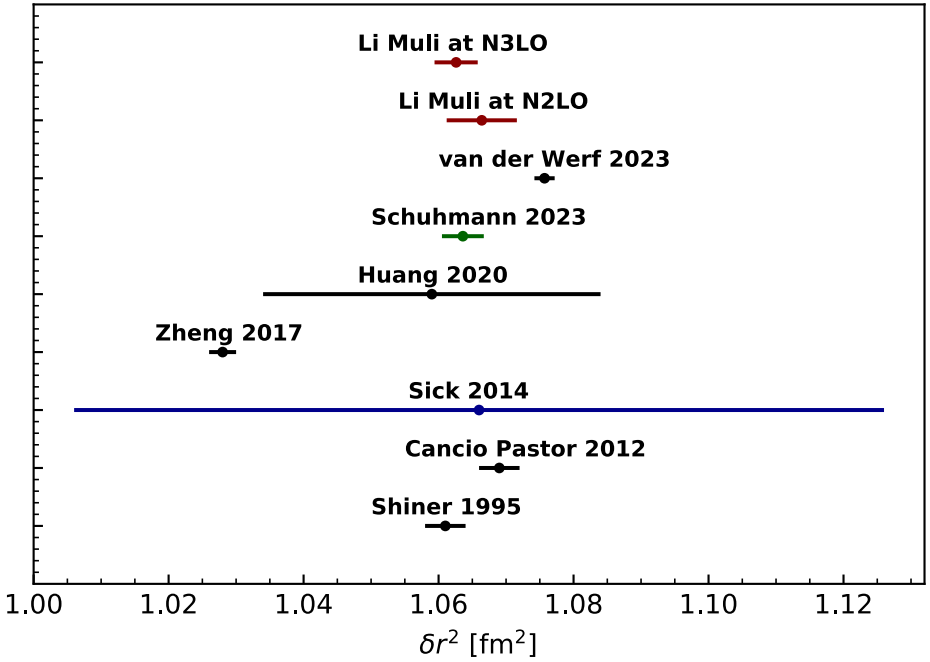

2

Ground and dipole-excited states in neutron-rich ^{6,8}He

FRANCESCA BONAITI, JGU MAINZ

In collaboration with:
Sonia Bacca (JGU Mainz)
Gaute Hagen (ORNL)
Gustav R. Jansen (ORNL)
Thomas Papenbrock (ORNL/UTK)

25TH EUROPEAN CONFERENCE ON FEW-BODY PROBLEMS IN PHYSICS @ MAINZ, GERMANY

AUGUST 3, 2023

At the extremes of the nuclear chart: halo nuclei

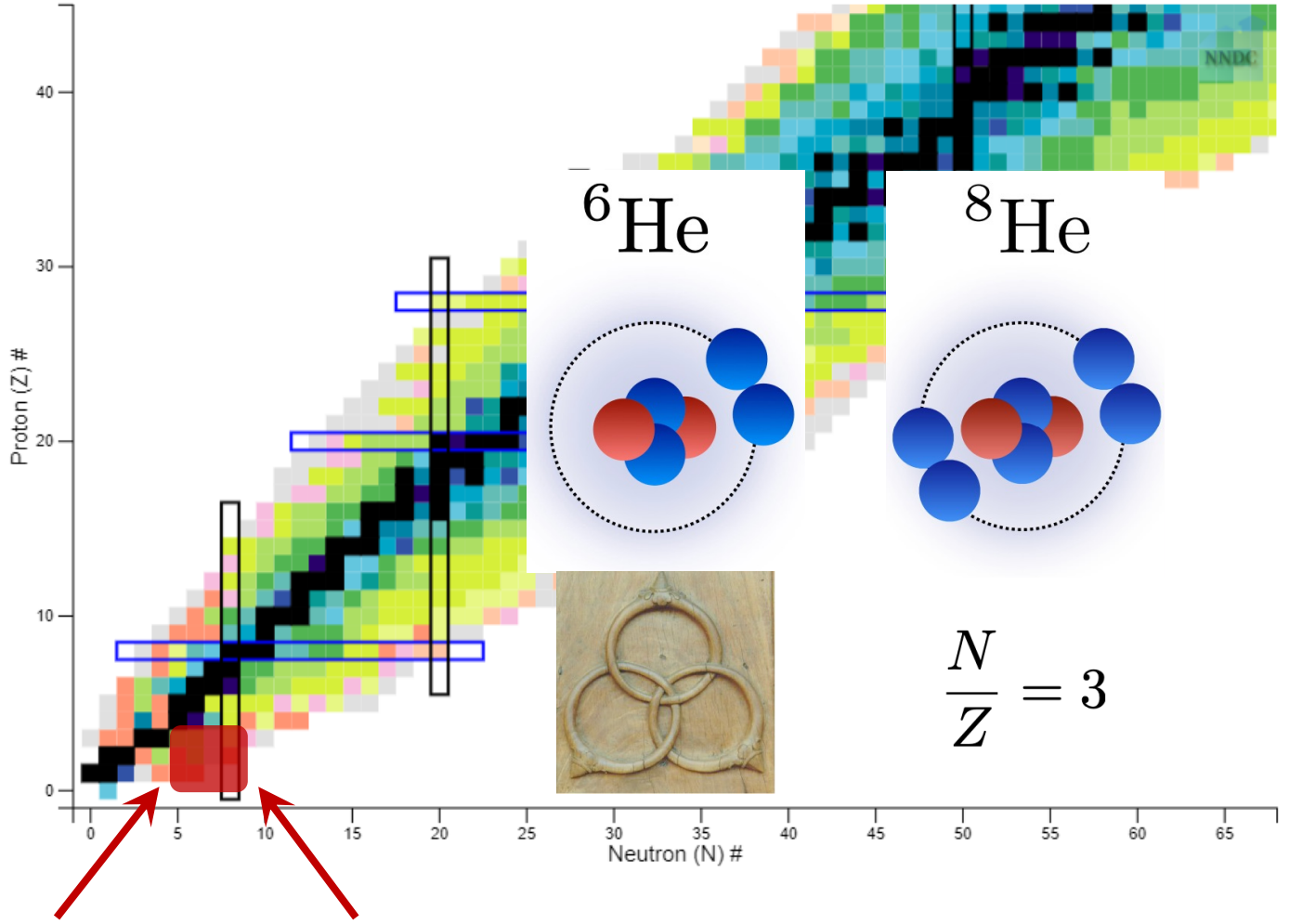

A lot is going on these days…

Article | Open Access | Published: 27 January 2021

Measuring the α-particle charge radius with muonic helium-4 ions

Julian J. Krauth, Karsten Schuhr

ELSEVIER

Physics Letters B

Volume 822, 10 November 2021, 136710

Nature **589**, 527–531 (2021) | Cit

Proton inelastic scattering reveals deformation in ^{8}He

M. Holl [a, b], R. Kanungo [a, b], Z.H. Sun [c, d], G. Hagen [c, d], J.A. Lay [e, f], A.M. Moro [e, f], P. Navrátil [b],

Article | Open Access | Published: 22 June 2022

Observation of a correlated free four-neutron system

M. Duer, T. Aumann, … M. V. Zhukov + Show authors

Nature **606**, 678–682 (2022) | Cite this article

See Antognini, Duer, Göbel's talks…

NEW measurement of dipole response of ^{6,8}He at low energy (SAMURAI collaboration)

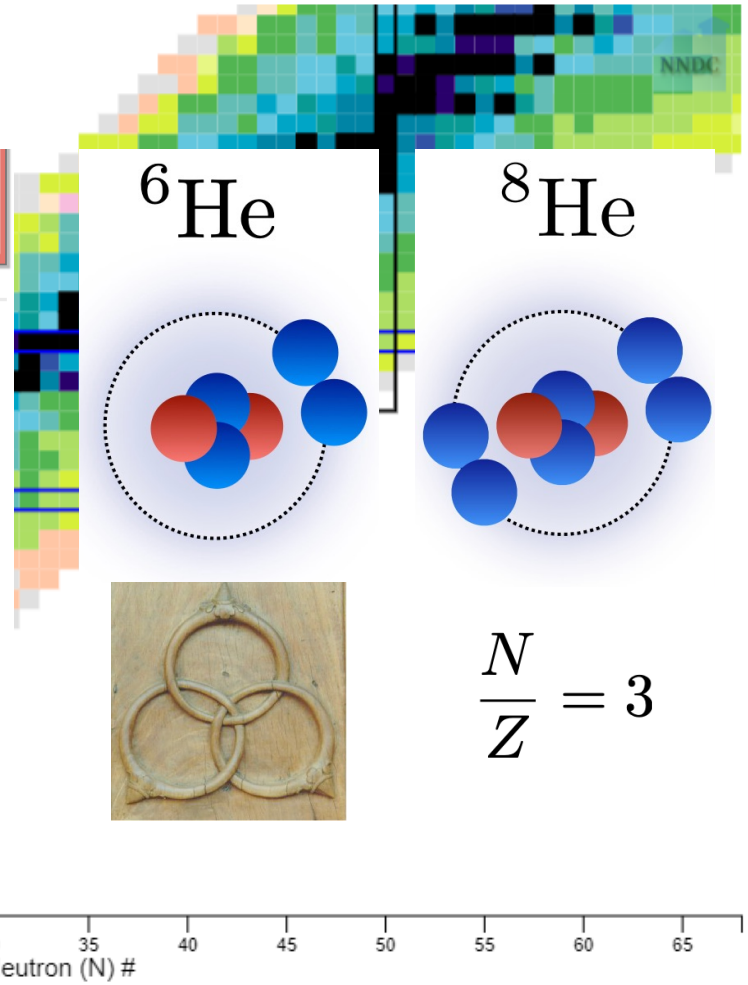

Electric dipole polarizability in ^{8}He: theory…

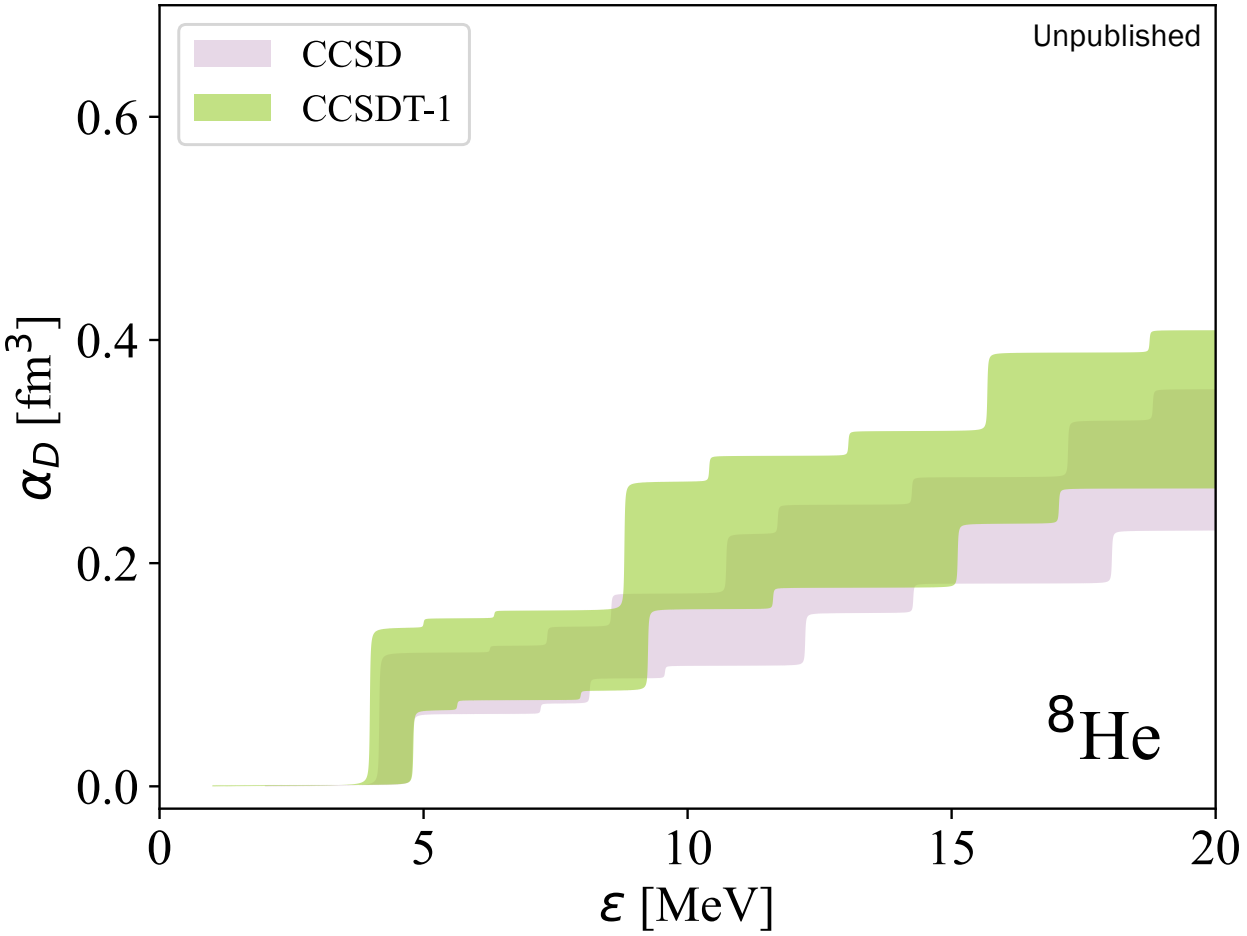

$$\alpha_D = 2\alpha \int_0^{\epsilon} d\omega\, \omega^{-1} R(\omega)$$

nuclear dipole response function

Electric dipole polarizability in ^{8}He: theory and experiment

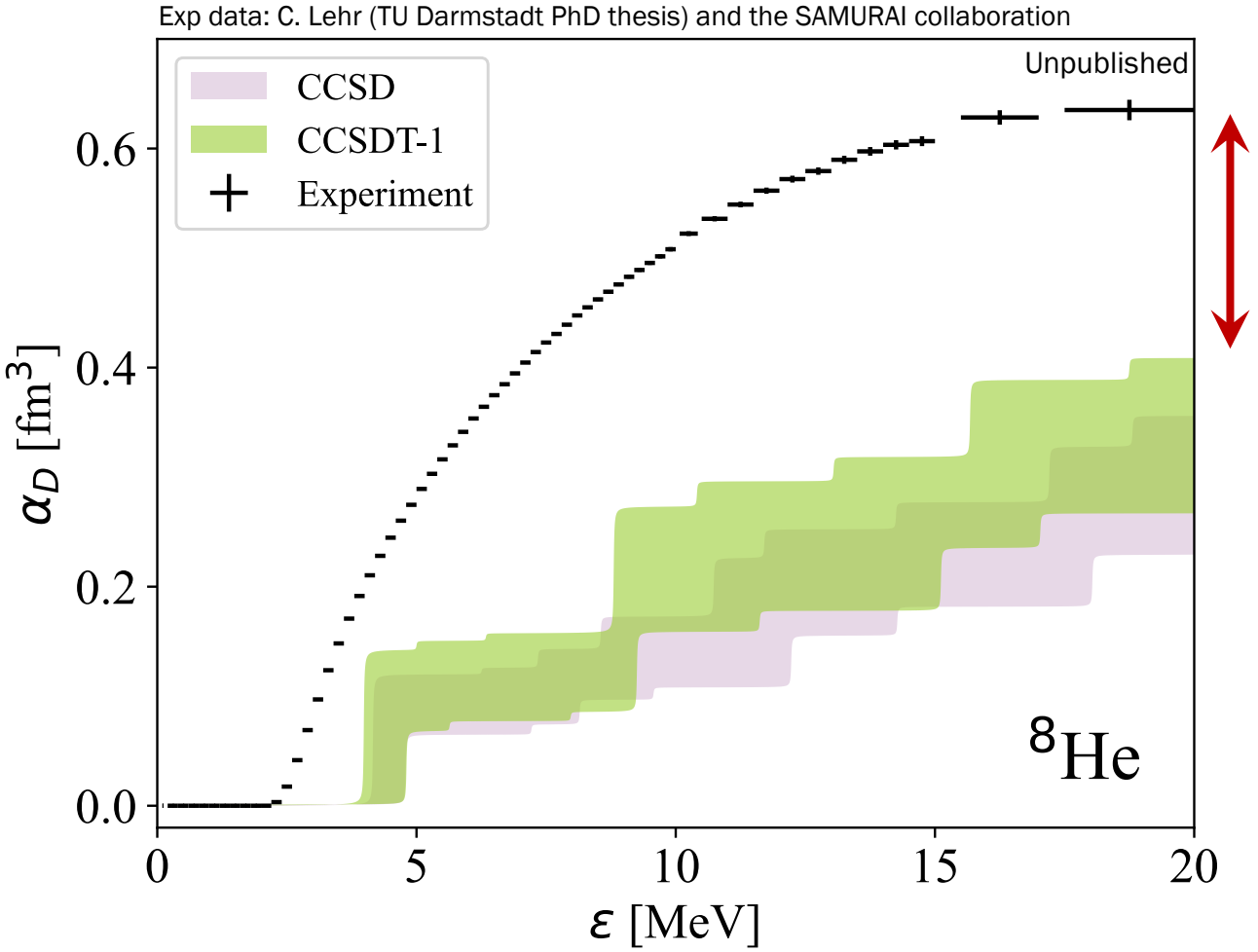

from “Oppenheimer”
© Universal Pictures

3

Multichannel nature of the lithium few-body puzzle

J. van de Kraats[1], D. J. M. Ahmed-Braun[1], J.-L. Li[2] and S. J. J. M. F. Kokkelmans[1]

[1]Coherence and Quantum Technology, Eindhoven University of Technology , The Netherlands

[2]Center for Integrated Quantum Science and Technology, Ulm University, Germany

TU/e EINDHOVEN UNIVERSITY OF TECHNOLOGY

QT/e CENTER FOR QUANTUM MATERIALS AND TECHNOLOGY EINDHOVEN

Quantum Delta the Netherlands

NWO

Lithium few-body puzzle

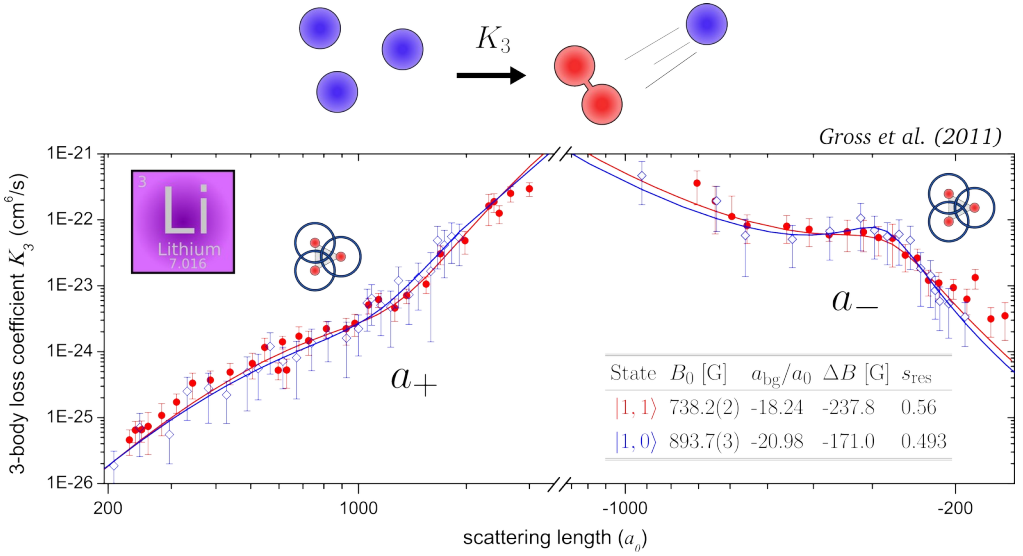

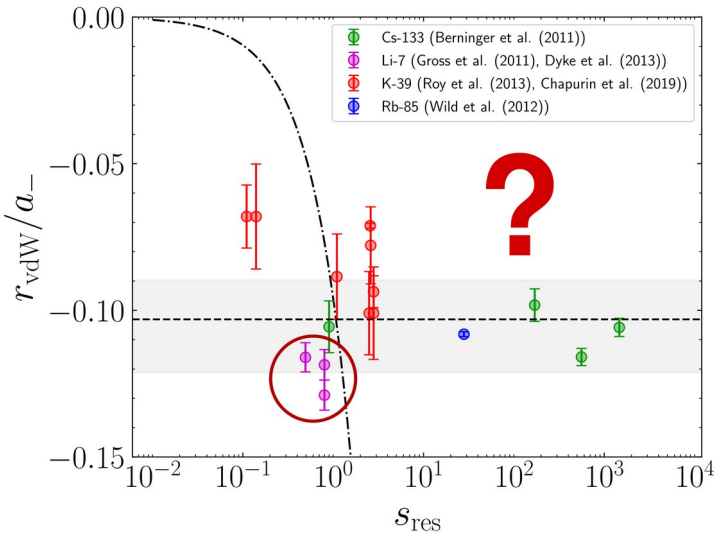

Question: What is missing from our current theoretical and numerical approaches to the lithium three-body complex?

Multichannel three-body physics

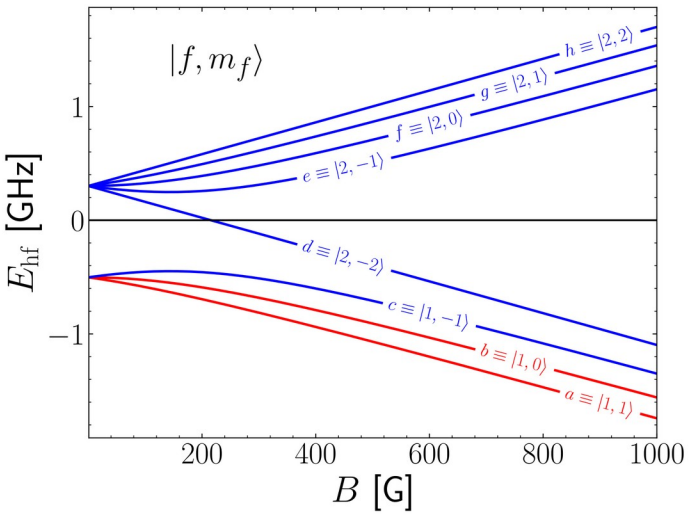

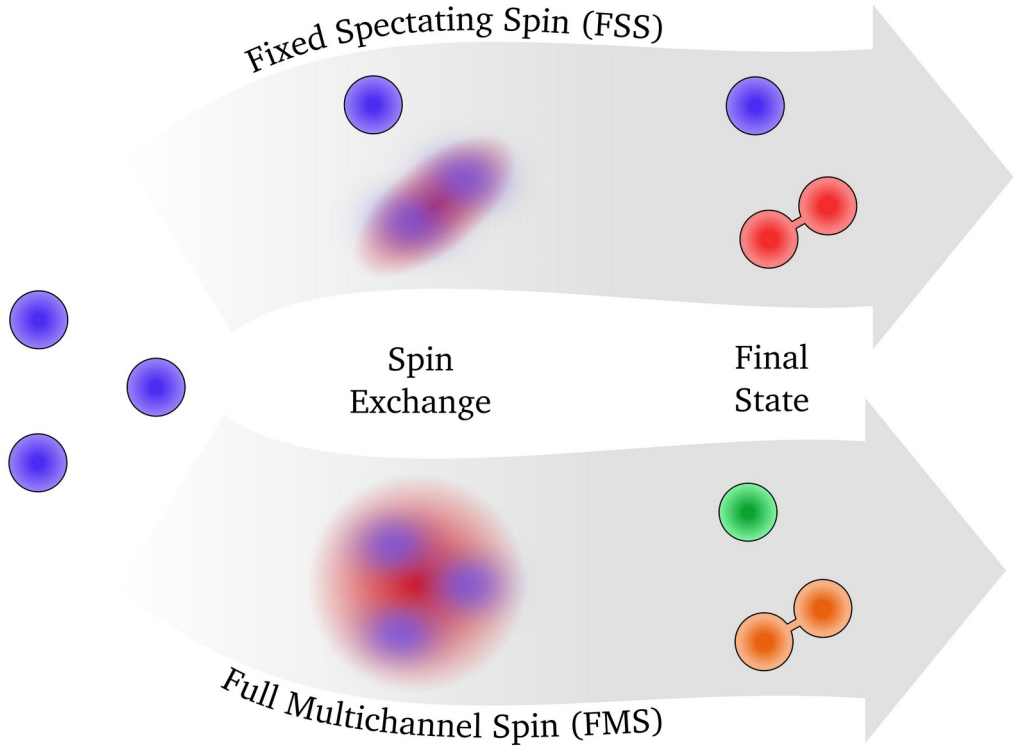

Results

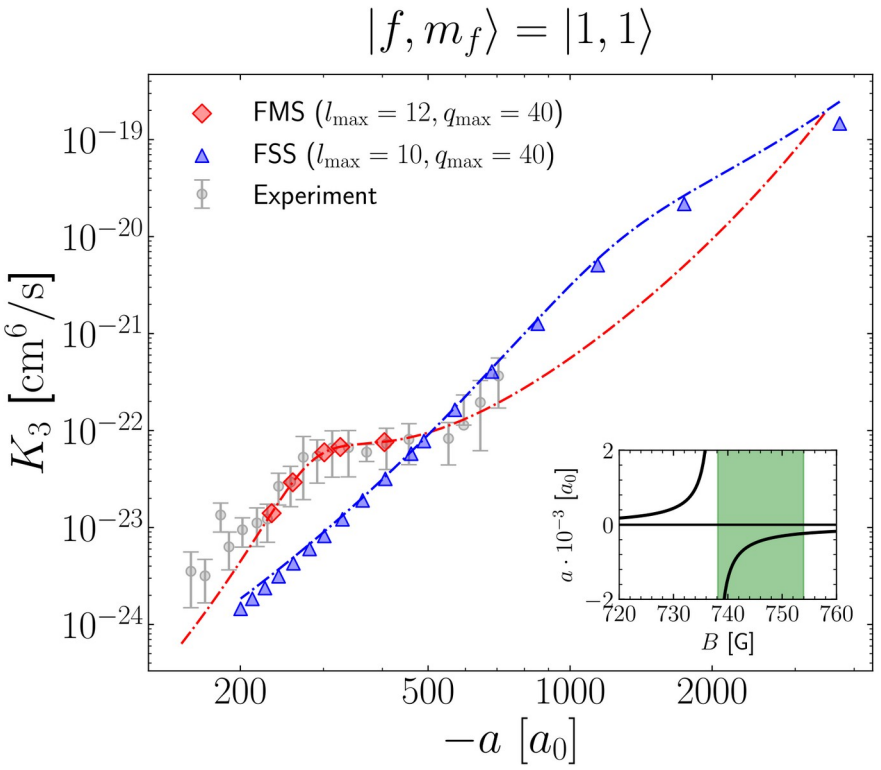

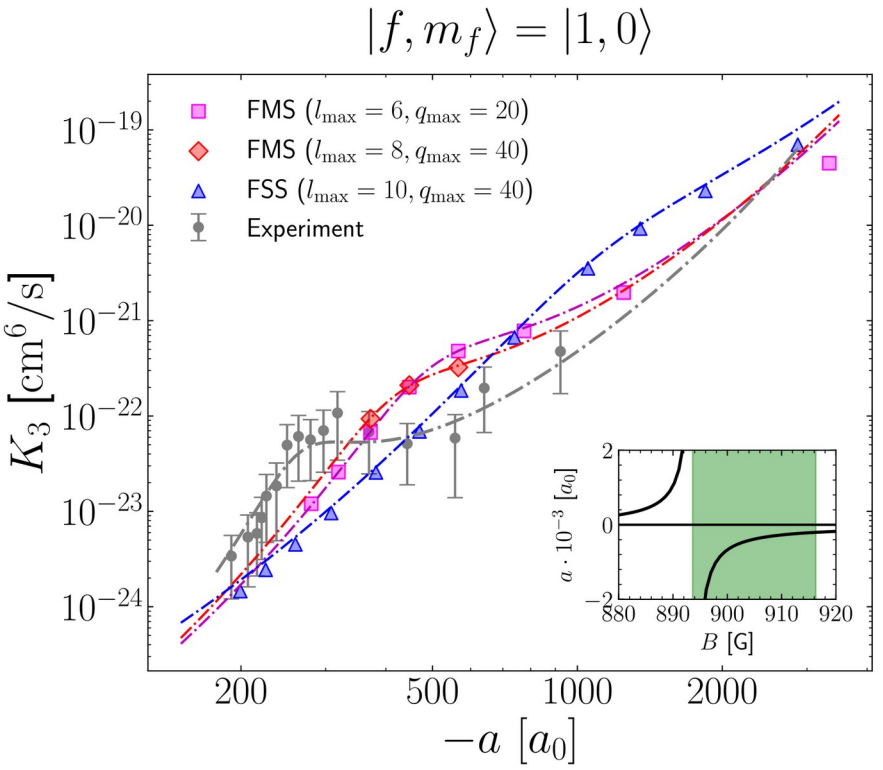

Our results clearly show the importance of multichannel physics in the lithium few-body puzzle

Core excitations in one-neutron halo nuclei

Live-Palm Kubushishi
Supervisor: Pierre Capel

Johannes Gutenberg-Universität Mainz

August 3, 2023

JOHANNES GUTENBERG UNIVERSITÄT MAINZ

JG|U

Halo nuclei

- **Light, neutron-rich** nuclei with **large matter radius**
- Low $\mathbf{S}_n$ or $\mathbf{S}_{2n}$: one or two loosely-bound neutrons
- Clusterised structure:
  neutrons can tunnel far from the core to form a halo
  $\rightarrow$ halo-nucleus $\equiv$ a compact core + valence neutron(s)
  $\rightarrow$ challenging to reproduce with usual few-body methods

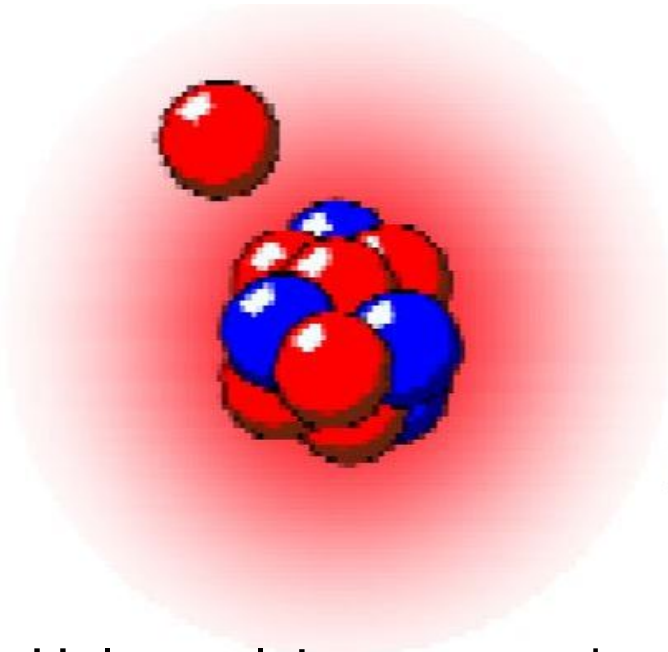

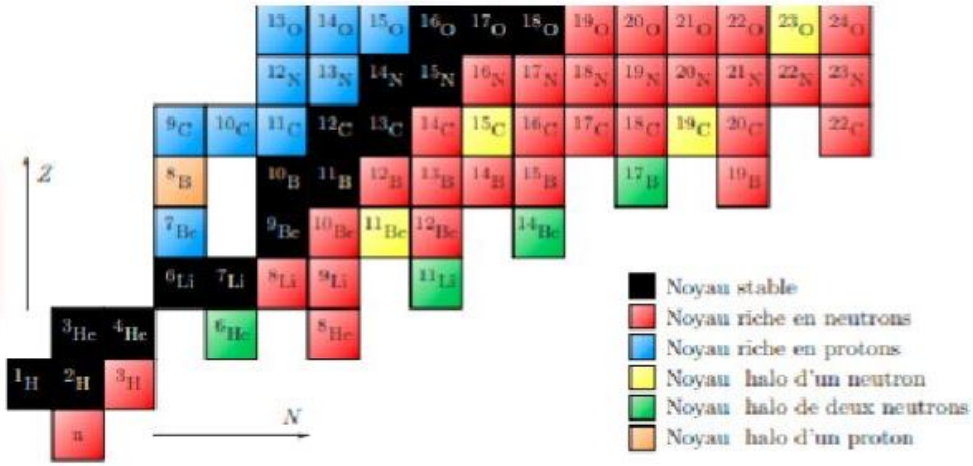

$\Rightarrow$ Halo-nuclei appear to be fascinating nuclear objects to study !

^{11}Be: resonant breakup & core excitations

- **Assumption**: $^{11}\mathrm{Be} \equiv {}^{10}\mathrm{Be}(0^+) + \mathrm{n} \Rightarrow$ single-particle description
  $\rightarrow$ **one-body** Hamiltonian: $\mathrm{H}_0(\mathbf{r}) = \mathrm{T}_{\mathbf{r}} + \mathrm{V}_{cn}(\mathbf{r})$
  $\rightarrow$ **single-particle description enough to fully describe breakup ?**
  e.g. ^{11}Be+C $\rightarrow$ ^{10}Be+n+C

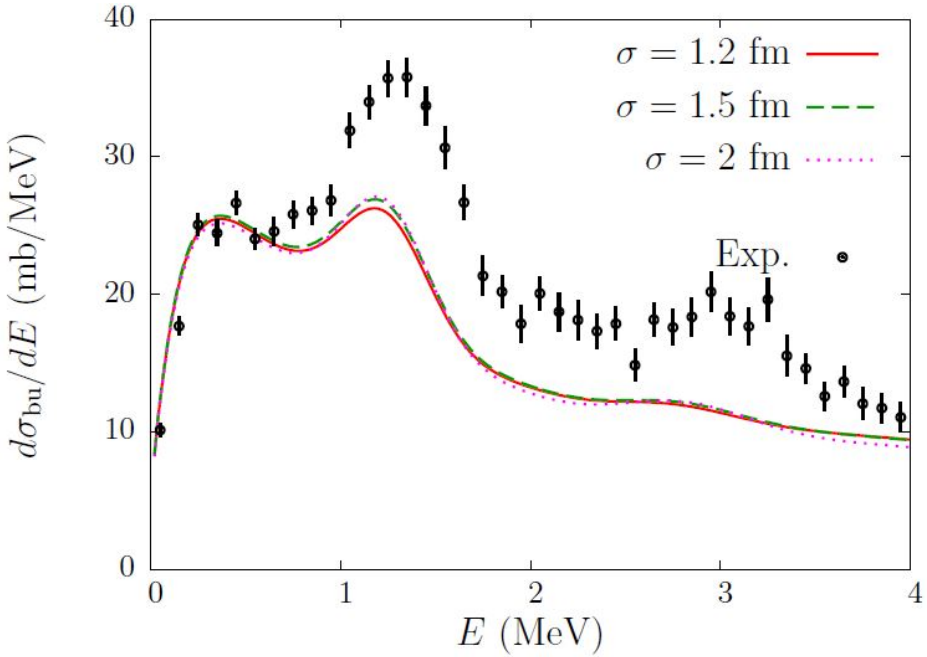

Figure: Capel, Philips & Hammer, PRC 98, 034610 (2018)

- Missing strength in resonances due to missing degree of freedom:
  $\rightarrow$ the ^{10}Be core can be excited to its 2^+ state $\rightarrow$ **s.p** not enough !

^{11}Be: results

And now, the results...

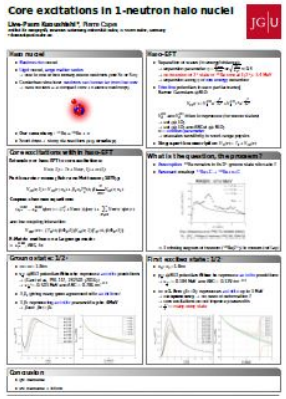

Some key-words:

- Halo-EFT
- Core excitations
- Structure calculations
- R-Matrix theory

5

Heavy-baryon spectroscopy in a quark-diquark approach

A. Torcato[1,2]
atorcato@lip.pt
A. Arriaga[1,3]
G. Eichmann[4]
M. T. Peña[1,2]

Context

Functional methods applied to baryons

Idea: Transform baryon qqq state into q(qq) state

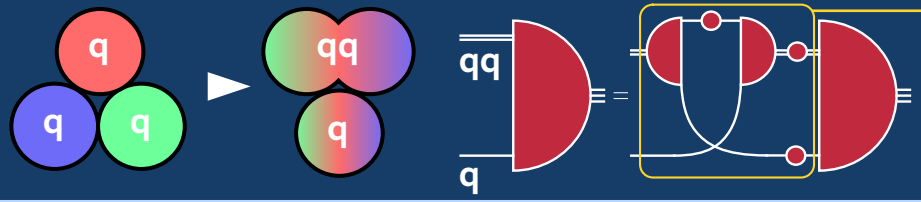

Objective

Calculate masses & structure variables

Idea: Transform q(qq) equation into eigenvalue form

$$\mathcal{K}\psi_i = \lambda_i \psi_i,\ \lambda_i(P^2 = -\mathrm{M}_i^2) = 1$$

Eigenvalues → calculate **masses**

Eigenvectors → calculate **structure variables**

Results

Published

Few Body Syst. 64, 45

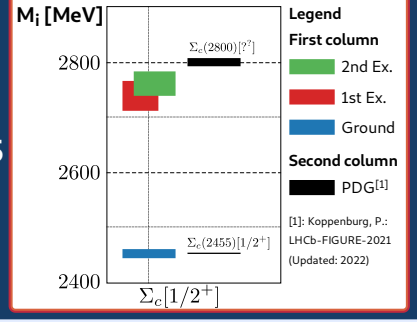

Ground state of nnc

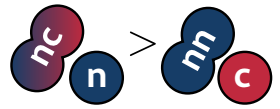

$\sim 60\%$ $\sim 40\%$

Check-out the poster, where we will answer...

- → How does one arrive at the q(qq) state?
- → What is the methodology for solving the equation?
- → What can we conclude from our results?
- → What awaits in the future? + Where is the wine & cheese?

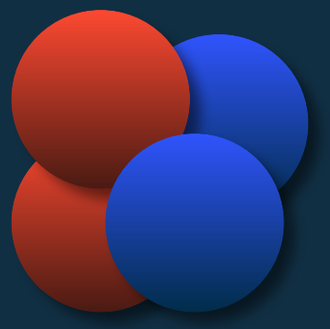

Bayesian Analysis of a Modified Power Counting in χEFT

Oliver Thim | Theoretical Subatomic Physics | Chalmers University of Technology

25th European conference on few-body problems in physics
Mainz, 2023-08-03

Introduction

- Predict nuclear properties in a well-founded EFT framework
  - A model: χEFT — from low energy QCD
  - Power counting (PC): orders contributions to observables; LO, NLO, …
- Weinberg PC has problems already at LO caused by the singular attraction of the one-pion exchange potential

  A. Nogga, R. G. E. Timmermans, and U. van Kolck, Phys. Rev. C **72**, 054006 (2005)

Introduction

- We investigate an alternative power counting due to Long & Yang
  - Promote counterterms based on RG arguments
  - Include sub-leading orders in perturbation theory

B. Long, C. J. Yang, Phys. Rev. C **85** (2012)
B. Long, C. J. Yang, Phys. Rev. C **86** (2012)

- Why?
  - An accurate order-by-order description is important for sound estimates of the EFT truncation error
  - Insight into what constitutes an adequate LO description

Results

Leading order:

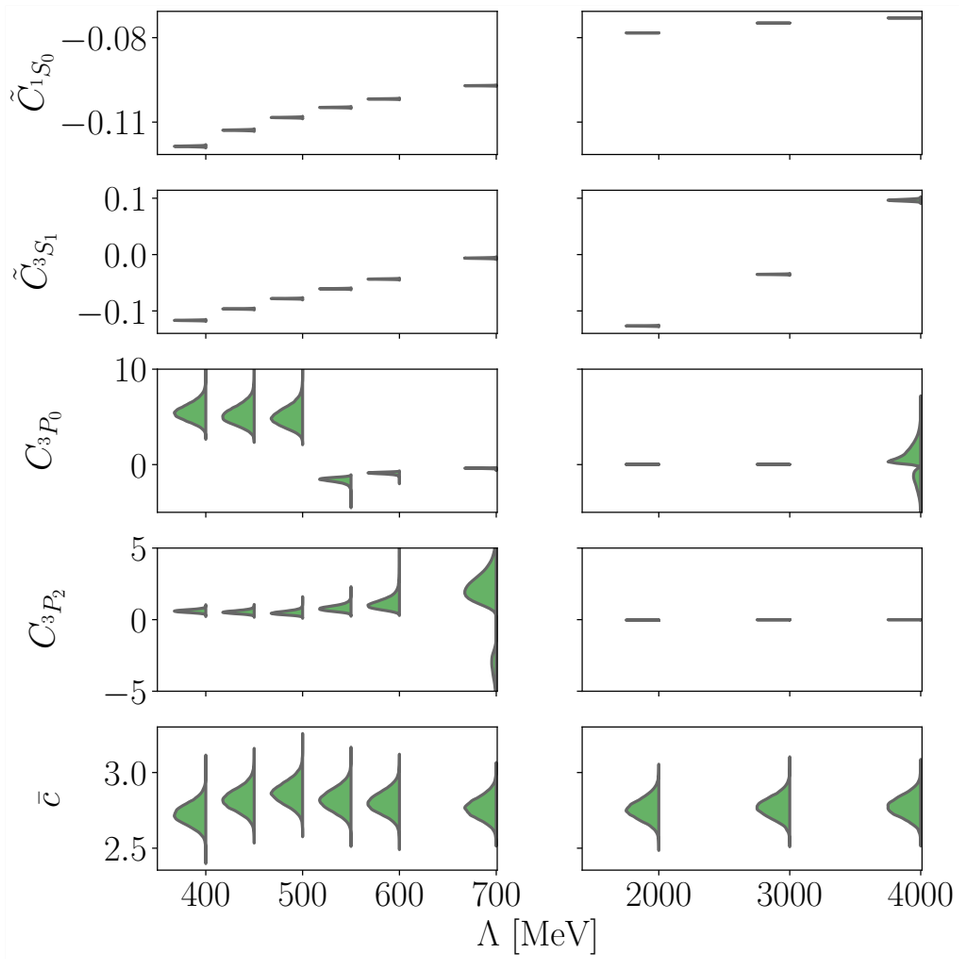

O. Thim, E. May, A. Ekström, C. Forssén, arXiv:2302.12624 (2023)

Sub-leading orders:

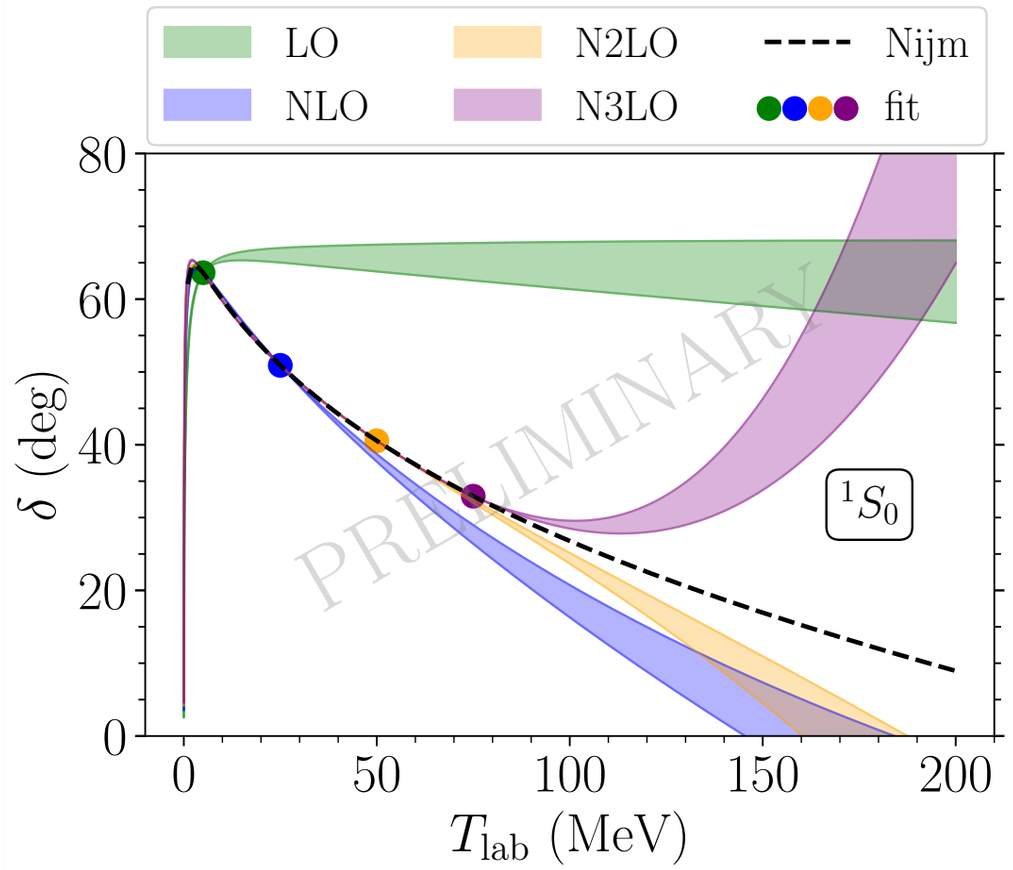

O. Thim, A. Ekström, C. Forssén, (in preparation)

Bayesian Analysis of χEFT in a Modified Weinberg Power Counting

Oliver Thim, Andreas Ekström, Christian Forssén

Introduction

A well-defined power counting in χEFT is crucial for:
- sound a priori estimates of the EFT truncation error.
- connecting quantum chromodynamics to properties of nuclei.

In several studies, e.g., Nogga *et al.*, the canonical power counting due to Weinberg has been up for debate. Yang *et al.* investigated the following renormalization group (RG) invariant modified leading order (LO) nucleon-nucleon potential and found that the nuclear-binding mechanism fails for nuclei with mass number $A > 4$. Low energy constants (LECs) overfitted to phase shifts might be a potential cause.

- We want to investigate if nuclei can be described in χEFT.
- In Thim *et. al.* we use **History Matching and Emulation** to perform a Bayesian formulation of χEFT.
- In Thim *et. al.* we use **History Matching and Emulation** to perform a Bayesian determine the joint probability density function for LECs and EFT truncation error and EFT error (with variance parametrized by a Gaussian process) given scattering data across a wide range of cutoffs.

$$\Pr(\theta|D,I) = \frac{\Pr(D|\theta,I)\cdot\Pr(\theta|I)}{\Pr(D|I)}$$

- In the modified power counting we follow (Quasi-Particle Peak) **orders** are included perturbatively in distorted wave Born approximation.

RG invariant LO potential

$$V(p',p) = \frac{1}{(2\pi)^3}\left[-\frac{g_A^2}{4f_\pi^2}\frac{(\sigma_1\cdot q)(\sigma_2\cdot q)}{q^2+m_\pi^2}(\tau_1\cdot\tau_2)\right.$$
$$\left.+\tilde{C}_{^1S_0}+\tilde{C}_{^3S_1}+(\tilde{C}_{^3P_0}+\tilde{C}_{^1P_1}+\tilde{C}_{^3P_2})p'p\right]$$

Include only partial waves with $l \leq 1$, as well as ${}^3D_1$ and ε_1.

- Found different LEC modes and phase shifts compared to Yang *et al.*
- Demonstrated both **robust Bayesian inference** across a wide range of cutoffs and RG-invariance in np ppds.
- This work at LO lays the foundation for a Bayesian analysis of an RG invariant formulation of χEFT at **sub-leading orders**.

- Posterior predictive distribution for the deuteron ground state energy.
- No EFT-error included in this ppd.
- Deeply bound state for $\Lambda > 700$ MeV.

Sub-Leading Orders

While sub-leading orders can be treated perturbatively with respect to LO

$$V_{\mathrm{II}} = \sum_{m=0}^{\infty} V_{\mathrm{II}}^{(m)}$$

$$\sum_{n=0}^{\infty}\left(\Omega_+ C^{(n)} V_{\mathrm{II}}^{(0)} \Omega_+ + \Omega_+ C^{(0)} V_{\mathrm{II}}^{(n)} \Omega_+ + \sum_{m=0}^{n-1} \Omega_+ C^{(m)} V_{\mathrm{II}}^{(n-m)} C^{(0)} V_{\mathrm{II}}^{(0)}\right)\Omega_+ , \ \ldots$$

phase cutoff

ν	Order	LECs
0	LO	$\tilde{C}_{^1S_0}^{(0)}$
1	NLO	$\tilde{C}_{^1S_0}^{(1)}$, $C_{^1S_0}^{(0)}$
2	N2LO	$\tilde{C}_{^1S_0}^{(2)}$, $C_{^1S_0}^{(1)}$, $D_{^1S_0}^{(0)}$
3	N3LO	$\tilde{C}_{^1S_0}^{(3)}$, $C_{^1S_0}^{(2)}$, $D_{^1S_0}^{(1)}$, $E_{^1S_0}^{(0)}$

shows signs of overfitting, which from 500 to 1500 MeV.

Bayesian posteriors and ppds

- Marginal posterior pdfs across cutoffs $\Lambda \in [400, 4000]$ MeV.
- An evidence analysis identified the relevant mode(s) for each cutoff.
- Interesting to compare our inference to the phase shift optimization by Yang *et al.* **We find similar LEC values and phase shifts in $^1S_0$ - waves and differences in the $^3P_0$ - waves.**

Outlook

- Extend sub-leading orders to all relevant partial waves and compute *NN* scattering **observables** perturbatively.
- Develop EFT **error model with correlations** and perform a Bayesian inference of LECs up to N^{3}LO.
- Predict observables in **heavier-mass nuclear systems.**

References

C. J. Yang, A. Ekström, C. Forssén, and G. Hagen, Phys. Rev. C **96**, 054311 (2017)
B. Long and C. J. Yang, Phys. Rev. C **85**, 024001 (2012)
A. Nogga, R. G. E. Timmermans, and U. van Kolck, Phys. Rev. C **72**, 054006 (2005)
H. W. Hammer, S. König, and U. van Kolck, Rev. Mod. Phys. **92**, 025004 (2020)
O. Thim, E. May, A. Ekström, C. Forssén, arXiv:2302.12624 [nucl-th] (2023)

Contact

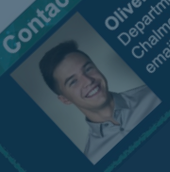

Oliver Thim
Department of Physics,
Chalmers University of Technology
email: oliver.thim@chalmers.se

CHALMERS

Swedish Research Council

European Research Council

Thank you!

Ab Initio Study of Low-Energy Antiproton-Nucleus Systems

Alireza Dehghani

IJCLAB, CNRS/IN2P3 & Université Paris-Saclay, Orsay, France

Team Members & Collaborators

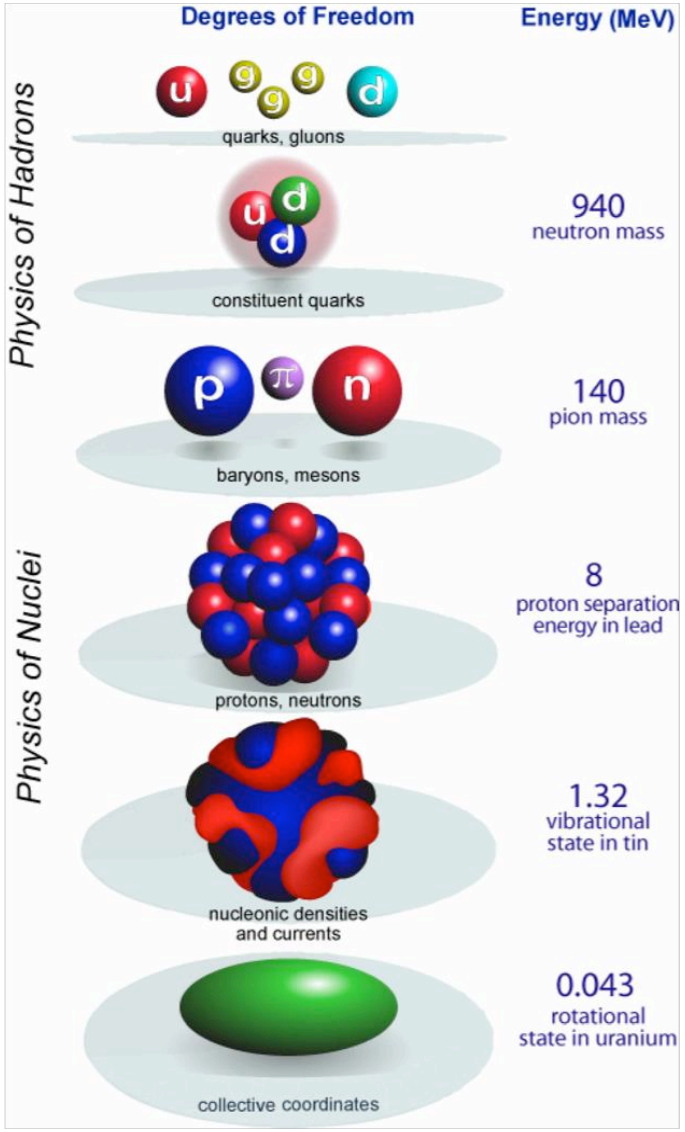

Thesis Directors:

Dr. Guillaume Hupin
Prof. Ubirajara van Kolck

Ab initio Nuclear Reactions Theory Team Members:

Dr. Lorenzo Contessi
Osama Yaghi (PhD student)
Alireza Dehghani (PhD student)

Collaborators (Antiprotonic Research):

Dr. Jaume Carbonell (IJCLab)
Prof. Slamowir Wycech (NCNR, Poland)

Why study Antiprotons?

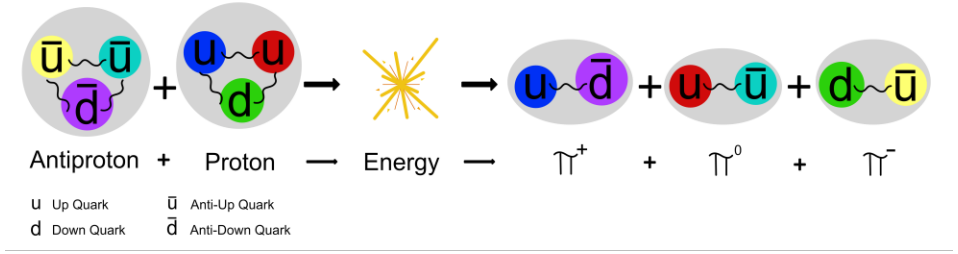

antiProton Unstable Matter Annihilation: PUMA

Aim: Using antiprotons as a probe for nuclear surface structure

What is measured?
neutron-to-proton annihilation ratio (which can be related to N/Z at the surface)

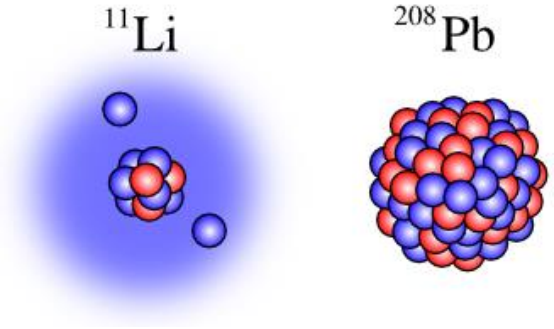

No-core shell model (NSCM) and NCSM/RGM

Ab initio expansion methods for nuclear structure:

- Direct calculation of the A-body system (all nucleons are active)
- Only input: 2- and 3-nucleons, e.g. Chiral-EFT interactions.

Applicability:

2 ≤ A ≤ 16: Full spectroscopy on structure properties

2 ≤ A ≤ 10: Elastic Channel E>0

2 ≤ A ≤ 6: Threebody Dynamics

$$\Psi^{(A)}_{NCSM} = |A\lambda J^{\pi} T\rangle = \sum_{\alpha} c_{\alpha} \; |A\alpha j_z{}^{\pi} t_z\rangle$$

Mixing coefficients(unknown)

A-body harmonic oscillator states

$$\Psi^{(A)}_{RGM} = \sum_{v} \int d\vec{r}\, g_v(\vec{r})\, \hat{A}_v \left| \Phi^{(A-a,a)}_{v\vec{r}} \right\rangle$$

Relative wave function (unknown)

Antisymmetrizer

Channel basis

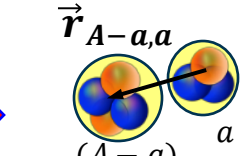

$$\psi^{(A-a)}_{\alpha_1} \psi^{(a)}_{\alpha_2} \, \delta(\vec{r} - \vec{r}_{A-a,a})$$

Cluster expansion technique

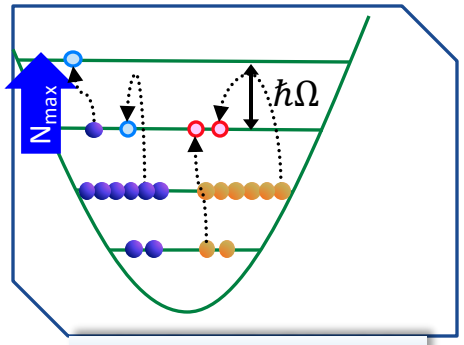

No-Core Shell Model (NCSM)

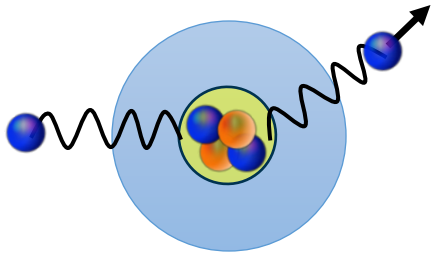

NCSM/RGM

Proton-Antiproton scattering phase shifts using R-Matrix and Complex Scaling (CS) Methods:

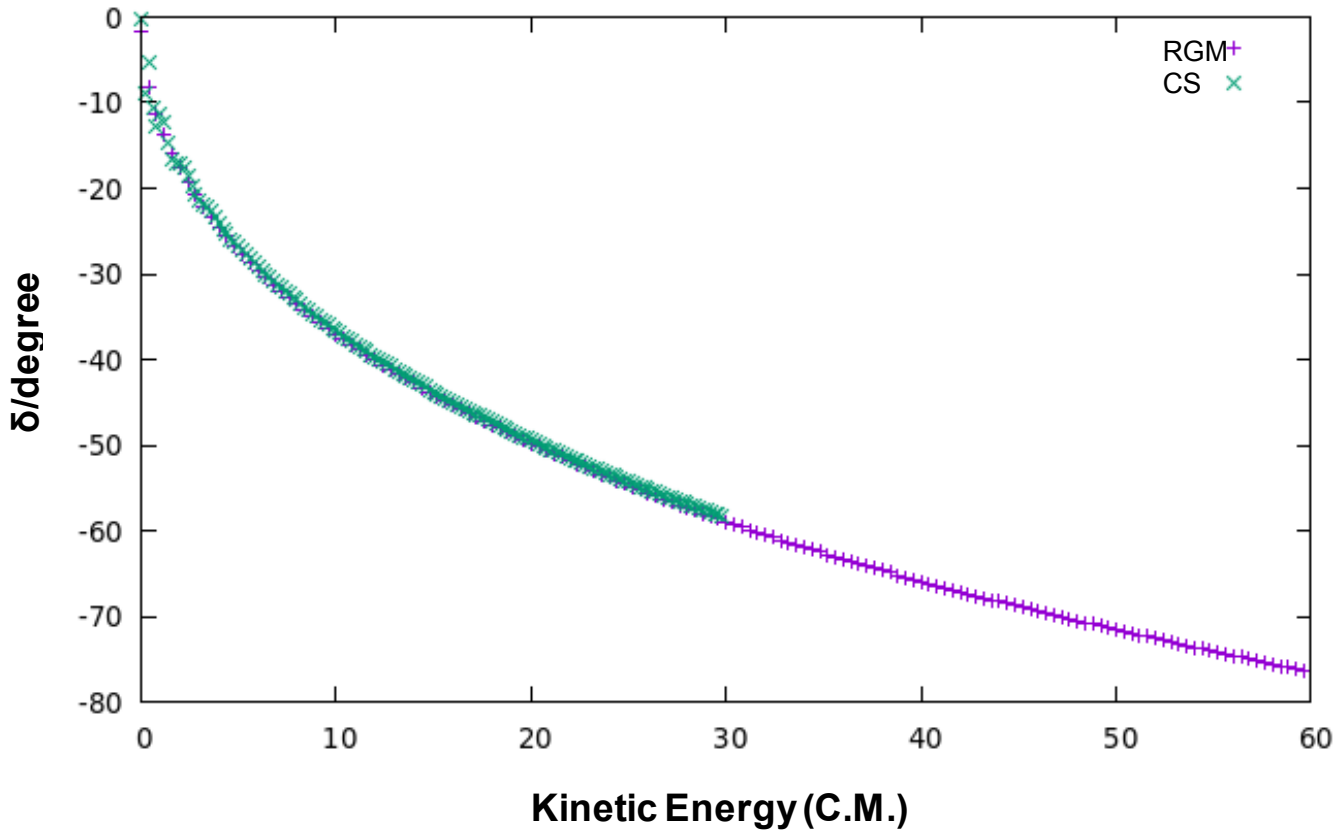

Antiproton-deuteron s-wave doublet phase shift using RGM with R-matrix:

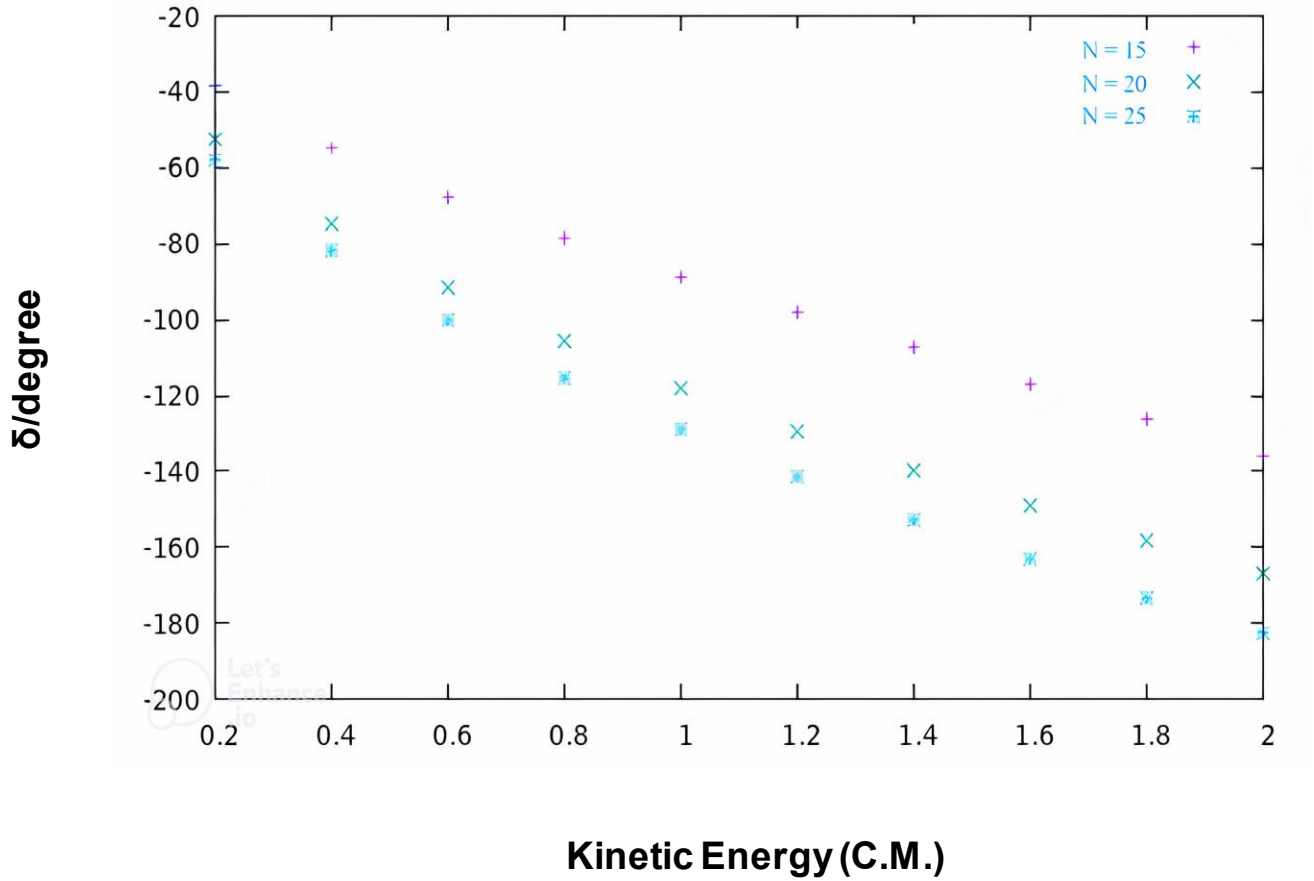

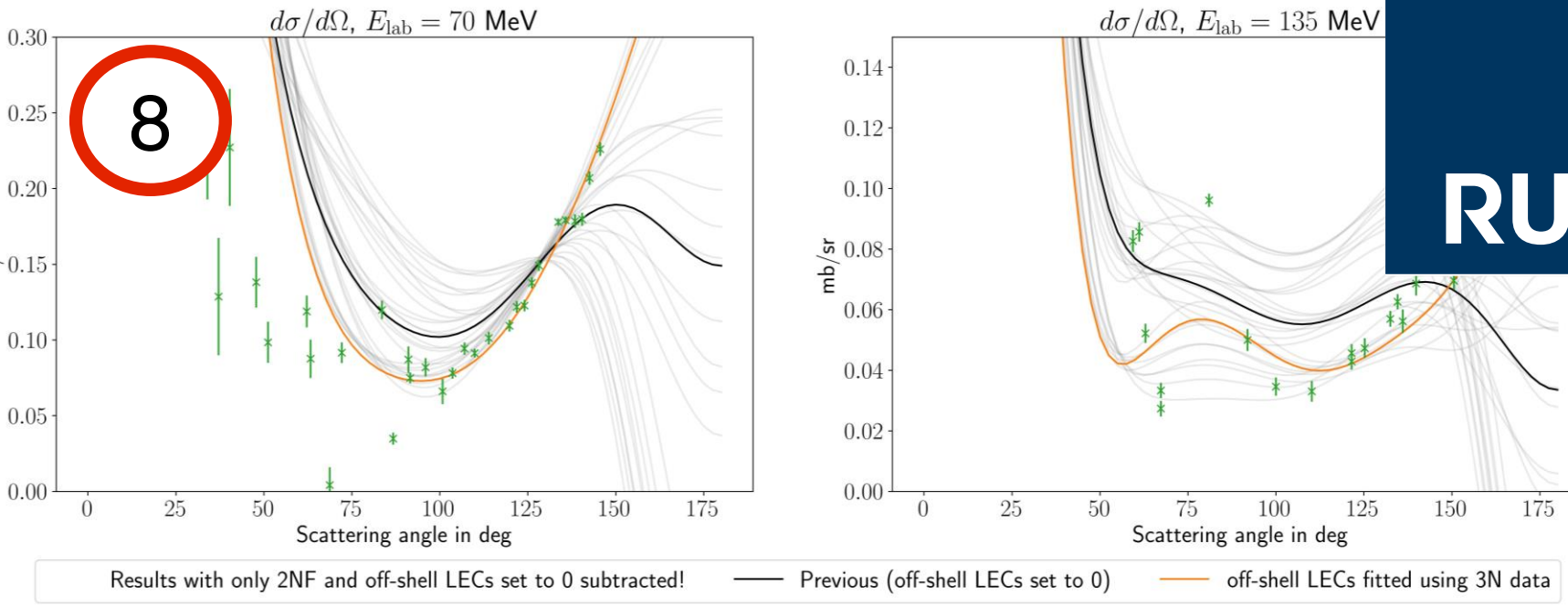

8

RUB

RUHR-UNIVERSITÄT BOCHUM

CONSTRAINING THE TWO-NUCLEON FORCE IN CHIRAL EFT FROM THREE-NUCLEON DATA

Observing the unobservable off-shell behavior?

Sven Heihoff, Evgeny Epelbaum

contact: sven.heihoff@rub.de

Off-shell Low-Energy Constants (off-shell LECs)

- 2N potential in chiral EFT in the order N^{3}LO in the $^1S_0$ partial wave:

$$\langle\, {}^1S_0, p' \big| V^{(4)} \big|\, {}^1S_0, p \rangle = D_{1S0}\, p^2\, p'^2 + D_{1S0}^{\text{off}} \left(\vec{p}'^2 - \vec{p}^2\right)^2 + \ \ldots$$

Off-shell Low-Energy Constants (off-shell LECs)

- 2N potential in chiral EFT in the order N^{3}LO in the ${}^1S_0$ partial wave:

$$\left\langle {}^1S_0, p' \middle| V^{(4)} \middle| {}^1S_0, p \right\rangle = D_{1S0}\, p^2\, p'^2 + D_{1S0}^{\text{off}} \left(\vec{p}'^2 - \vec{p}^2\right)^2 + \ \ldots$$

- We can only observe $p = p'$ → D_{1S0}^{off} can not be determined by using 2N experimental data

Off-shell Low-Energy Constants (off-shell LECs)

- 2N potential in chiral EFT in the order N^{3}LO in the ${}^1S_0$ partial wave:

$$\langle {}^1S_0, p' | V^{(4)} | {}^1S_0, p \rangle = D_{1S0}\, p^2\, p'^2 + D_{1S0}^{\text{off}} \left(\vec{p}'^2 - \vec{p}^2\right)^2 + \ \ldots$$

- We can only observe $p = p'$ → D_{1S0}^{off} can not be determined by using 2N experimental data
- Off-shell LECs are somewhat similar to transformation angles γ_{i} of a unitary transformation

$$\hat{U} = \exp\left(\gamma_1 \hat{T}_1 + \gamma_2 \hat{T}_2 + \ \gamma_3 \hat{T}_3\right), \qquad \langle \vec{p}' | \hat{T}_1 | \vec{p} \rangle = \frac{m_{\text{N}}}{2\Lambda_{\text{b}}^4} \left(\vec{p}'^2 - \vec{p}^2\right)/2$$

$$\langle \vec{p}' | \delta\hat{H} | \vec{p} \rangle = \langle \vec{p}' | \hat{U}^\dagger \hat{H}^{(0)} \hat{U} - \hat{H}^{(0)} | \vec{p} \rangle = \Sigma_i\, \gamma_i \left\langle \vec{p}' \left| \left[\hat{H}_{\text{kin}}^{(0)}, \hat{T}_i \right] \right| \vec{p} \right\rangle + \cdots = \gamma_1 \frac{1}{\Lambda_{\text{b}}^4} \left(\left(\vec{p}'^2 - \vec{p}^2\right)/2 \right)^2 + \cdots$$

Off-shell Low-Energy Constants (off-shell LECs)

- 2N potential in chiral EFT in the order N^{3}LO in the ${}^1S_0$ partial wave:

$$\langle {}^1S_0, p' | V^{(4)} | {}^1S_0, p \rangle = D_{1S0}\, p^2\, p'^2 + D_{1S0}^{\text{off}} \left(\vec{p}'^2 - \vec{p}^2\right)^2 + \ \ldots$$

- We can only observe $p = p'$ → D_{1S0}^{off} can not be determined by using 2N experimental data
- Off-shell LECs are somewhat similar to transformation angles γ_{i} of a unitary transformation

$$\hat{U} = \exp\left(\gamma_1 \hat{T}_1 + \gamma_2 \hat{T}_2 + \gamma_3 \hat{T}_3\right), \qquad \langle \vec{p}' | \hat{T}_1 | \vec{p} \rangle = \frac{m_{\text{N}}}{2\Lambda_{\text{b}}^4} \left(\vec{p}'^2 - \vec{p}^2\right)/2$$

$$\langle \vec{p}' | \delta\hat{H} | \vec{p} \rangle = \langle \vec{p}' | \hat{U}^\dagger \hat{H}^{(0)} \hat{U} - \hat{H}^{(0)} | \vec{p} \rangle = \Sigma_i\, \gamma_i \left\langle \vec{p}' \left| \left[\hat{H}_{\text{kin}}^{(0)}, \hat{T}_i \right] \right| \vec{p} \right\rangle + \cdots = \gamma_1 \frac{1}{\Lambda_{\text{b}}^4} \left(\left(\vec{p}'^2 - \vec{p}^2\right)/2 \right)^2 + \cdots$$

- **Conclusion:** Fixing off-shell LECs is equivalent to fixing arbitrary transformation angles!

Unitary Transformation in 3N Systems and Technicalities

- 3N forces are induced by the unitary transformation

$$\gamma_1 \langle \vec{p}_1', \vec{p}_2', \vec{p}_3' \left| \left[\hat{V}_{\text{cont}}^{(0)}, \hat{T}_1 \right] \right| \vec{p}_1, \vec{p}_2, \vec{p}_3 \rangle = \gamma_1 \frac{m_N}{4\Lambda_b^4} |\vec{p}_3' - \vec{p}_3|^2 \, (C_S + C_T \vec{\sigma}_1 \vec{\sigma}_2) + \text{permutations.}$$

Unitary Transformation in 3N Systems and Technicalities

- 3N forces are induced by the unitary transformation

$$\gamma_1 \langle \vec{p}_1', \vec{p}_2', \vec{p}_3' \left| \left[\hat{V}_{\text{cont}}^{(0)}, \hat{T}_1 \right] \right| \vec{p}_1, \vec{p}_2, \vec{p}_3 \rangle = \gamma_1 \frac{m_N}{4\Lambda_b^4} |\vec{p}_3' - \vec{p}_3|^2 \, (C_S + C_T \vec{\sigma}_1 \vec{\sigma}_2) + \text{permutations.}$$

- This is observable → γ_i can be determined → off-shell LECs can be determined!

Unitary Transformation in 3N Systems and Technicalities

- 3N forces are induced by the unitary transformation

$$\gamma_1 \langle \vec{p}_1', \vec{p}_2', \vec{p}_3' \left| \left[\hat{V}_{\text{cont}}^{(0)}, \hat{T}_1 \right] \right| \vec{p}_1, \vec{p}_2, \vec{p}_3 \rangle = \gamma_1 \frac{m_N}{4\Lambda_b^4} |\vec{p}_3' - \vec{p}_3|^2 \, (C_S + C_T \vec{\sigma}_1 \vec{\sigma}_2) + \text{permutations.}$$

- This is observable → γ_i can be determined → off-shell LECs can be determined!
- Induced 3N forces appear at N^{3}LO and there are similar terms in N^{4}LO

  → Determination necessary for complete N^{3}LO calculation

Unitary Transformation in 3N Systems and Technicalities

- 3N forces are induced by the unitary transformation

$$\gamma_1 \langle \vec{p}_1', \vec{p}_2', \vec{p}_3' \left| \left[\hat{V}_{\text{cont}}^{(0)}, \hat{T}_1 \right] \right| \vec{p}_1, \vec{p}_2, \vec{p}_3 \rangle = \gamma_1 \frac{m_N}{4\Lambda_b^4} |\vec{p}_3' - \vec{p}_3|^2 \, (C_S + C_T \vec{\sigma}_1 \vec{\sigma}_2) + \text{permutations.}$$

- This is observable → γ_i can be determined → off-shell LECs can be determined!
- Induced 3N forces appear at N^{3}LO and there are similar terms in N^{4}LO
  → Determination necessary for complete N^{3}LO calculation

- **Technicalities**:
  - Iterating Faddeev equation takes a lot of time → emulator based on RBF interpolation
  - Fitting off-shell LECs takes ~ 1 min instead of ~ 1 week thanks to emulator, cost: on average 3% error
  - Creating a reliable database of experimental 3N data

Improvement of 3N Data Description

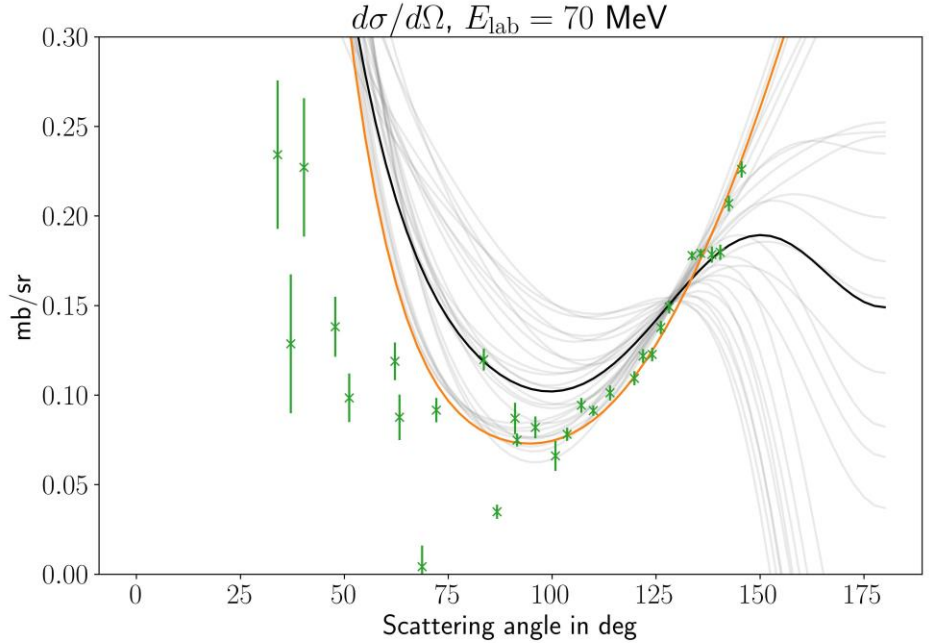

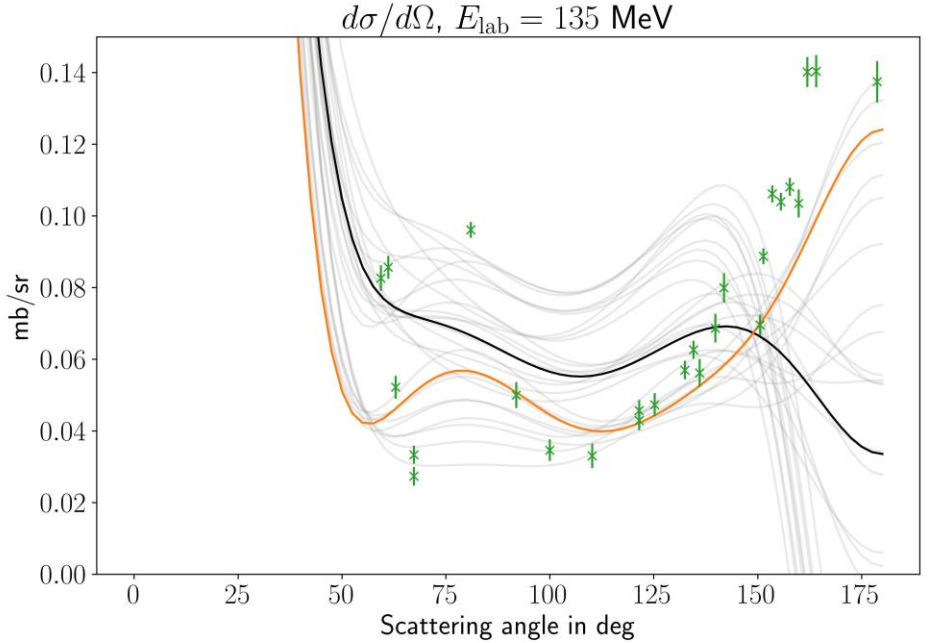

Results with only 2NF and off-shell LECs set to 0 subtracted! — Previous (off-shell LECs set to 0) — off-shell LECs fitted using 3N data

Experimental data from Kimiko et. al, Phys. Rev. C 65, 034003 (2002), Phys. Rev. C 70, 014001 (2004) and Phys. Rev. Lett. 95, 162301 (2005)

9

Ab initio description of the antiproton-deuteron annihilation

Pierre-Yves Duerinck[1,2,3]

Supervisors: Jérémy Dohet-Eraly[1] and Rimantas Lazauskas[2]

[1]Physique nucléaire et physique quantique (PNPQ), ULB, Brussels
[2]Institut Pluridisciplinaire Hubert Curien (IPHC), Unistra, Strasbourg
[3]F.R.S.-FNRS research fellow

25th European Conference on Few-body Problems in Physics
August 03, 2023

Motivation

- PUMA experiment (CERN): aims to study nucleus skin densities of short-lived nuclear isotopes using low-energy antiprotons as a probe.
- Study of the proton and neutron densities by measuring the annihilation products and $p\bar{p}/n\bar{p}$ annihilation ratio.

- Remaining questions:
  1. Validity of the $N\bar{N}$ models ?
  2. Model dependence ?
  3. Theoretical uncertainties ?

$\longrightarrow$ **Microscopic treatment of the antiproton-nucleus system**.

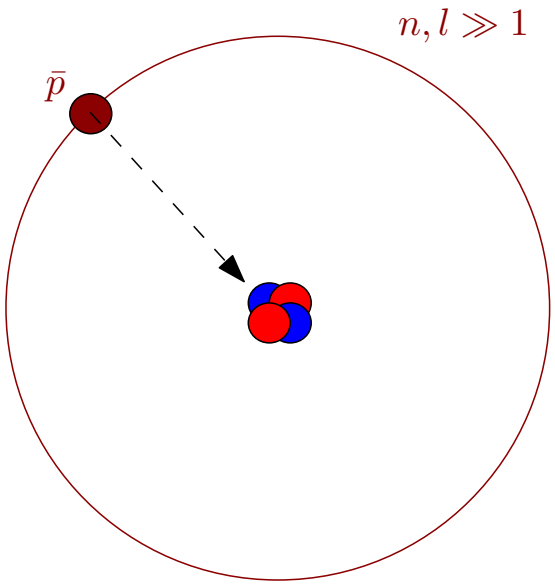

Figure: Antiproton-nucleus system

Present work: antiproton-deuteron annihilation (poster 10)

- Antiproton-deuteron ($\bar{p}d$) system:
  1. In the absence of strong nuclear interaction: formation of an hydrogenic state with energy
  $$E_n^{(C)} = -2.22\,\mathrm{MeV} + \epsilon_\mathrm{n}, \qquad \epsilon_\mathrm{n} = -\frac{16.7}{\mathrm{n}^2}\,\mathrm{keV}$$
  2. The hadronic interaction shifts and broadens the energy levels: $E_n = E_R - i\frac{\Gamma}{2}$

- Non-relativistic description by solving the Faddeev equations in configuration space.
- Calculation of the $\bar{p}d$ scattering lengths/volumes and level shifts with different NN and $N\bar{N}$ interactions.
- Model dependence on the $N\bar{N}$ input: comparison between optical and coupled-channel models.

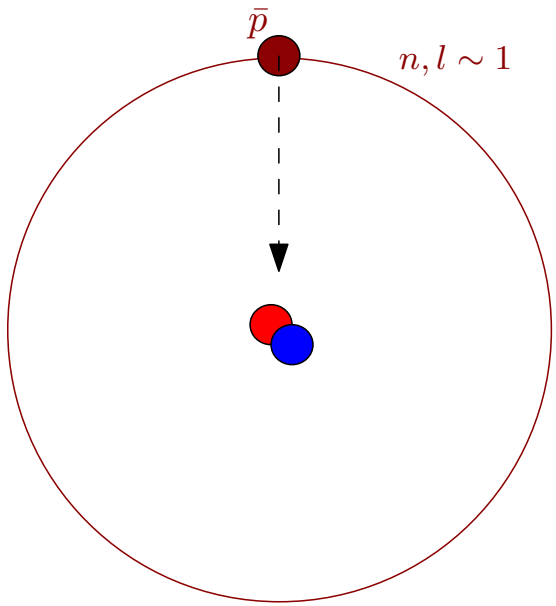

Figure: Antiproton-deuteron system

10

Molecular nature of the $D_{s0}^*(2317)$ and B_{s0}^*

25th European Conference on Few-body Problems in Physics

Hee-Jin Kim

Inha University

In collaboration with Prof. Hyun-Chul Kim

Outline

- *Introduction*
- *General formailsm*
- *Results*
- *Summary*

Introduction

Introduction

- The $D_{s0}^{*}(2317)$ state was first observed in 2003 by the BaBar Collaboration at SLAC in the inclusive $D_s^+\pi^0$ invariant mass distribution from e^+e^- annihilation data[1].
- The mass of the $D_{s0}^{*}(2317)$ shows a deviation from the P-wave $c\bar{s}$ state in the conventional quark model predictions.
- The proximity of its mass to D^0K^+ threshold and narrow width $\Gamma_{D_{s0}^{*}(2317)} < 3.8$ MeV indicate the possibility of the DK molecule state.
- The spin-parity assignment of $J^P = 0^+$ is favorable by the parity conservation.
- The molecule interpretation of the $D_{s0}^{*}(2317)$ has been supported by several theoretical calculations: Chiral unitary approaches, Effective Lagrangian methods, and Lattice QCD.
- We investigate the hadron molecule feature of the $D_{s0}^{*}(2317)$ and predict the B_{s0}^{*} state within the meson-exchange framework using the *fully off-mass-shell* coupled-channel formalism.

[1] B. Aubert *et al*.(BABAR Collaboration), Phys.Rev.Lett.90.242001(2003)

General Formalism

Effective Lagrangian

- **Heavy chiral Lagrangian**

The coupling constants between heavy and light mesons are determined by the interaction Lagrangian based on the *Heavy Quark Effective Field Theory*(HQEFT).

$$\mathcal{L}_{\rm heavy} = ig\mathrm{Tr}[H_b\gamma_\mu\gamma_5\mathcal{A}^\mu_{ba}\bar{H}_a] + i\beta\mathrm{Tr}[H_b v^\mu(\mathcal{V}_\mu-\rho_\mu)_{ba}\bar{H}_a] + i\lambda\mathrm{Tr}[H_b\sigma_{\mu\nu}F^{\mu\nu}_{ba}(\rho)\bar{H}_a] + g_\sigma\bar{H}_a H_a\sigma$$

A heavy-light meson is made up by a heavy quark Q and a light antiquark $\bar{q}$.

→ heavy quark spin symmetry(HQSS), heavy quark flavor symmetry(HQFS) + chiral symmetry

$$H^a = \frac{1+\not{v}}{2}(P^{*a}_\mu\gamma^\mu - P^a\gamma_5), \quad \bar{H} = \gamma_0 H^\dagger\gamma_0 = (P^{*\dagger a}_\mu\gamma^\mu + P^{\dagger a}\gamma_5)\frac{1+\not{v}}{2}$$

pseudoscalar heavy field: $P^a = \{D^+, D^0, D_s^+\}$ or $\{B^-, \bar{B}^0, \bar{B}_s^0\}$

vector heavy field: $P^{*a}_\mu = \{D^{*+}_\mu, D^{*0}_\mu, D^{*+}_{s\mu}\}$ or $\{B^{*-}_\mu, \bar{B}^{*0}_\mu, \bar{B}^{*0}_{s\mu}\}$

- **SU(3) symmetric Lagrangians for the light flavors**

$$\mathcal{L}_{\mathcal{PPV}} = -\frac{i}{2}g_{\mathcal{PPV}}\,\mathrm{Tr}([\mathcal{M},\partial_\mu\mathcal{M}]V_\mu),$$

$$\mathcal{L}_{\mathcal{PP}\sigma} = 2g_{\mathcal{PP}\sigma}m_{\mathcal{P}}\mathcal{M}\mathcal{M}\sigma$$

Feynman amplitudes

- **Decay to isospin violated channel $D_{s0}^*(2317) \to D_s\pi^0$**

  Isospin violation decay implies the mixing of the isoscalar and isovector channels → π^0-η mixing

  - *$\pi^0\eta$ mixing :* mass term in the chiral Lagrangian violate the isospin symmetry

$$\mathcal{L}_{\rm mass} = \frac{B_0 f_\pi^2}{4}\,{\rm Tr}\,\hat{M}U \quad \Longrightarrow \quad \mathcal{L}_{\rm mixing} = -\frac{B_0}{\sqrt{3}}(m_u - m_d)\pi^0\eta$$

$\hat{M} = {\rm diag}(m_u, m_d, m_s),\ U = \exp(2i\mathcal{M}/f_\pi)$

  - Diagonalize with the mixing angle ϵ :

$$|D_s^+\pi^0\rangle = |D_s^+\tilde{\pi}^0\rangle\cos\epsilon - |D_s^+\tilde{\eta}\rangle\sin\epsilon$$
$$|D_s^+\eta\rangle = |D_s^+\tilde{\pi}^0\rangle\sin\epsilon + |D_s^+\tilde{\eta}\rangle\cos\epsilon$$

$$\tan 2\epsilon = \frac{\sqrt{3}}{2}\frac{m_d - m_u}{m_s - (m_u + m_d)/2}, \quad \epsilon = 0.012$$

- **Kernel matrix**

  Consider four $C = S = +1$ channels : $|1\rangle = |D_s^+\pi^0\rangle,\ |2\rangle = |D^0K^+\rangle,\ |3\rangle = |D^+K^0\rangle,\ |4\rangle = |D_s^+\eta\rangle$

  Kernel matrix element: $\mathcal{V}_{ba} \equiv \langle b|\mathcal{V}|a\rangle$

$$\hat{\mathcal{V}} = \begin{pmatrix} \mathcal{V}_{D_s^+\pi^0\to D_s^+\pi^0} & \mathcal{V}_{D_s^+\pi^0\to D^0K^+} & \mathcal{V}_{D_s^+\pi^0\to D^+K^0} & \mathcal{V}_{D_s^+\pi^0\to D_s^+\eta} \\ \mathcal{V}_{D^0K^+\to D_s^+\pi^0} & \mathcal{V}_{D^0K^+\to D^0K^+} & \mathcal{V}_{D^0K^+\to D^+K^0} & \mathcal{V}_{D^0K^+\to D_s^+\eta} \\ \mathcal{V}_{D^+K^0\to D_s^+\pi^0} & \mathcal{V}_{D^+K^0\to D^0K^+} & \mathcal{V}_{D^+K^0\to D^+K^0} & \mathcal{V}_{D^+K^0\to D_s^+\eta} \\ \mathcal{V}_{D_s^+\eta\to D_s^+\pi^0} & \mathcal{V}_{D_s^+\eta\to D^0K^+} & \mathcal{V}_{D_s^+\eta\to D^+K^0} & \mathcal{V}_{D_s^+\eta\to D_s^+\eta} \end{pmatrix}$$

  We construct the *off-mass-shell* kernel matrix in the full-channel momentum space.

Coupled-channel equation

- **Scattering amplitudes**

$$\mathcal{V}^t_\sigma(t) = 4F^2(t) g_{DD\sigma} g_{PP\sigma} m_D m_P \frac{1}{t - m^2_\sigma}$$

$$\mathcal{V}^t_V(t) = -F^2(t) g_{DDV} g_{PPV} \frac{(p_1 + k_1)\cdot(p_2 + k_2)}{t - m^2_V}$$

$$\mathcal{V}^u_{D^*}(u) = F^2(u) g^2_{DD^*P} \frac{(p_1 + k_2)\cdot(p_2 + k_1)}{u - m^2_{D^*}},$$

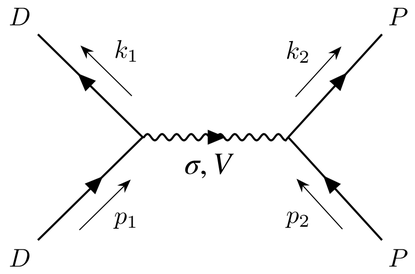

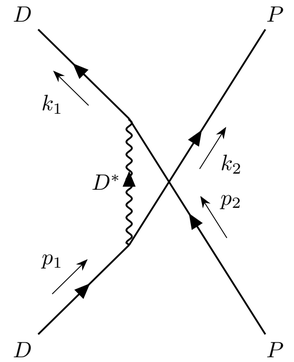

- **Blankenbecler-Sugar equation**

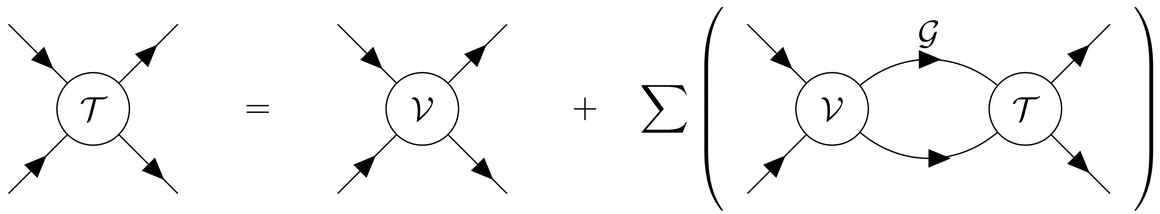

$$T = V + VGT$$

Matrix inversion method: $T^J = V^J + V^J G T^J \implies T^J = (1 - V^J G)^{-1} V^J$

$$\mathcal{T}^J_{fi} = \begin{pmatrix} \mathcal{T}^J_{D_s^+\pi^0\to D_s^+\pi^0} & \mathcal{T}^J_{D_s^+\pi^0\to D^0K^+} & \mathcal{T}^J_{D_s^+\pi^0\to D^+K^0} & \mathcal{T}^J_{D_s^+\pi^0\to D_s^+\eta} \\ \mathcal{T}^J_{D^0K^+\to D_s^+\pi^0} & \mathcal{T}^J_{D^0K^+\to D^0K^+} & \mathcal{T}^J_{D^0K^+\to D^+K^0} & \mathcal{T}^J_{D^0K^+\to D_s^+\eta} \\ \mathcal{T}^J_{D^+K^0\to D_s^+\pi^0} & \mathcal{T}^J_{D^+K^0\to D^0K^+} & \mathcal{T}^J_{D^+K^0\to D^+K^0} & \mathcal{T}^J_{D^+K^0\to D_s^+\eta} \\ \mathcal{T}^J_{D_s^+\eta\to D_s^+\pi^0} & \mathcal{T}^J_{D_s^+\eta\to D^0K^+} & \mathcal{T}^J_{D_s^+\eta\to D^+K^0} & \mathcal{T}^J_{D_s^+\eta\to D_s^+\eta} \end{pmatrix}$$

Results

T-matrix near the pole position

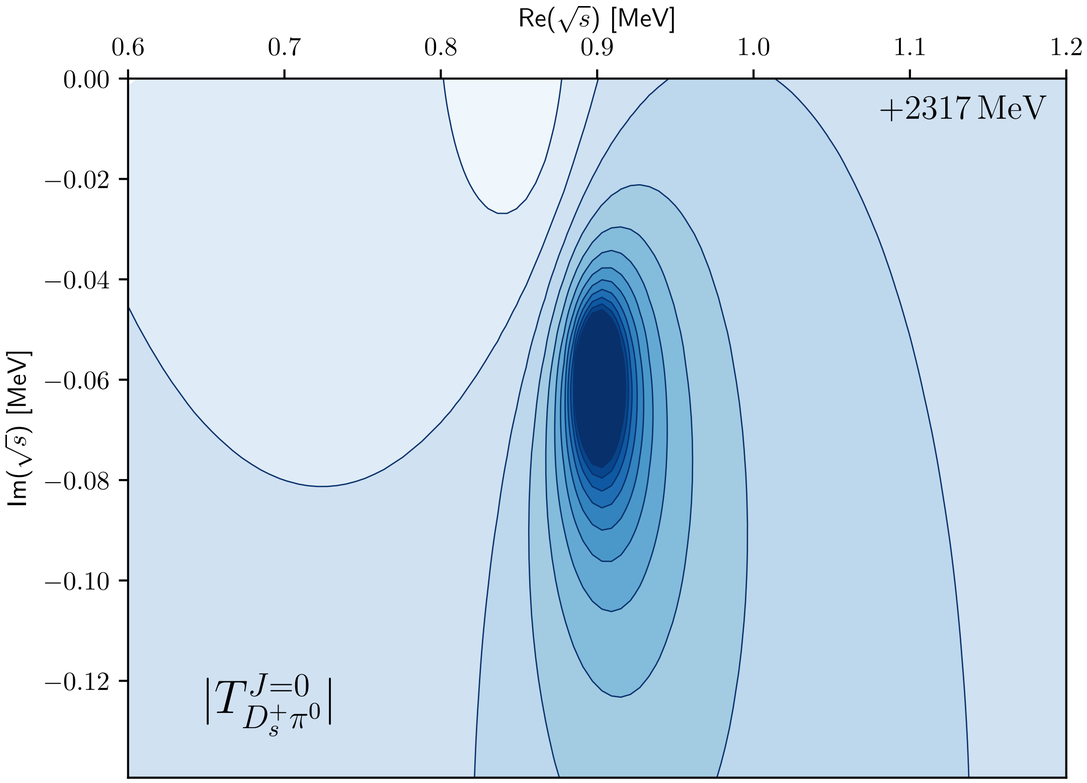

$$\sqrt{s}_R = 2317.90 - i0.0593\,\text{MeV}$$

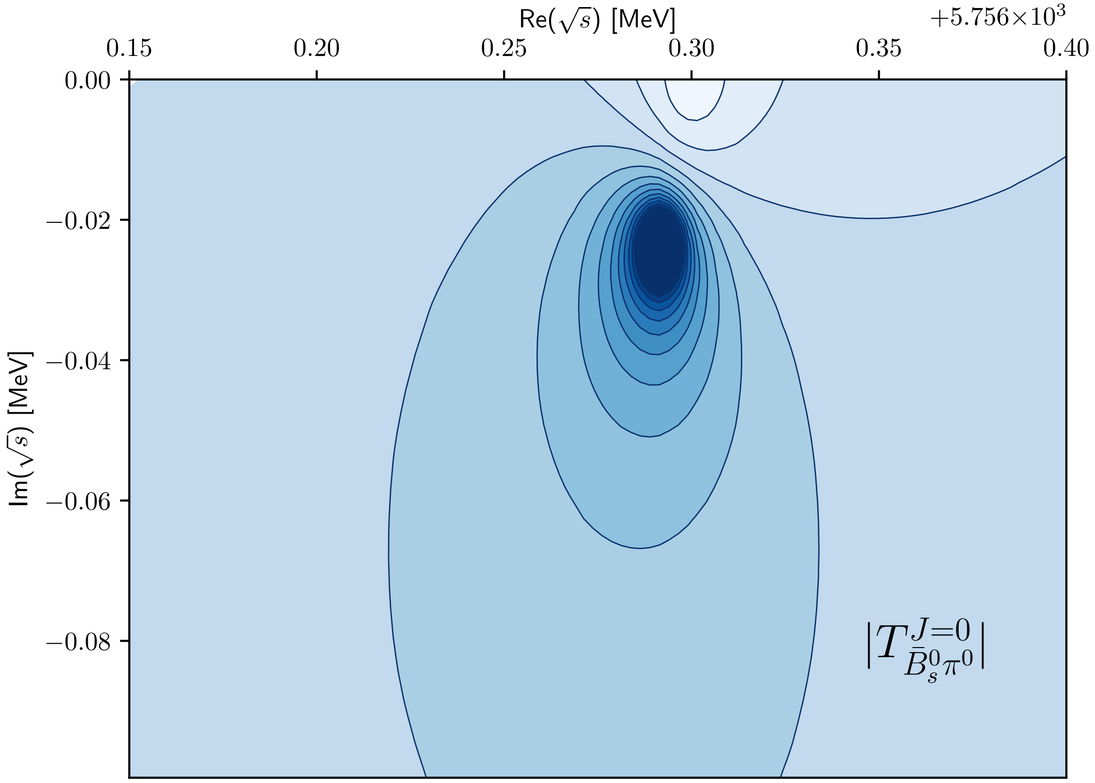

$$\sqrt{s}_R = 5756.32 - i0.0228\,\text{MeV}$$

$$\Gamma_{D_{s0}^*\to D_s^+\pi^0} = \frac{g_1^2}{m_{D_{s0}^*}}\rho_{D_s^+\pi^0}(m^2_{D_{s0}^*}) = \frac{g_1^2}{m^2_{D_{s0}^*}}\frac{p_{\text{cm}}}{4\pi} = 13.86\,\text{keV} < 3.8\,\text{MeV}$$

$$\Gamma_{\bar{B}_{s0}^*\to\bar{B}_s^0\pi^0} = 25.54\,\text{keV}$$

Summary

Summary

- investigated the dynamical generation of the $D_{s0}^*(2317)$ through the coupled-channel formalism with the fully off-mass-shell kernel amplitudes.
- considered the isospin violation arises from mass difference between u and d quark.
- found the pole near the observed $D_{s0}^*(2317)$ mass in the second Riemann sheet.
- searched the bottom-strange scalar meson in the appropriate Riemann sheet as well.
- predicted the pole position for B_{s0}^* as $\sqrt{s}_R = 5756.32 - i0.0228\,\mathrm{MeV}$.
- the off-mass-shell effect substantially contributes to the total decay width.
- showed that the meson-exchange framework works well in the heavy-light system.

Thank you

Getting LQCD Calculations Outside the Box

Tafat Weiss-Attia

The Racah Institute of Physics,
The Hebrew University of Jerusalem

EFB25 conference,
Mainz, August 2023

האוניברסיטה העברית בירושלים
THE HEBREW UNIVERSITY OF JERUSALEM

LQCD

- The nuclear interaction and the corresponding properties of nuclei are low-energy manifestations of QCD.
- At low energies, QCD is non-perturbative, requiring the use of lattice QCD (LQCD).
- To obtain physical quantities, LQCD calculations demand extrapolation into free-space.

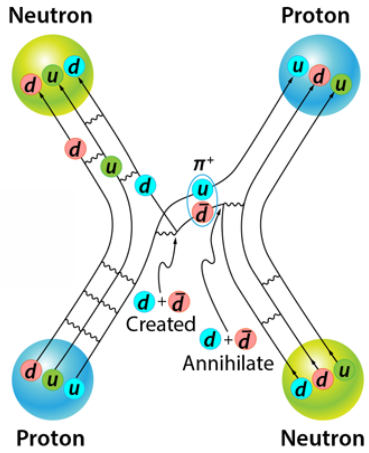

APS/ Alan Stonebraker

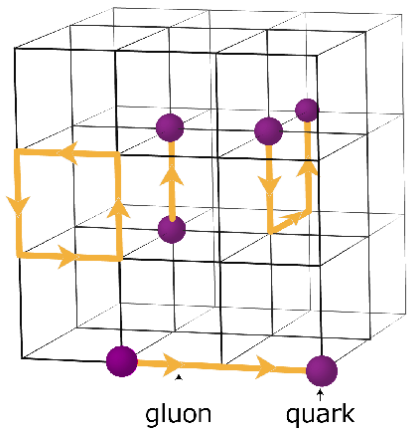

LQCD

- The nuclear interaction and the corresponding properties of nuclei are low-energy manifestations of QCD.
- At low energies, QCD is non-perturbative, requiring the use of lattice QCD (LQCD).
- To obtain physical quantities, LQCD calculations demand extrapolation into free-space.

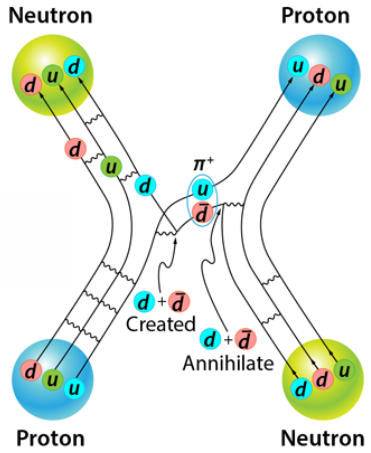

APS/ Alan Stonebraker

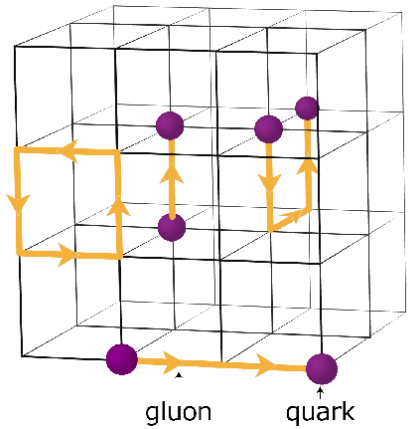

LQCD

- The nuclear interaction and the corresponding properties of nuclei are low-energy manifestations of QCD.
- At low energies, QCD is non-perturbative, requiring the use of lattice QCD (LQCD).
- To obtain physical quantities, LQCD calculations demand extrapolation into free-space.

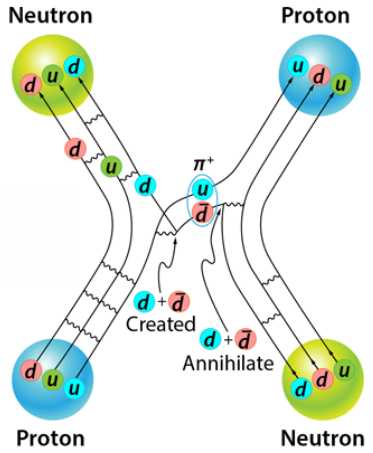

APS/ Alan Stonebraker

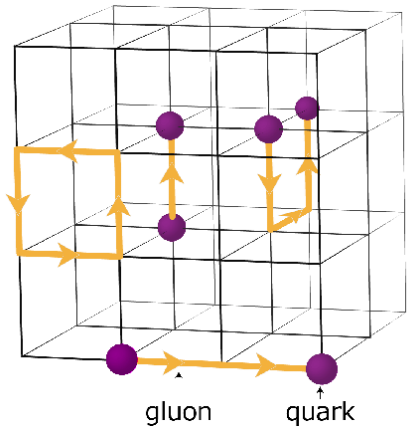

Extrapolation methods

- Lüscher two-body formulas and generalizations,

$$B_2(L) - B_2^{\text{free}} = \frac{6\kappa_2 |\mathcal{A}_2|^2}{\mu_2 L} e^{-\kappa_2 L} + O(e^{-\sqrt{2}\kappa_2 L})$$

$$k \cot \delta_0(k) = \frac{1}{\pi L} S\left[\left(\frac{Lk}{2\pi}\right)^2\right]$$

M. Lüscher, Commun. Math. Phys. **104**, 177 (1986); Nucl. Phys. B **354**, 531 (1991).

Extrapolation methods

- Pionless effective field theory ($\not\pi$EFT).

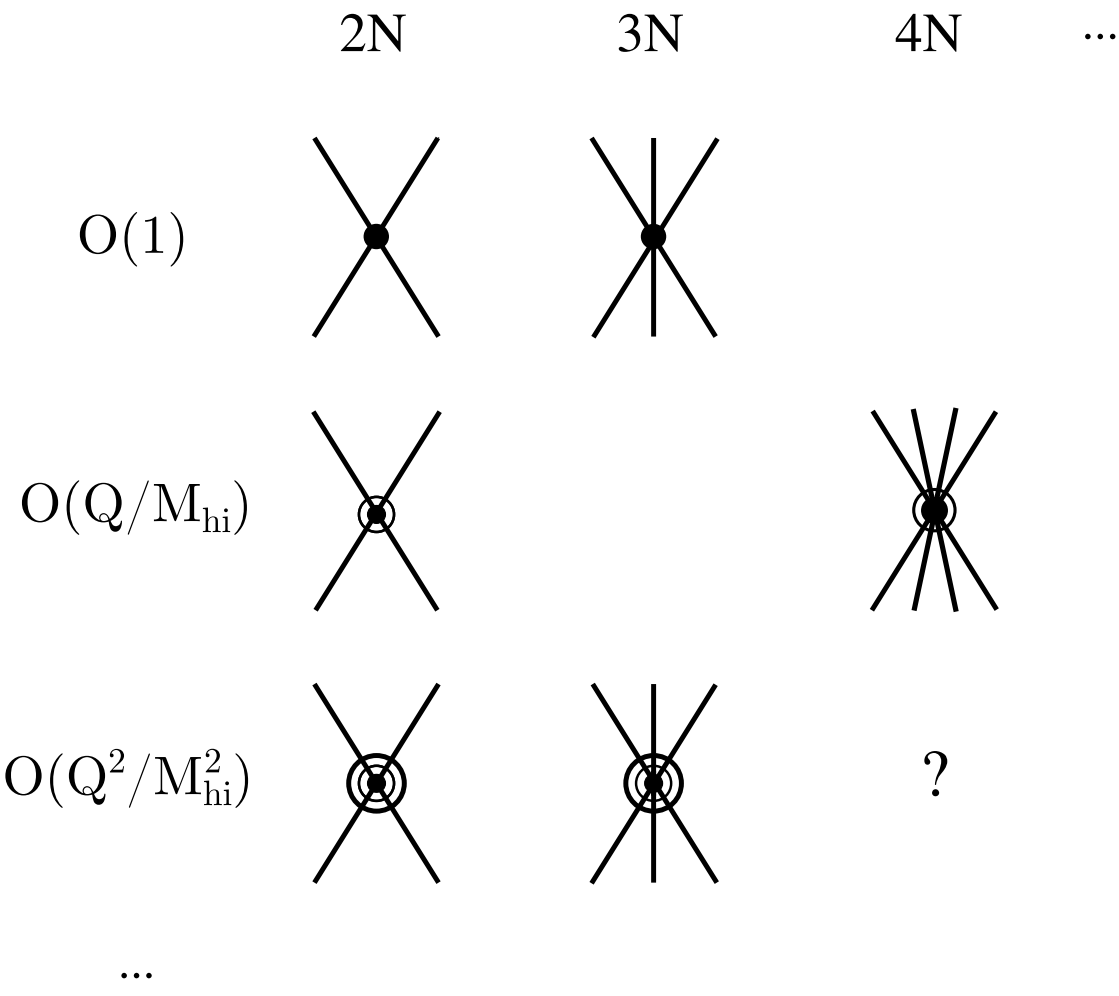

W. Hammer, S. König, and U. van Kolck, Rev. Mod. Phys. **92**, 025004 (2020).

Current work

- Replace LQCD results with artificial finite-range data, calculated with the Minnesota potential.
- Promote LO ≠EFT to NLO.
- Compare between extrapolations performed with the Lüscher formalism and with finite-volume ≠EFT.

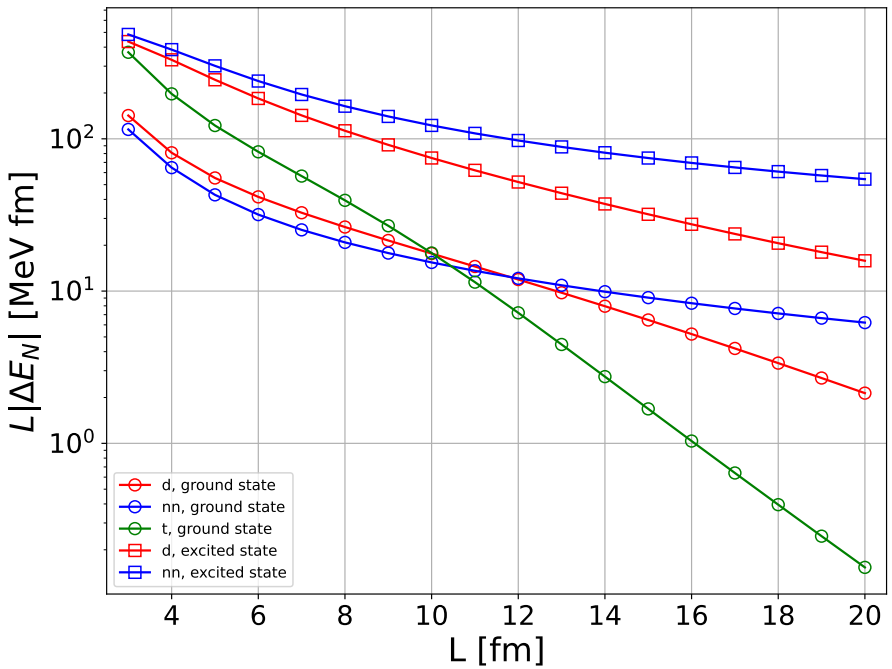

Current work

- Replace LQCD results with artificial finite-range data, calculated with the Minnesota potential.
- Promote LO ≠EFT to NLO.
- Compare between extrapolations performed with the Lüscher formalism and with finite-volume ≠EFT.

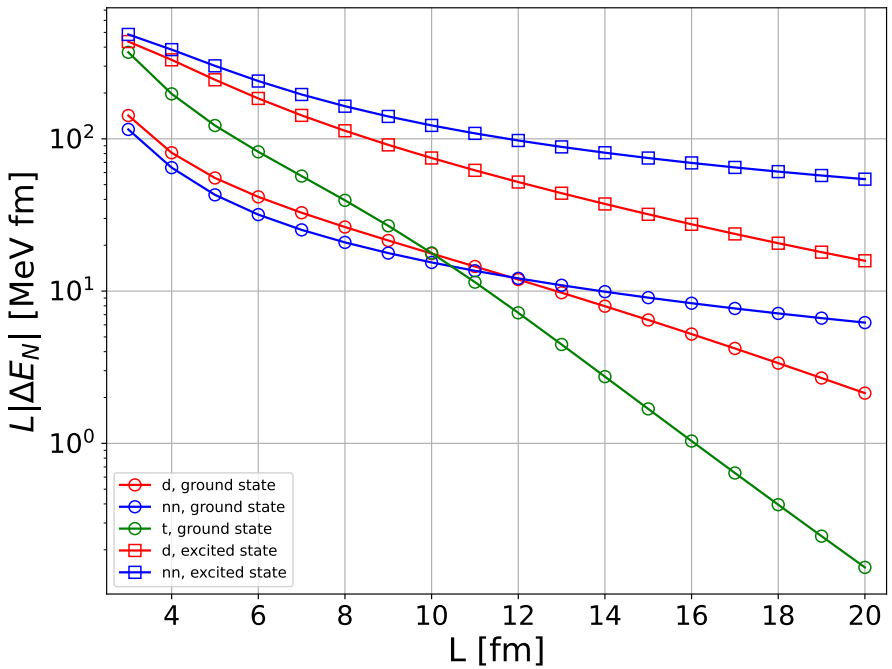

Current work

- Replace LQCD results with artificial finite-range data, calculated with the Minnesota potential.
- Promote LO ≠EFT to NLO.
- Compare between extrapolations performed with the Lüscher formalism and with finite-volume ≠EFT.

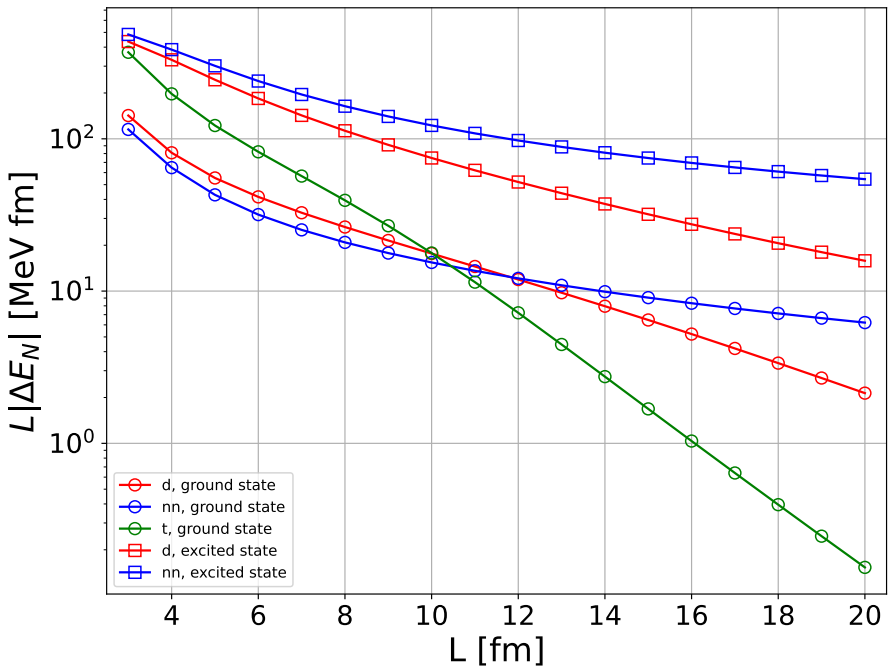

Free Space Results

The deuteron binding energy:

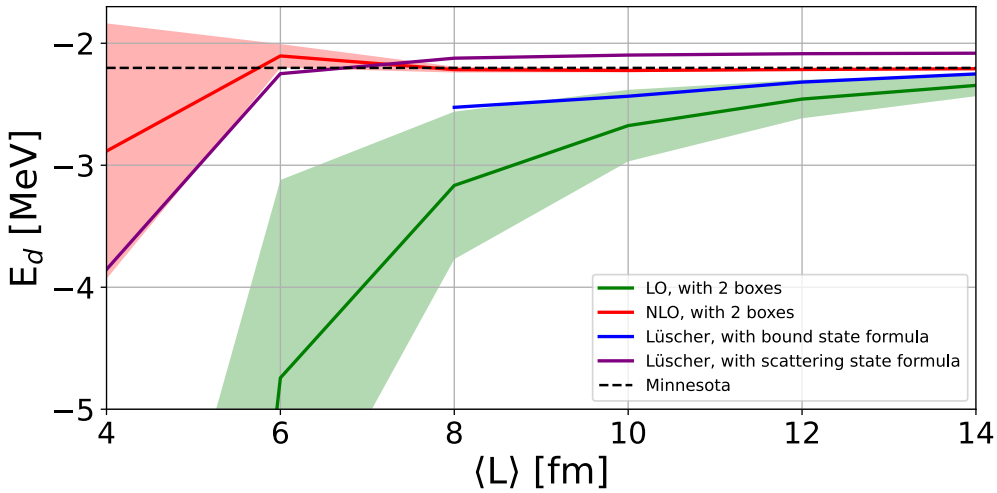

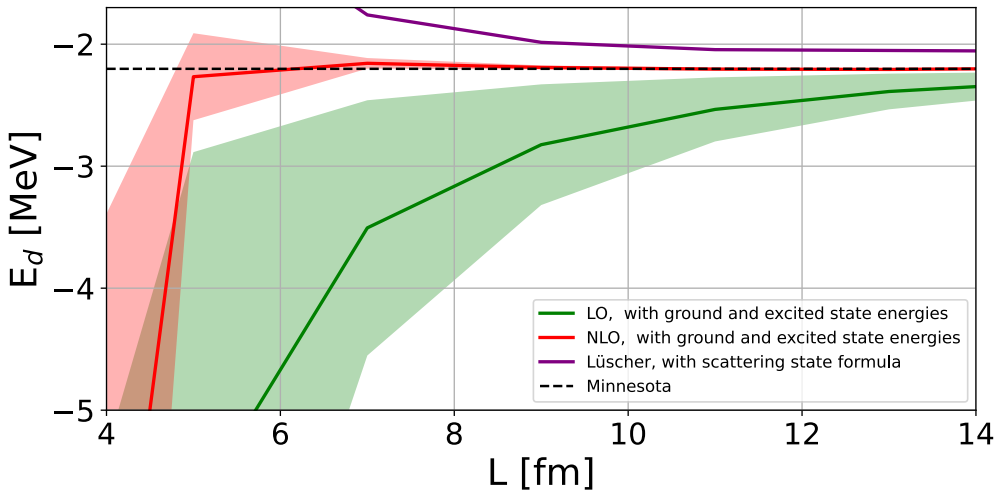

Free-space results

n-d with spin 3/2 scattering parameters:

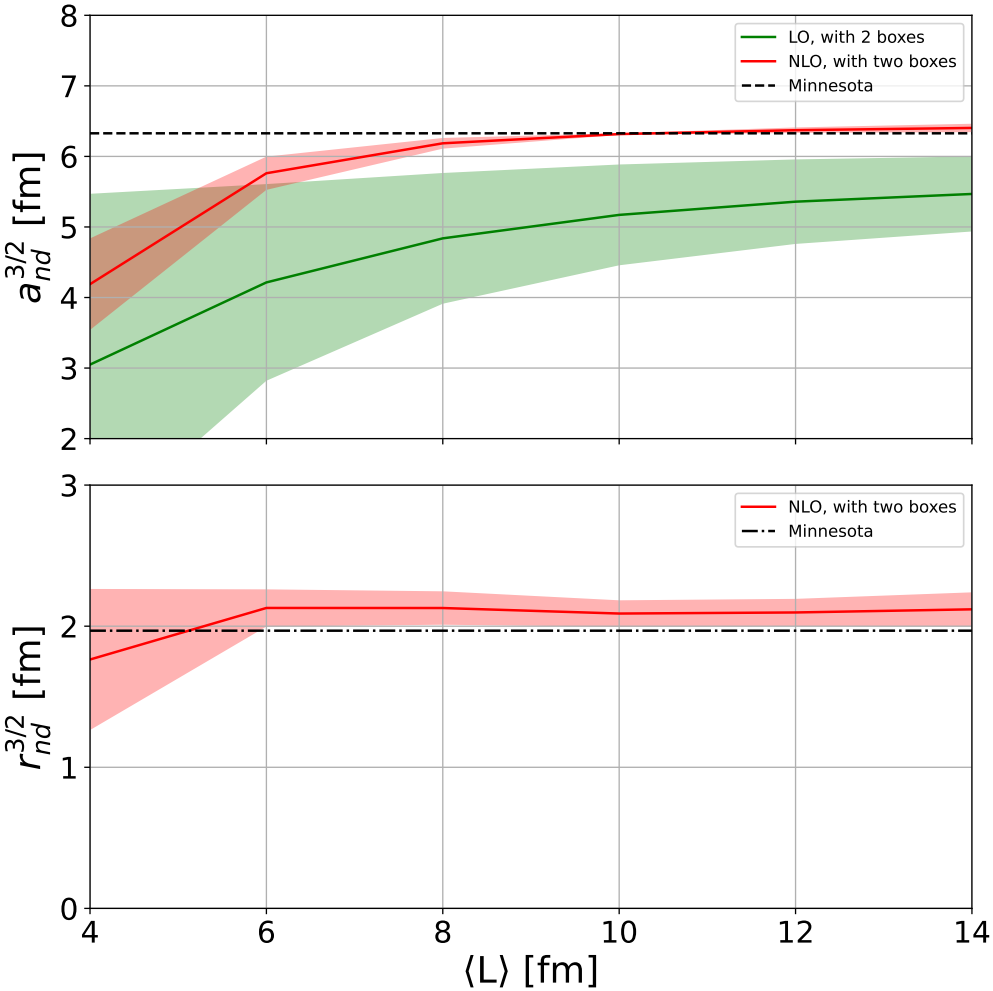

Effective theory for few-body physics in the Gaudin-Yang model

Timothy George Backert

Poster 12

- experimentally realizable
- strong attractive δ-interaction

→ for $V_{\text{ext}} \neq 0$ non-integrable

- usually: numerical calculations

1D spin-1/2 Fermi gas

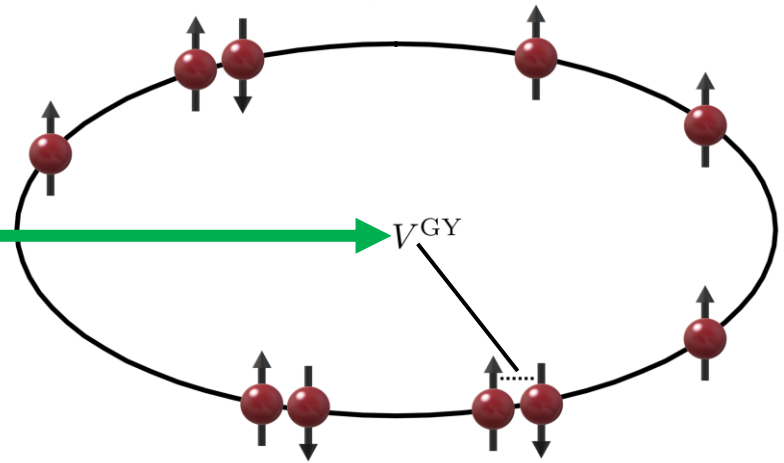

Effective theory for few-body physics in the Gaudin-Yang model

Timothy George Backert

TECHNISCHE UNIVERSITÄT DARMSTADT

Poster 12

- experimentally realizable
- strong attractive δ-interaction

→ for $V_{\text{ext}} \neq 0$ non-integrable

- ~~usually: numerical calculations~~
- our approach: effective theory

→ analytical insights

1D spin-1/2 Fermi gas

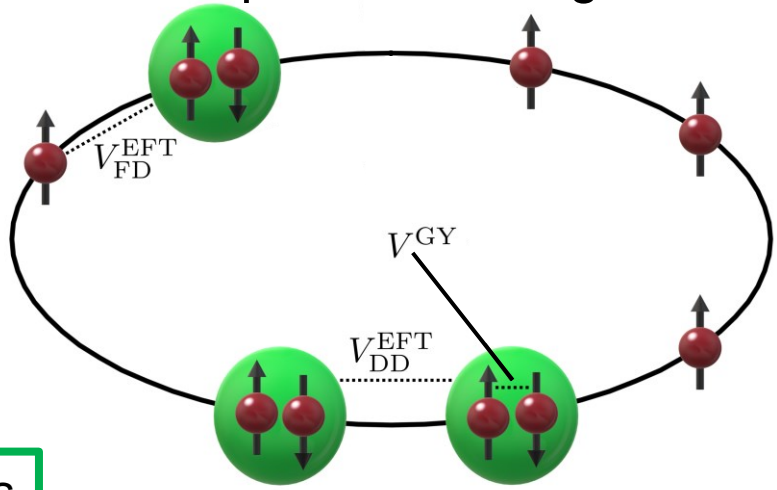

Effective theory for few-body physics in the Gaudin-Yang model

Timothy George Backert

TECHNISCHE UNIVERSITÄT DARMSTADT

- physical insights while setting up EFT
- simplification:

strong —Fermi-Bose mapping→ weak

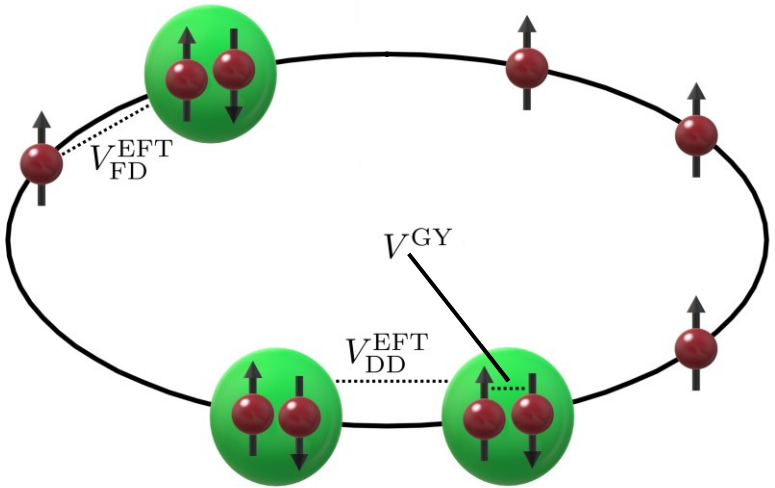

Effective theory for few-body physics in the Gaudin-Yang model

Timothy George Backert

TECHNISCHE UNIVERSITÄT DARMSTADT

- physical insights while setting up EFT
- simplification:

strong —Fermi-Bose mapping→ weak

Join me at my poster!

No.13

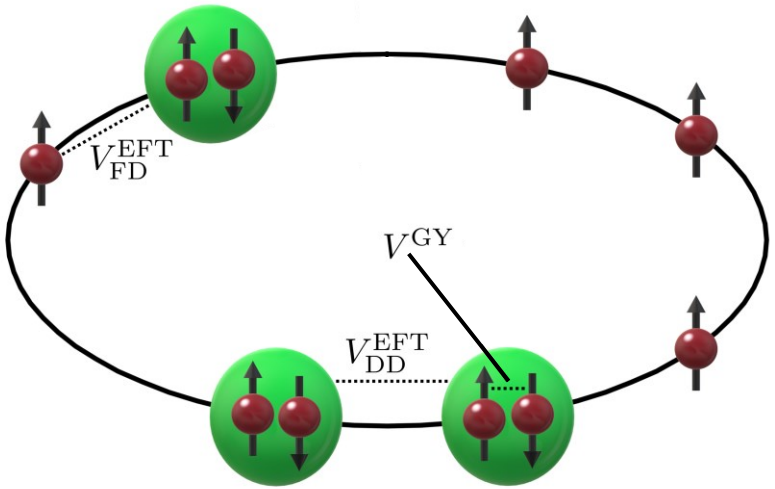

13

Strangeness of the gravitational form factors

Ho-Yeon Won, Hyun-Chul Kim, and June-Young Kim

INHA UNIVERSITY

25 EFB

Contents

- What is the gravitational form factors?
- Flavor structure of the *D*-term
- Necessity of the $\bar{c}$ form factor
- What we will show

Gravitational form factors

$T^{\mu\nu}$: energy − momentum tensor current

$$\langle N(p')|T^{\mu\nu}|N(p)\rangle$$

$$= \bar{u}(p')\left[A(t)\frac{P^\mu P^\nu}{M_N} + J(t)\frac{iP^{\{\mu}\sigma^{\nu\}\rho}\Delta_\rho}{2M_N} + D(t)\frac{\Delta^\mu\Delta^\nu - g^{\mu\nu}\Delta^2}{4M_N} + \bar{c}(t)M_N g^{\mu\nu}\right]u(p)$$

Normalized mass

$$\sum_{a=q,g} A_a(t) = 1$$

Spin

$$\sum_{a=q,g} J_a(t) = \frac{1}{2}$$

***D*-term related to the shear force inside the nucleon. There is no constraint.**

$\bar{c}$ related to the pressure inside the nucleon.

$$\sum_{a=q,g} \bar{c}_a(t) = 0$$

Our target: flavor structure of *D*-term and $\bar{c}$

$P = (p' + p)/2$

$\Delta = p' - p, \qquad t = \Delta^2$

Flavor structure of the *D*-term

- For the first time, Burkert et al. have measured the proton *D*-term.
- However, Burkert et al. assumed
  1. Large N_c limit, $d_1^u \approx d_1^d$
  2. Flavor SU(2) symmetry without the strange quarks

We will show the importance of the strange quarks in the *D*-term!

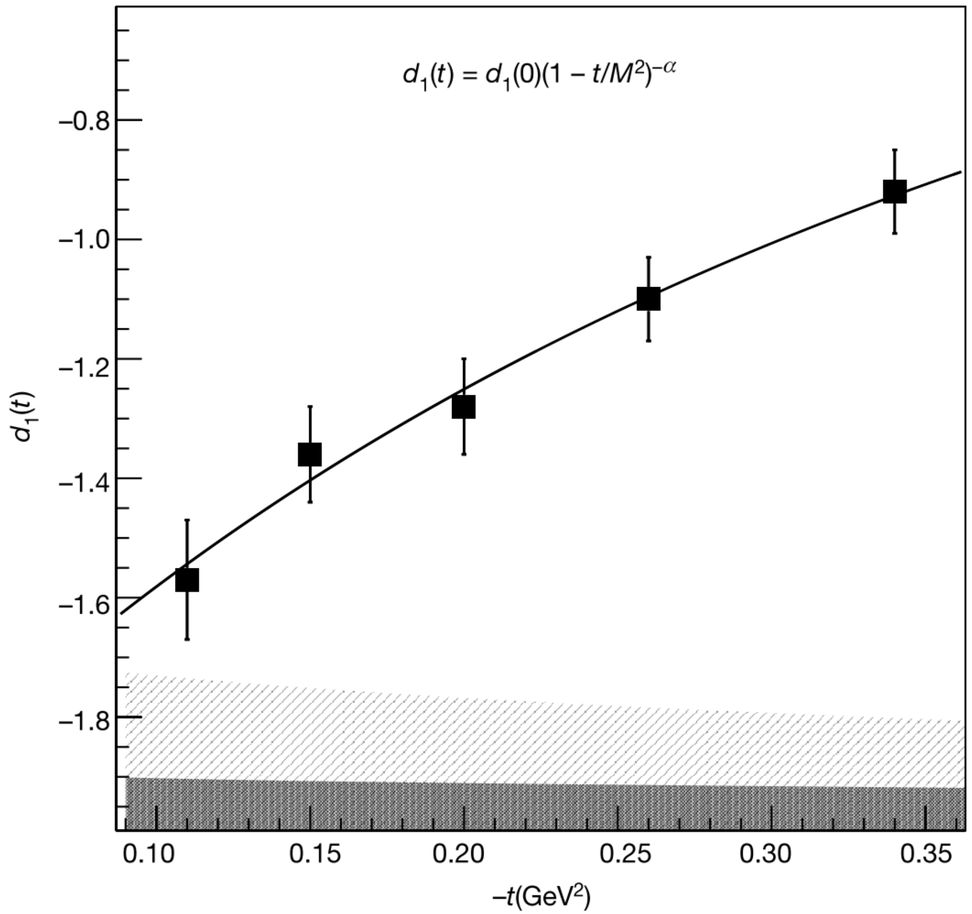

V. D. Burkert et al., Nature 557 (2018)

Necessity of the $\bar{c}$ form factor

- **EMT conservation law & global stability condition**

$$\sum_{a=q,g} \partial_\mu T_a^{\mu\nu} = 0 \Leftrightarrow \sum_{a=q,g} \bar{c}_a(t) = 0 \Leftrightarrow \int d^3r \sum_{a=q,g} p_a(r) = 0$$

- **For the forward limit ($t \to 0$) with the same spin polarization in the rest frame**

$$\langle N(p)|T_q^{00}|N(p)\rangle = 2m^2 \left[A_q(0) + \bar{c}_q(0)\right]$$

To investigate the nucleon mass in terms of the quark flavor, we must consider the $\bar{c}_q$.

In our poster, we will show

- Field-theoretical results of the gravitational form factors
- Flavor-decomposed GFFs of the proton considering the strange quarks for the first time
- Flavor-decomposed proton mass M_p^q/M_p **vs** the quark momentum fraction $\langle x \rangle_p^q$ via the presence of the $\bar{c}_q$

Thank you for your attention

14

Two-dimensional transverse charge distributions of the Δ baryon: Interpolation between the nonrelativistic and ultrarelativistic limits

Ki-Hoon Hong*, June-Young Kim and Hyun-Chul Kim***

**Department of Physics, Inha University, Incheon 22212, Republic of Korea*

***Theory Center, Jefferson Lab, Newport News, Virginia 23606, USA*

- **In this work, we calculate the charge distributions of the moving Δ^+ and Δ^0 baryons in 2D Elastic frame. We will show the relativistic effects by changing their longitudinal momentum of them from an ultra-relativistic limit to a nonrelativistic limit.**

✓ Elastic frame(EF)

$$p_f = (P^0, \frac{\vec{\Delta}_\perp}{2}, P_z), \;\; p_i = (P^0, -\frac{\vec{\Delta}_\perp}{2}, P_z)$$

$$P = \frac{1}{2}(p_f + p_i) = (P^0, \vec{0}, P_z)$$

$$\Delta = p_f - p_i = (0, \vec{\Delta}_\perp, 0)$$

$$P^0 = \sqrt{\frac{\vec{\Delta}^2}{4} + m^2 + P_z^2}$$

$P_z = 0$

✓ Breit frame(BF) ($P_z = 0$)

$$p_f = (P_0, \frac{\vec{\Delta}}{2}), \quad p_i = (P_0, -\frac{\vec{\Delta}}{2})$$

$$P = \frac{1}{2}(p_f + p_i) = (P^0, \vec{0})$$

$$\Delta = p_f - p_i = (0, \vec{\Delta})$$

$$P^0 = \sqrt{\frac{\vec{\Delta}^2}{4} + m^2}$$

$P_z \to \infty$ ✓ Infinite momentum frame(IMF)

◆ Matrix element of the electromagnetic current operator J^μ:

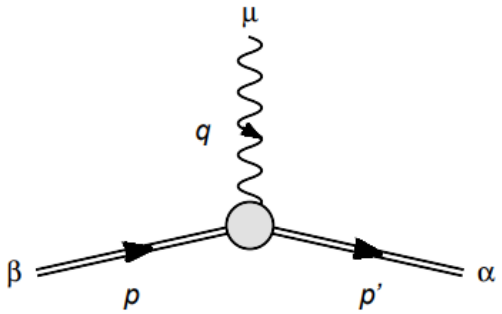

$$\langle \Delta(p', \sigma') | J^\mu(0) | \Delta(p, \sigma) \rangle$$

$$= -\bar{u}_\alpha(p', \sigma') \left\{ \left[F_1^*(t) g^{\alpha\beta} + F_3^*(t) \frac{\Delta^\alpha \Delta^\beta}{4M^2} \right] \gamma^\mu + \left[F_2^*(t) g^{\alpha\beta} + F_4^*(t) \frac{\Delta^\alpha \Delta^\beta}{4M^2} \right] \frac{i\sigma^{\mu\nu} q_\nu}{2M} \right\} u_\beta(p, \sigma)$$

❖ *Numerical Results (Δ^+ Charge Distribution)*

◆ Polarized spin along z-direction

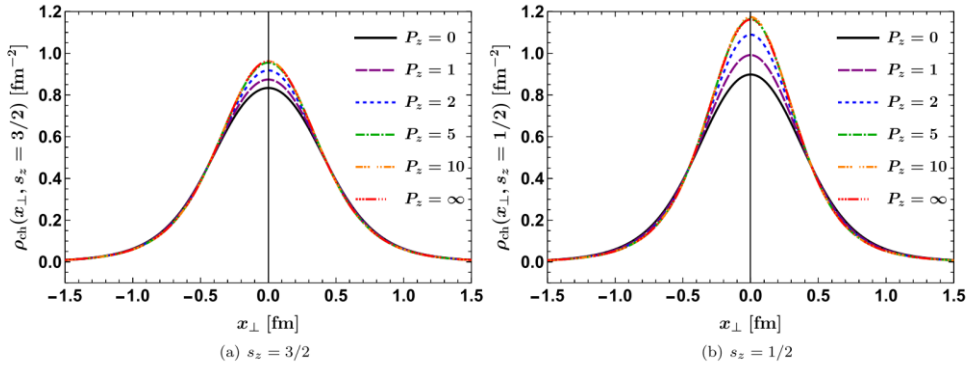

(a) $s_z = 3/2$ (b) $s_z = 1/2$

FIG. 1. The y-axis profiles of the transverse charge distributions of the moving Δ^+ baryon as the longitudinal momentum P_z increases from $P_z = 0$ to $P_z = \infty$. Its spin is polarized along the z-axis with $s_z = 3/2$ and $s_z = 1/2$, respectively. In the left (right) panel, $\rho_{\rm ch}$ with $s_z = 3/2$ ($s_z = 1/2$) is depicted.

◆ Transverse polarized spin along x-directionç

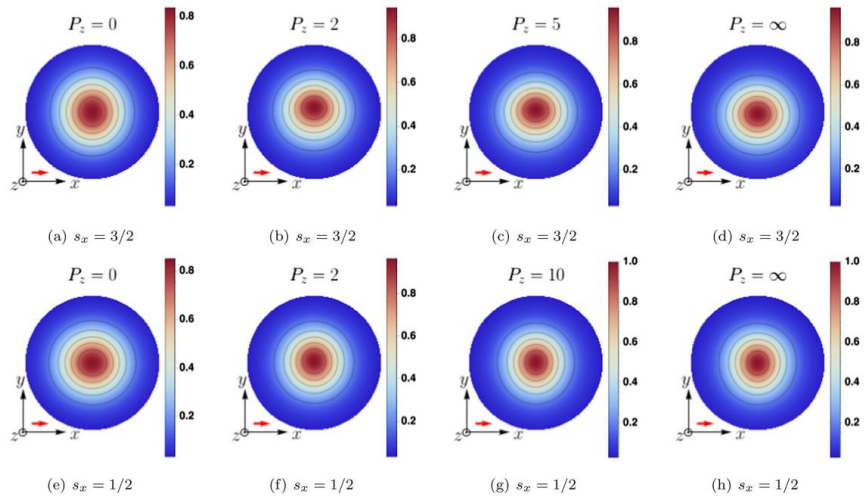

(a) $s_x = 3/2$ (b) $s_x = 3/2$ (c) $s_x = 3/2$ (d) $s_x = 3/2$

(e) $s_x = 1/2$ (f) $s_x = 1/2$ (g) $s_x = 1/2$ (h) $s_x = 1/2$

FIG. 5. (a)–(d) 2D charge distributions of the moving Δ^+ baryon transversely polarized along x-axis with $s_x = 3/2$; (e)–(h) 2D charge distributions of the moving Δ^+ baryon transversely polarized along x-axis with $s_x = 1/2$.

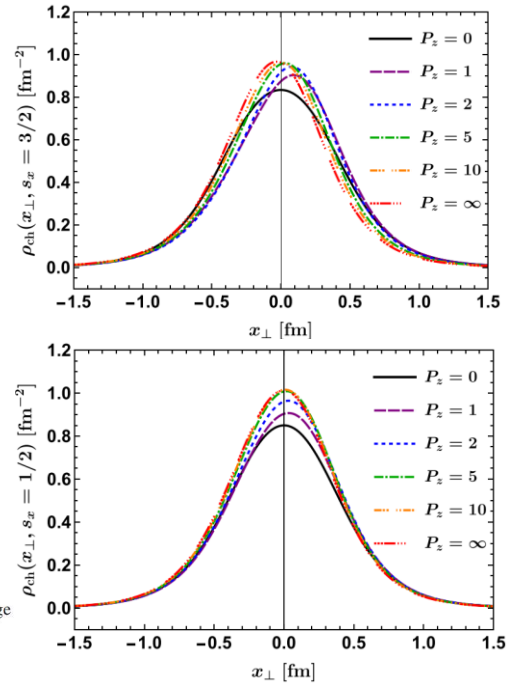

❖ *Numerical Results (Δ^0 Charge Distribution)*

◆ Polarized spin along z-direction

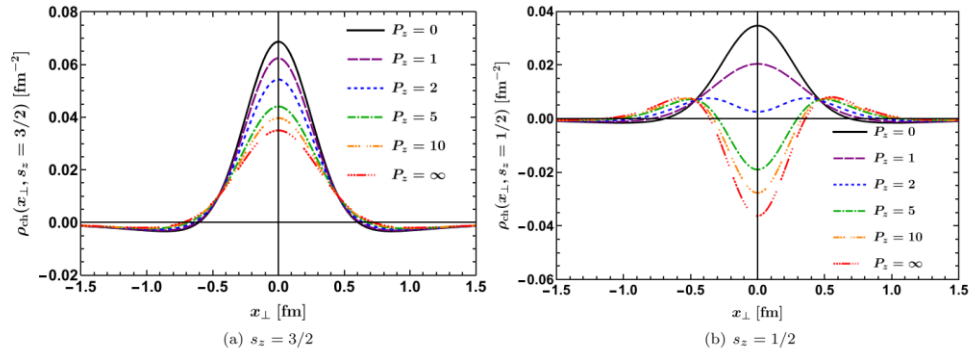

(a) $s_z = 3/2$ (b) $s_z = 1/2$

FIG. 2. The y-axis profiles of the transverse charge distributions of the moving Δ^0 baryon as the longitudinal momentum P_z increases from $P_z = 0$ to $P_z = \infty$. Its spin is polarized along the z-axis with $s_z = 3/2$ and $s_z = 1/2$, respectively. In the left (right) panel, $\rho_{\rm ch}$ with $s_z = 3/2$ ($s_z = 1/2$) is depicted.

◆ Transverse polarized spin along x-direction

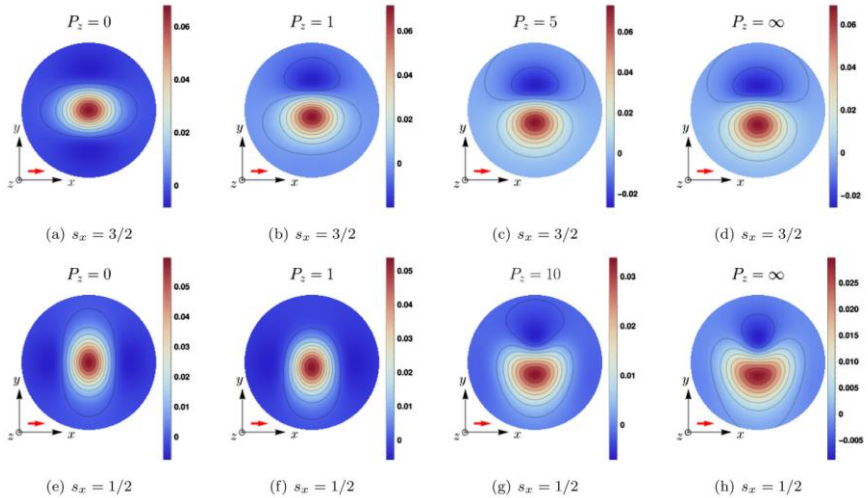

(a) $s_x = 3/2$ (b) $s_x = 3/2$ (c) $s_x = 3/2$ (d) $s_x = 3/2$

(e) $s_x = 1/2$ (f) $s_x = 1/2$ (g) $s_x = 1/2$ (h) $s_x = 1/2$

FIG. 10. (a)–(d) 2D charge distributions of the moving Δ^0 baryon transversely polarized along x-axis with $s_x = 3/2$; (e)–(h) 2D charge distributions of the moving Δ^0 baryon transversely polarized along x-axis with $s_x = 1/2$.

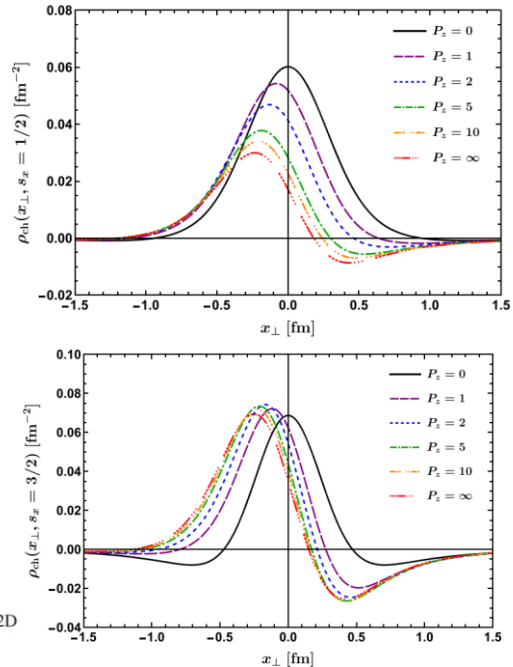

Two-dimensional transverse charge distributions of the Δ baryon: Interpolation between the nonrelativistic and ultrarelativistic limits

Ki-Hoon Hong,[1,*] June-Young Kim,[2,†] and Hyun-Chul Kim[1,3,‡]

[1]*Department of Physics, Inha University, Incheon 22212, Republic of Korea*
[2]*Theory Center, Jefferson Lab, Newport News, Virginia 23606, USA*
[3]*School of Physics, Korea Institute for Advanced Study (KIAS), Seoul 02455, Republic of Korea*

(Received 23 January 2023; accepted 21 March 2023; published 7 April 2023)

We investigate how the charge distributions of both the unpolarized and transversely polarized Δ baryon change as the longitudinal momentum (P_z) of the Δ baryon increases from $P_z = 0$ to $P_z = \infty$ in a Wigner phase-space perspective. When the Δ baryon is longitudinally polarized, its two-dimensional charge distribution is kept to be spherically symmetric with P_z varied, whereas when the Δ baryon is transversely polarized along the x-axis, the quadrupole contribution emerges at the rest frame ($P_z = 0$). When P_z grows, the electric dipole and octupole moments are induced. The induced dipole moment dominates over other higher multipole contributions and governs the deformation of the charge distribution of the Δ baryon.

DOI: 10.1103/PhysRevD.107.074004

15

Microscopic theory of infinite nuclear matter and connections to the nuclear energy functional

Francesco Marino

Università di Milano and INFN

25th European conference on few-body problems in physics, Mainz

Infinite nuclear matter

We study infinite nuclear matter using density functional theory (DFT) and the *ab initio* Self-consistent Green's functions (SCGF) method

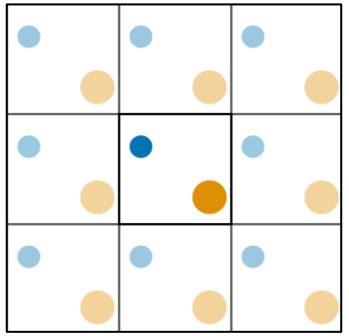

Finite number of particles in a finite box

Infinite nuclear matter

We study infinite nuclear matter using density functional theory (DFT) and the *ab initio* Self-consistent Green's functions (SCGF) method

Equation of state of homogeneous matter

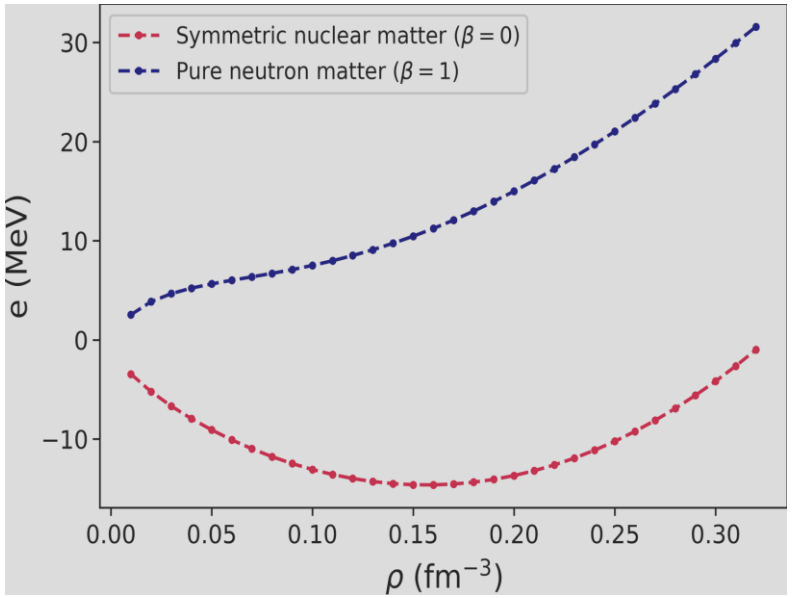

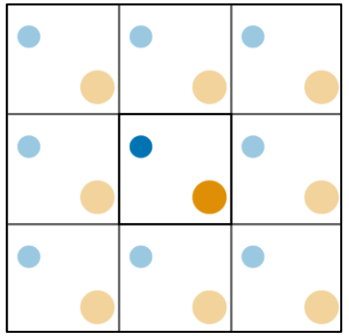

Finite number of particles in a finite box

Infinite nuclear matter

We study infinite nuclear matter using density functional theory (DFT) and the *ab initio* Self-consistent Green's functions (SCGF) method

Equation of state of homogeneous matter

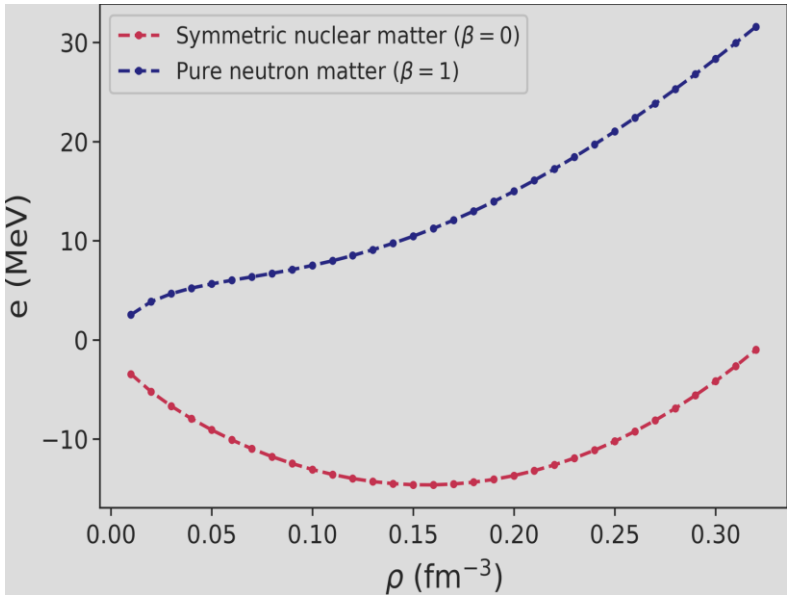

Nuclear matter **perturbed** by an external **potential**

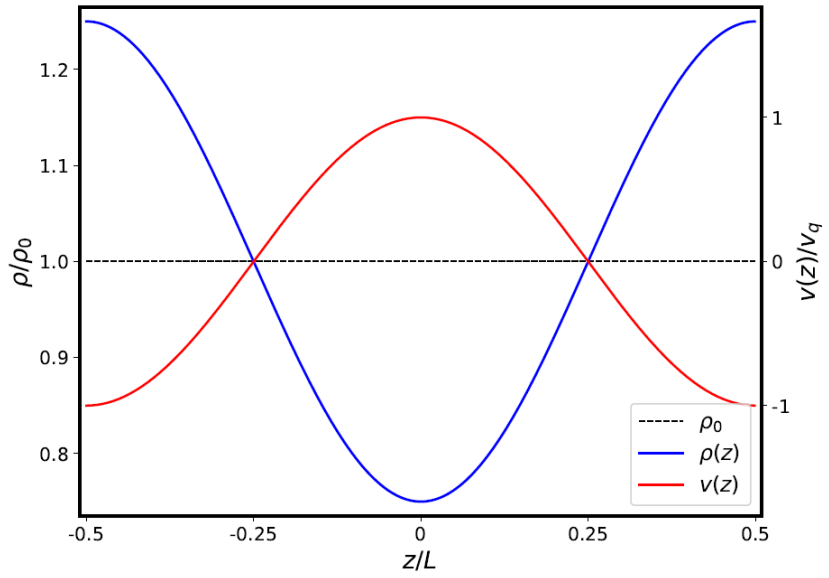

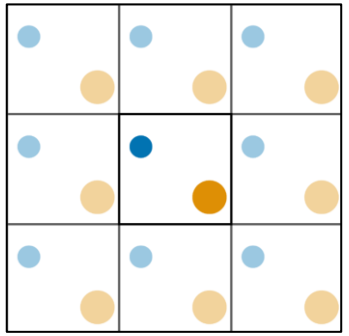

Finite number of particles in a finite box

Density functional theory

$$\delta\rho(\boldsymbol{x}) = 2\chi(q)\, v_q \cos(\boldsymbol{q}\cdot\boldsymbol{x})$$

$\chi(q)$: **static response function**

PNM static response, DFT

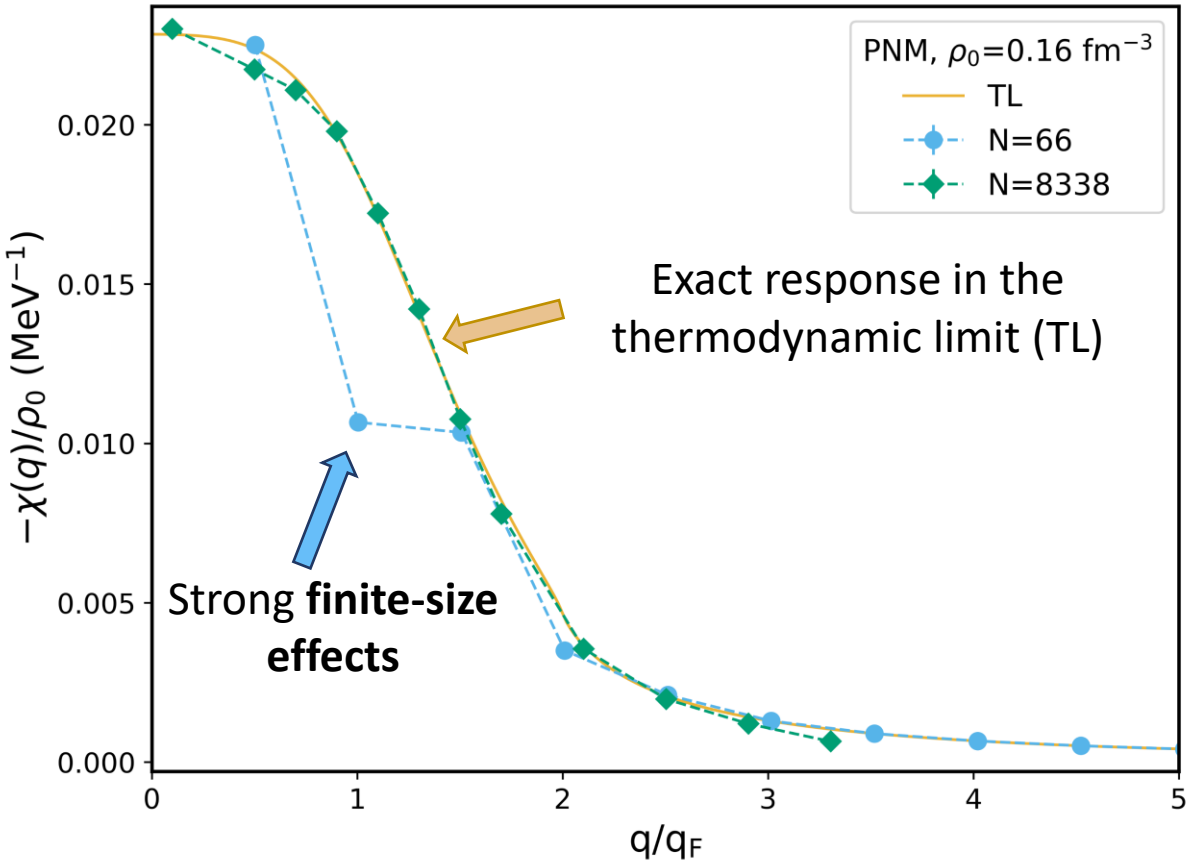

Density of perturbed matter

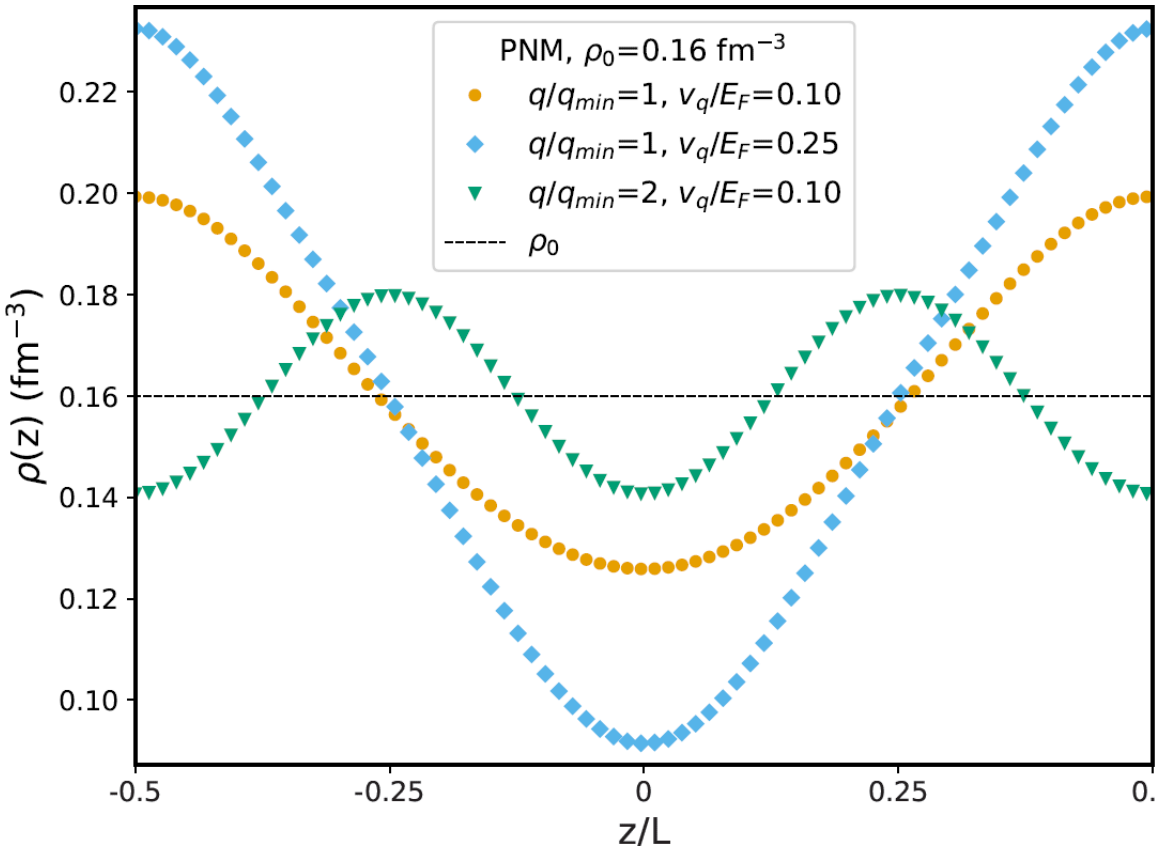

Self-consistent Green's functions

Dyson equation for the one-body propagator $g(\omega)$

$$g(\omega) = g^{(0)}(\omega) + g^{(0)}(\omega)\Sigma^{(*)}(\omega)g(\omega)$$

$\Sigma^{(*)}$: self-energy

Spectral representation of the one-body propagator

$$g(\boldsymbol{k},\omega) = \sum_j \frac{|Z_j|^2}{\omega - \epsilon_j(\boldsymbol{k})}$$

Poles (ϵ_j) and **amplitudes** (Z_j) are obtained from the Dyson equation

Equation of state

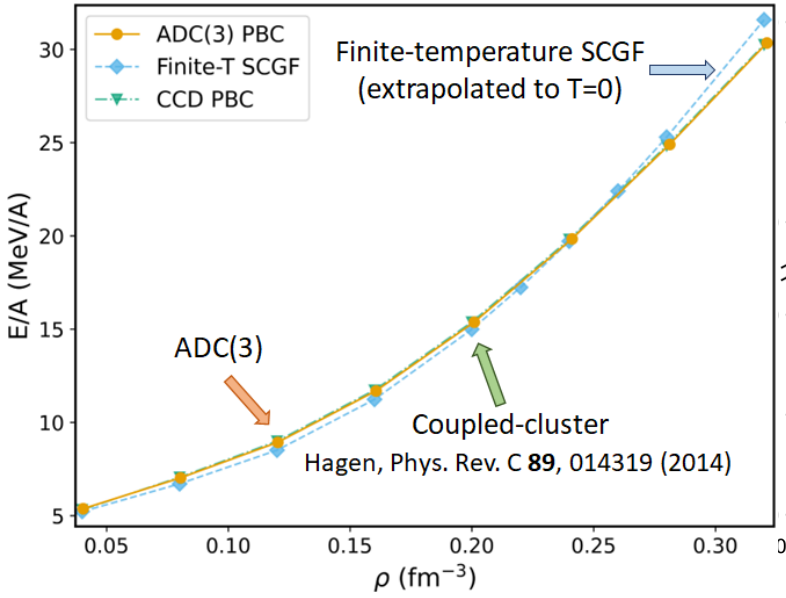

Momentum distribution

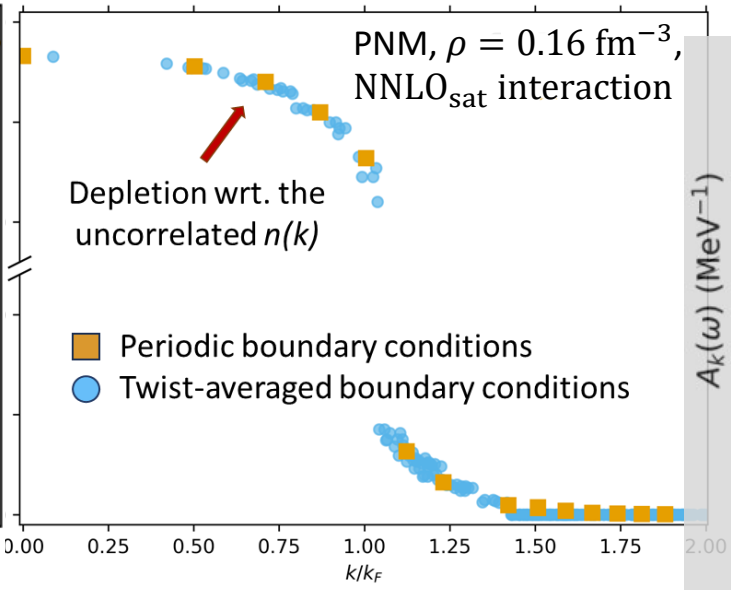

Spectral function

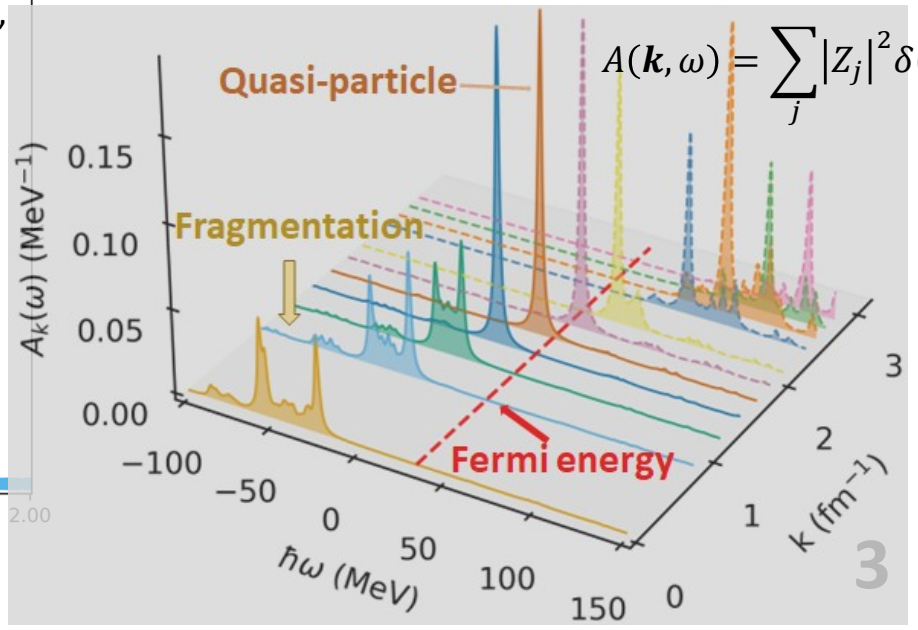

$$A(\boldsymbol{k},\omega) = \sum_j |Z_j|^2 \delta(\omega - \epsilon_j)$$

Thank you for your attention!

Collaborators

Argonne: Alessandro Lovato

Milano: Carlo Barbieri, Gianluca Colò, Xavier Roca-Maza, Enrico Vigezzi

Trento: Francesco Pederiva

Borromean states in a one-dimensional three-body system

Tobias Schnurrenberger[1], Lucas Happ[2], Maxim Efremov[1]
[1]German Aerospace Center (DLR), Institute of Quantum Technologies, 89081 Ulm; [2]RIKEN Nishina Center, Strangeness Nuclear Physics Laboratory, Wako 351-0198, Japan

16

$$\left[-\frac{\alpha_x}{2}\frac{d^2}{d\xi^2}-\frac{\alpha_y}{2}\frac{d^2}{d\eta^2}+v\left(\xi+\frac{1}{2}\eta\right)+v\left(\xi-\frac{1}{2}\eta\right)\right]\psi^{(3)}(\xi,\eta)=\varepsilon^{(3)}\psi^{(3)}(\xi,\eta)$$

- One-dimensional three-body system
- Two identical heavy particles and a different particle of smaller mass
- No bound state supported by the heavy-light interaction potential
- No heavy-heavy interaction potential

- Heavy bosons, $\Psi^{(3)}(\xi\to\pm\infty,\eta\to\pm\infty)=0$
- Solve the corresponding two-body problem (heavy-light) analytically
- Numerical calculation of the three-body spectrum and wave-functions with the Faddeev equations

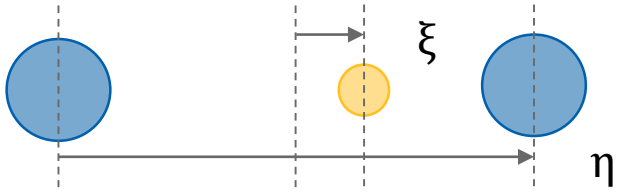

Figure 1: One-dimensional heavy-light-heavy system.

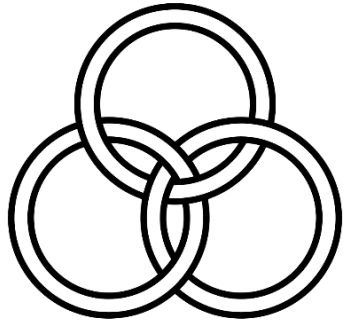

Figure 2: Real world analogy: Borromean rings [1].

[1] https://en.m.wikipedia.org/wiki/File:Borromean-rings_minimal-overlap.svg

Borromean states in a one-dimensional three-body system

Tobias Schnurrenberger[1], Lucas Happ[2], Maxim Efremov[1]
[1]German Aerospace Center (DLR), Institute of Quantum Technologies, 89081 Ulm; [2]RIKEN Nishina Center, Strangeness Nuclear Physics Laboratory, Wako 351-0198, Japan

$$\left(-\frac{1}{2}\frac{d^2}{d\xi^2}+\mathrm{v}(\xi)\right)\psi^{(2)}(\xi)=\varepsilon^{(2)}\psi^{(2)}(\xi) \qquad \mathrm{v}(\xi)=-v_0\left[\delta\left(\xi+\frac{1}{2}\right)-\alpha\delta\left(\xi-\frac{1}{2}\right)\right]$$

- Depending on v_0 and α, there are either, one virtual state, one bound state or two bound states
- Solve the three-body system for parameters corresponding to the transition: one bound → one virtual state

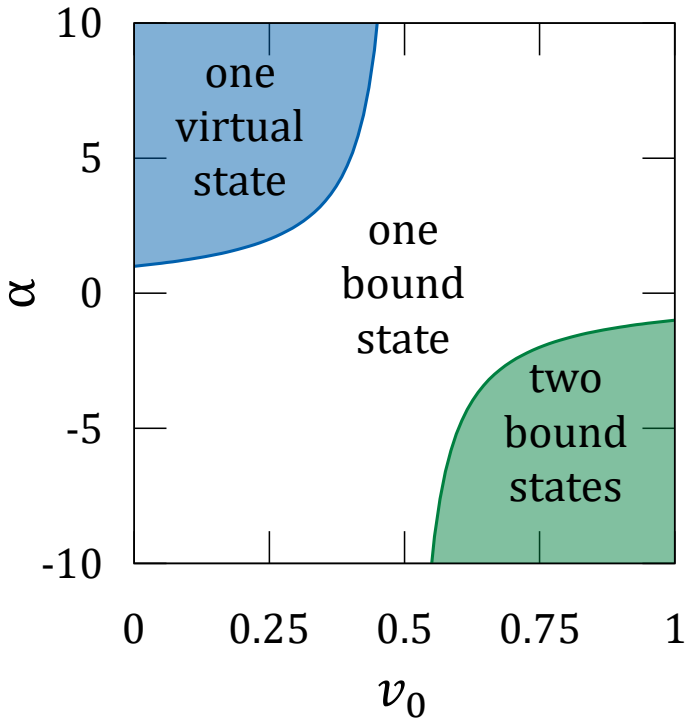

Figure 3: Parameter space of the two-body problem.

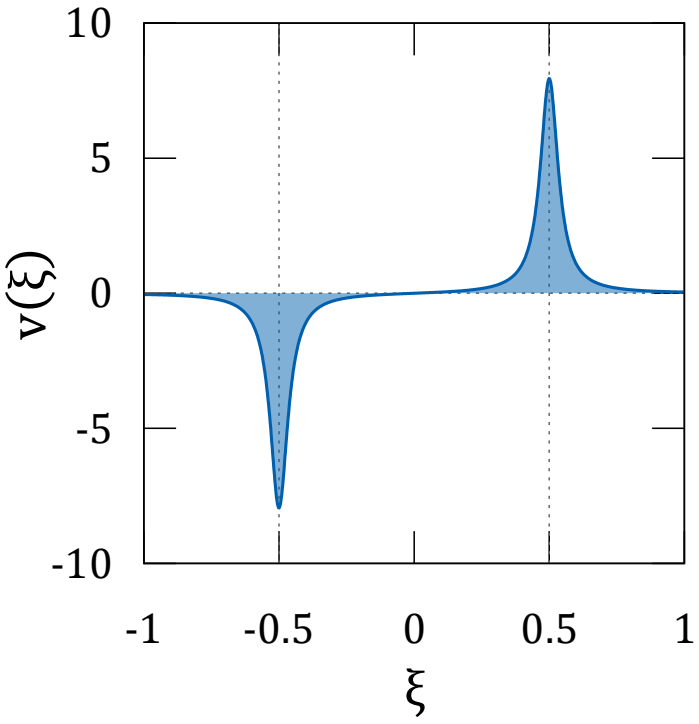

Figure 4: Heavy-light interaction potential.

Borromean states in a one-dimensional three-body system

Tobias Schnurrenberger[1], Lucas Happ[2], Maxim Efremov[1]
[1]German Aerospace Center (DLR), Institute of Quantum Technologies, 89081 Ulm; [2]RIKEN Nishina Center, Strangeness Nuclear Physics Laboratory, Wako 351-0198, Japan

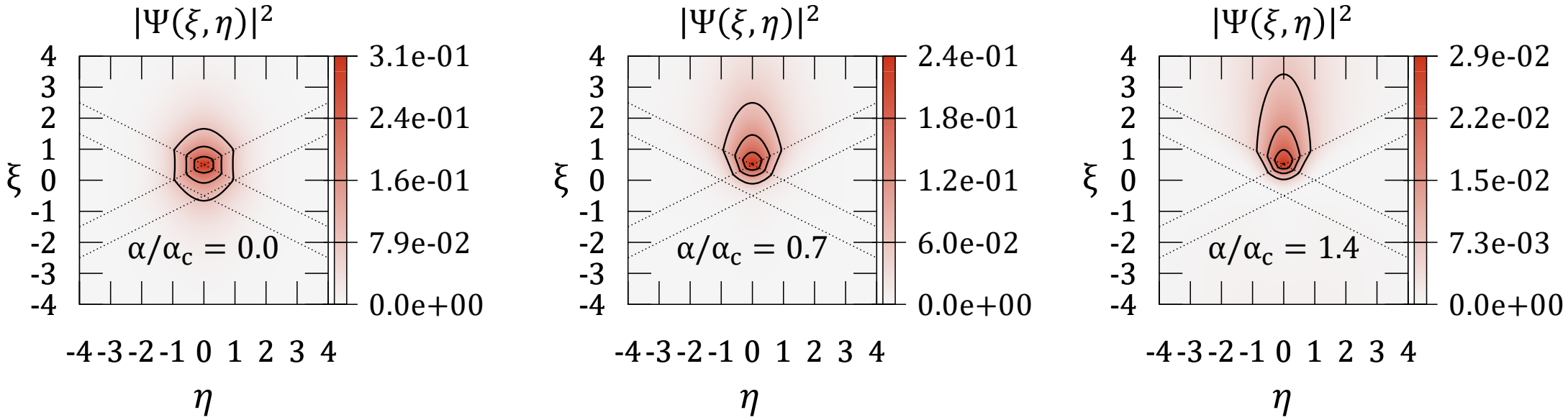

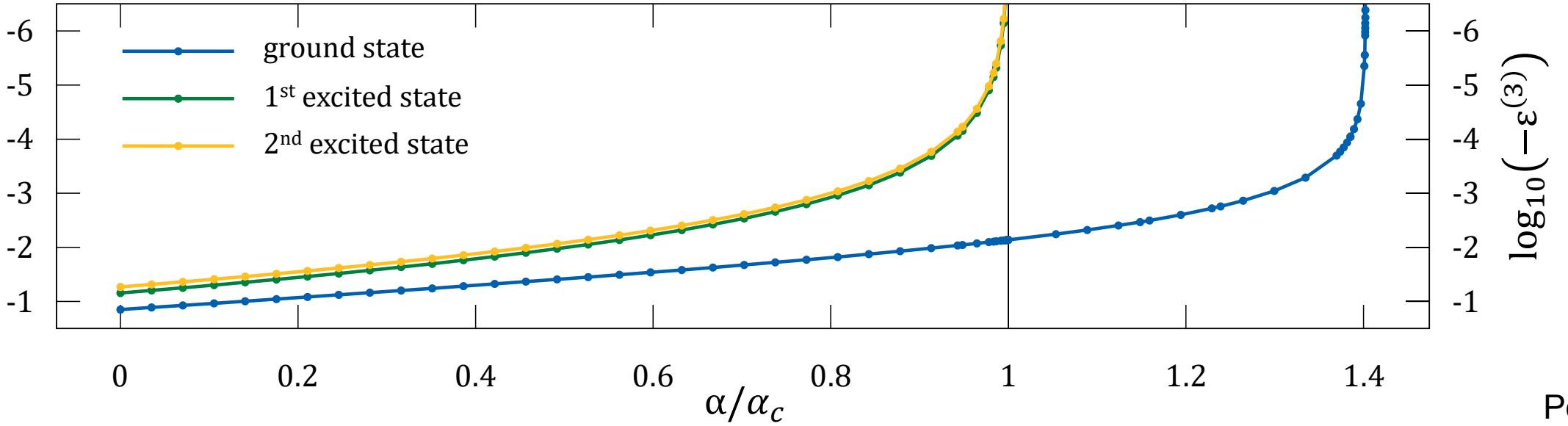

Poster 17

17

Relativistic Calculations of Electron and Positron Scattering Length for Argon

Michał P. Piłat [1*] Paweł Syty [1] Józef E. Sienkiewicz [1]

[1]Division of Theoretical Physics and Quantum Information, Faculty of Applied Physics and Mathematics, Gdańsk University of Technology, Fahrenheit Universities,
Gabriela Narutowicza str. 11/12, 80-233 Gdańsk, Poland

03.08.2023

$$\left(\frac{\mathrm{d}}{\mathrm{d}r} + \frac{\kappa}{r}\right) P_k = (\frac{2}{\alpha} + \alpha(\epsilon - V - V_{pol}))Q_k - X^{(Q)} \tag{1}$$

$$\left(\frac{\mathrm{d}}{\mathrm{d}r} - \frac{\kappa}{r}\right) Q_k = -\alpha(\epsilon - V - V_{pol})Q_k + X^{(P)} \tag{2}$$

$$V_{pol} = -\frac{1}{2}\frac{\alpha_d r^2}{\left(r^3 + r_0^3\right)^2}, \tag{3}$$

$$a = -\lim_{k\to 0}\frac{\tan(\delta)}{k}, \qquad \frac{1}{a} = -\lim_{k\to 0} k \cdot \cot(\delta) \tag{4}$$

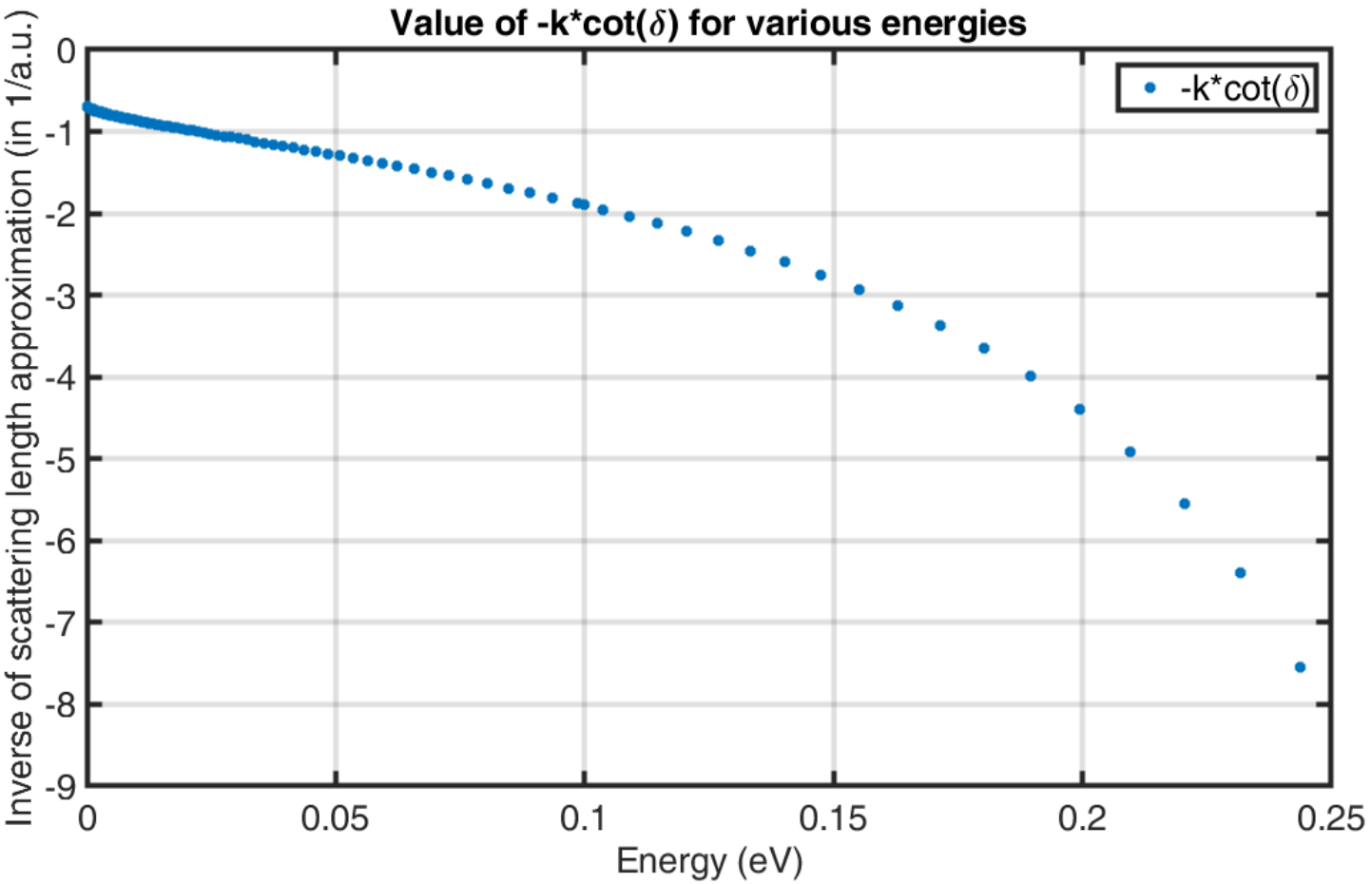

Figure: Graph of the $-k \cdot \cot(\delta)$ for various energies. Scattering length is the inverse of the limit of this expression as $k \to 0$.

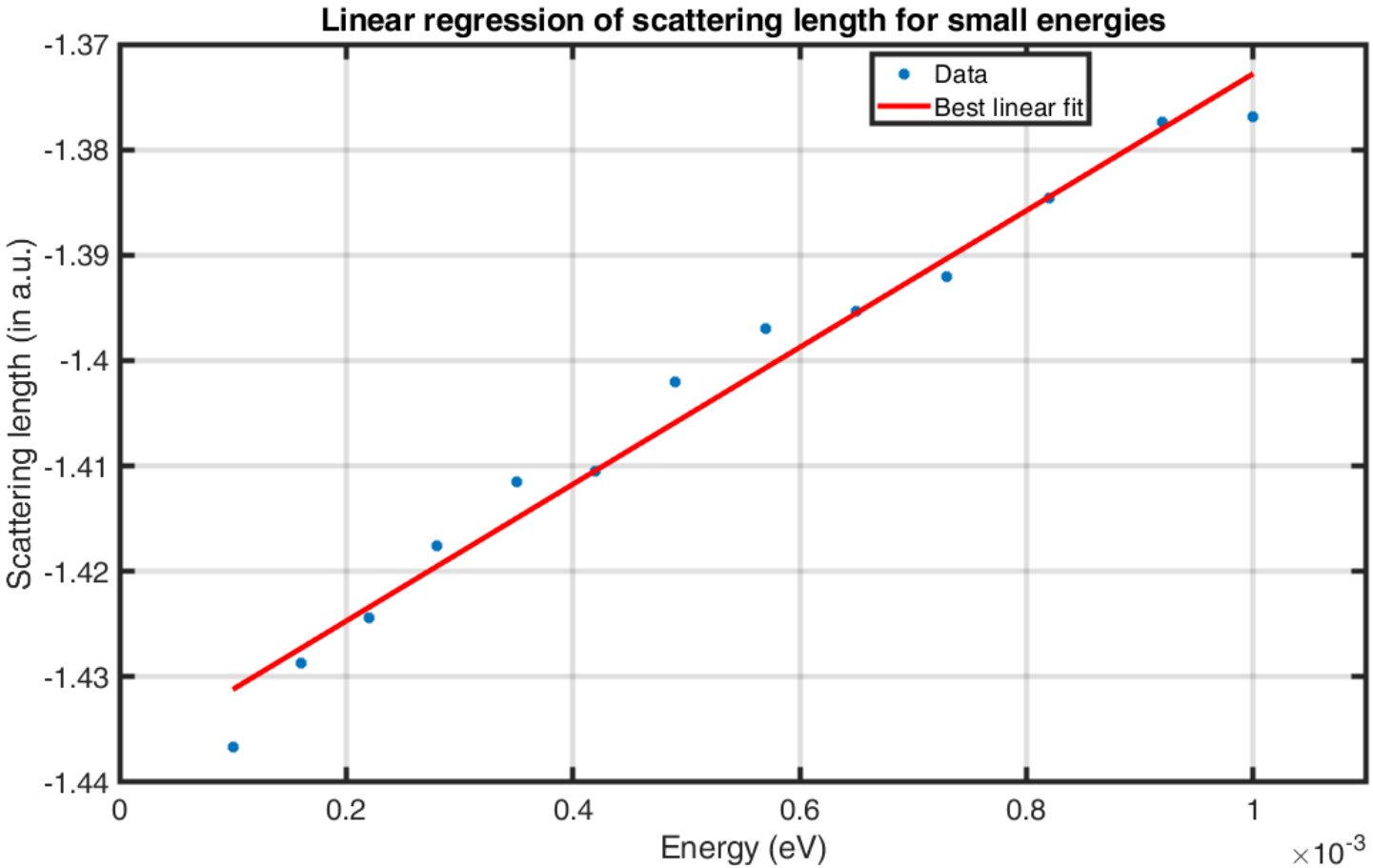

Figure: Close-up of the upper graph. Linear regression was used to estimate the limit value at $k = 0$.

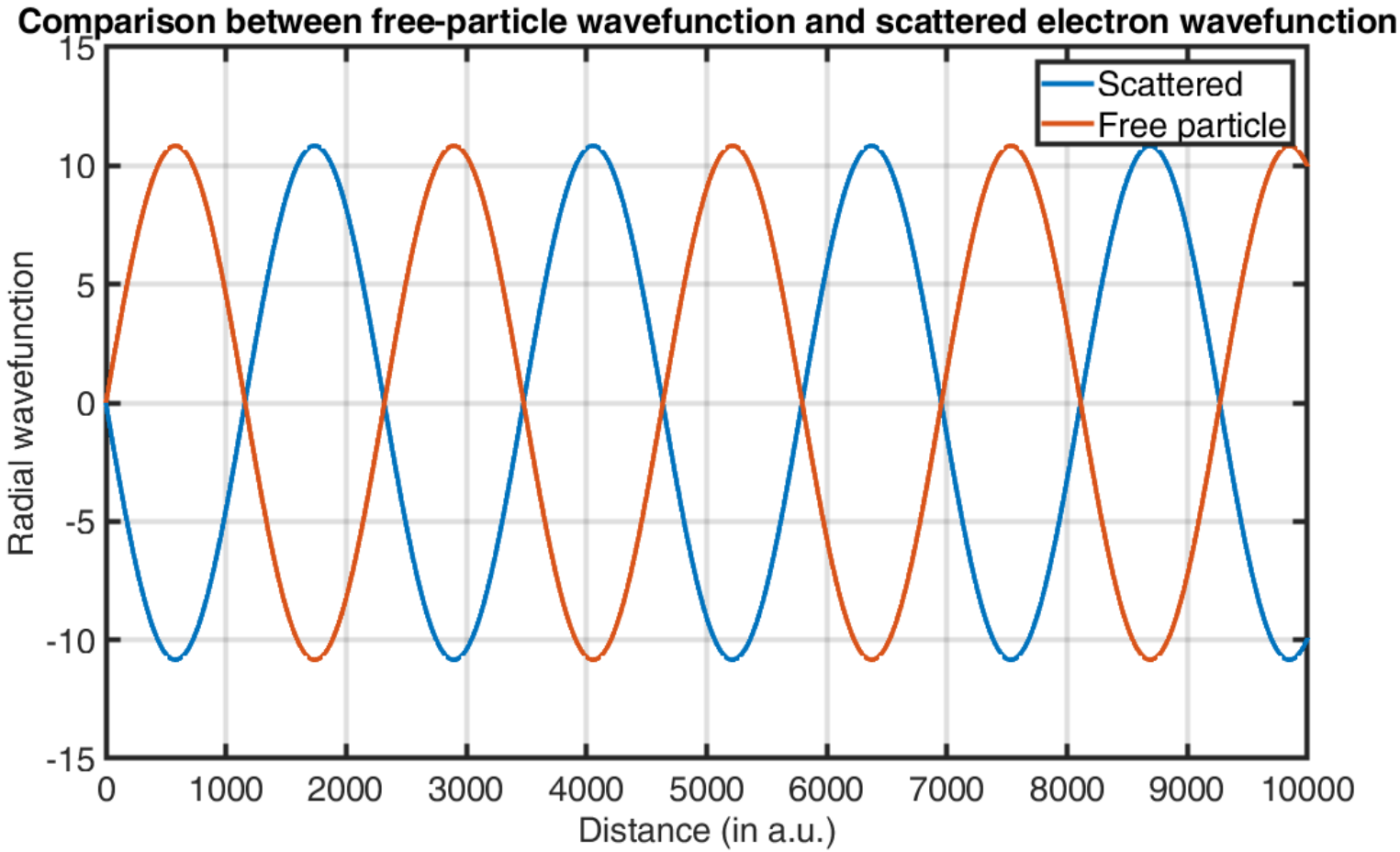

Figure: Comparison of the scattered wavefunction and free-particle wavefunction for $E = 0.00001eV$. Phaseshift between those functions is used to calculate scattering length.

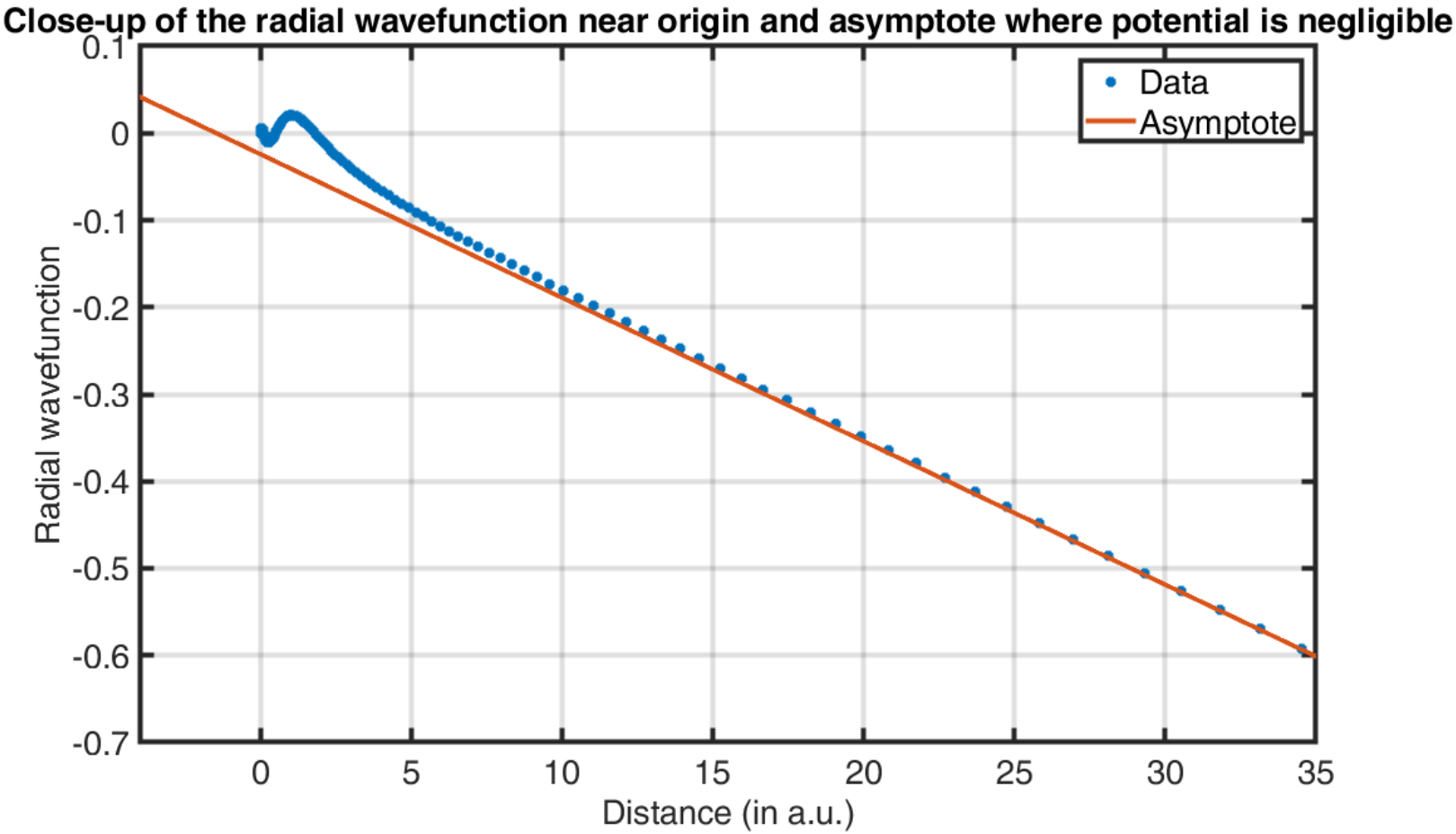

Figure: Close-up of the radial wavefunction for $E = 0.00001eV$ and the linear asymptote. We can treat the intersection of the asymptote with x-axis as a value of scattering length.

Table: Calculation of scattering length for electron using both methods and comparison with other works, in bold are experimental values.

Method	Asymptotic behaviour	Interpolation near origin
DHF	-1.4596	-1.4503
Layer 1	-1.4377	-1.4542
Layer 2	-1.4087	-1.4491
Layer 3	-1.3702	-1.3461
Other works	-1.39 -1.441, **-1.488**, **-1.449**, **-1.593**, **-1.442**, **-1.459**,	

Table: Calculation of scattering length for positron using both methods and comparison with other works, in bold are experimental values.

Method	Asymptotic behaviour	Interpolation near origin
DHF	-4.4613	-4.502
Layer 1	-4.4057	-4.4267
Layer 2	-4.3965	-4.4330
Layer 3	-4.4056	-4.5345
Other works	-4.41, -4.6991, -5.30, -5.05, -4.30, **-4.9±0.7**	

18

Laboratory on Energy and Matter for
Nuclear Sciences Development
TUNISIA

Accurate determination of radiative properties in the carbon isoelectronic sequence by using the MCDHF method

Presented by : Dhia Elhak Salhi

Atomic and Plasma Group: Prof. Dr. Haikel JELASSI and Soumaya MANAI

Interest of nuclear fusion

$$^{2}D + ^{3}T \rightarrow \alpha + n + 17.5MeV$$

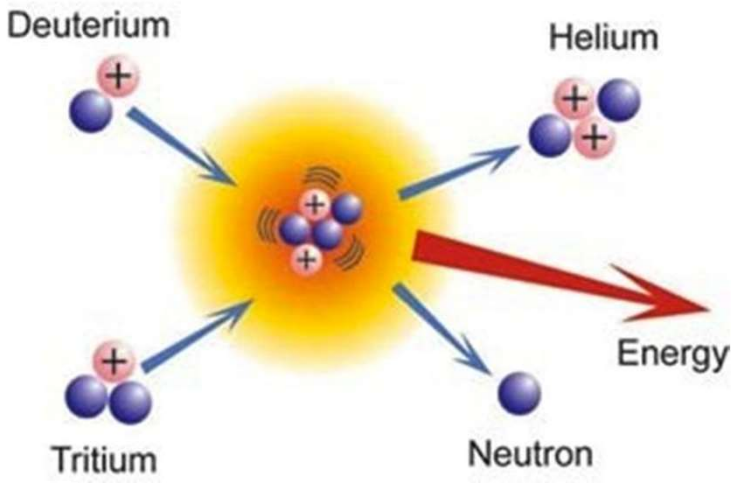

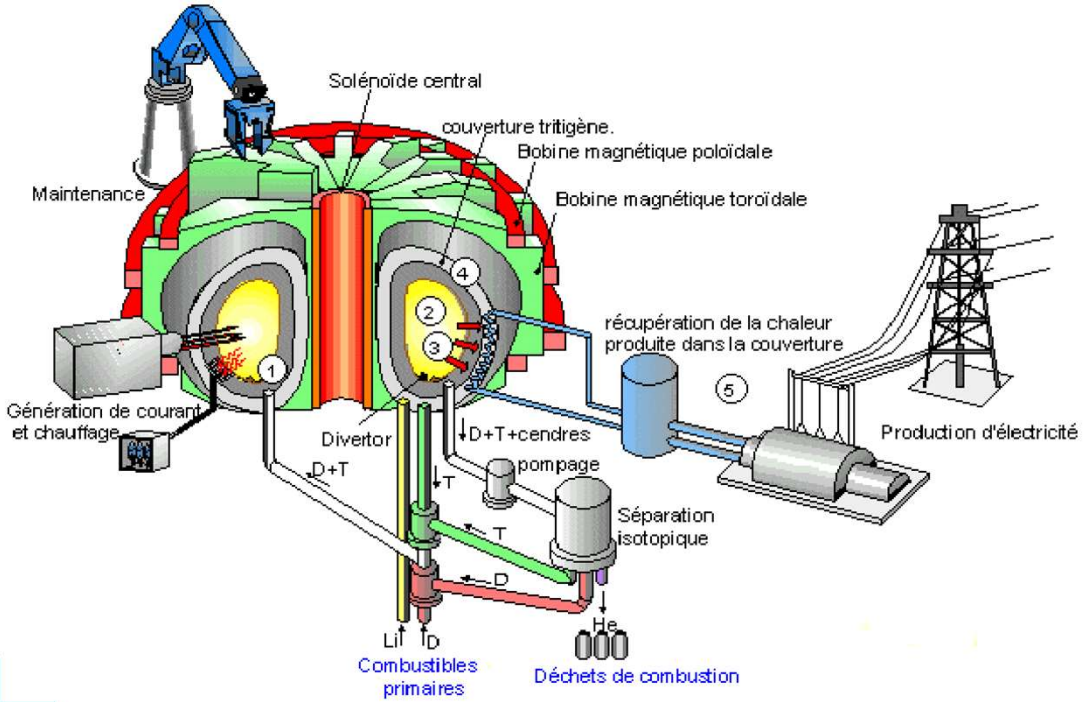

Diagram of the ITER reactor
Source : CEA/IRFM

❖ **Importance of atomic data**

For the gaseous impurities (example: neon), their injection lowers the edge temperature, and for this limits the erosion of the wall of the tokamak.

❖ Objectives

Use best performing relativistic atomic codes

Generate new atomic data for C-like (Z= 10-22) using the $2s^2 2p^2$, $2p^4$ and $2s^1 2p^3$ configurations, resulting in a total of 20 energy levels.

Improve uncertainty for certain energy levels, wavelength values, oscillator strength values and radiative transition rates

Assess the accuracy of the results for these elements of the carbon isoelectronic sequence.

❖ Multi-Configuration-Dirac-Hartree-Fock Theory (MCDHF)

CSF (Configuration State Function) :

$$\Psi(\gamma \Pi J M) = \sum_{\nu}^{\mathrm{NCF}} c_\nu \Phi(\gamma_\nu \Pi J M)$$

Normalization condition :

$$\sum_{\nu}^{\mathrm{NCF}} c_\nu^2 = 1$$

$$\begin{pmatrix} c\left(\frac{d}{dr} + \frac{\kappa_a}{r}\right) & -2c^2 + V_a(r) \\ -V_a(r) & c\left(\frac{d}{dr} - \frac{\kappa_a}{r}\right) \end{pmatrix} \begin{pmatrix} P_a(r) \\ Q_a(r) \end{pmatrix} = \sum_b \varepsilon_{a,b} \begin{pmatrix} P_b(r) \\ Q_b(r) \end{pmatrix} + \begin{pmatrix} X_a^Q(r) \\ X_a^P(r) \end{pmatrix}$$

$$V_a(r) = V_N(r) + \sum_{b,k} a^k(b,b) Y^k(b,b)$$

$$\begin{aligned} E &= \sum_{\mu=1}^{NCF} \sum_{\nu=1}^{NCF} c_\mu c_\nu \left\langle \Phi(\gamma_\mu \Pi J M) \left| H_{DC} \right| \Phi(\gamma_\nu \Pi J M) \right\rangle \\ &= \sum_{\mu=1}^{NCF} c_\mu^2 H_{\mu\mu} + 2 \sum_{\mu<\nu}^{NCF} c_\mu c_\nu H_{\mu\nu} \\ &= \sum_{\mu=1}^{NCF} c_\mu^2 \left[E_{AV}^\mu + \Delta E^\mu \right] + 2 \sum_{\mu<\nu}^{NCF} c_\mu c_\nu H_{\mu\nu} \end{aligned}$$

$$E_{\mathrm{AV}}(jj) = \frac{\sum_n (2J_n + 1) E(J_n)}{\sum_n (2J_n + 1)}$$

❖ Relativistic corrections

$$\boxed{H_{DC}\Psi = E\Psi}$$

$$H_{DC} = \sum_{i=1}^{N} \left(c\boldsymbol{\alpha}_i \cdot \boldsymbol{p}_i + (\beta_i - 1)\, c^2 + V\left(r_i\right) \right) + \sum_{i<j}^{N} V(i,j)$$

Breit interaction :

is due to the interaction of a moving electron in a magnetic field generated by another electron

$$V_{ij} = \frac{1}{r_{ij}} - \frac{\boldsymbol{\alpha}_i \cdot \boldsymbol{\alpha}_j}{r_{ij}} \cos\left(\frac{\omega_{ij} r_{ij}}{c}\right) + c^2 (\boldsymbol{\alpha} \cdot \nabla)_i (\boldsymbol{\alpha} \cdot \nabla)_j \frac{\cos\left(\frac{\omega_{ij} r_{ij}}{c}\right) - 1}{\omega_{ij}^2 r_{ij}}$$

QED electrodynamic effects:

- The self-energy corresponding to the emission of an electron by a photon or an electron pair which will then be reabsorbed

- The vacuum polarization

❖ Calculation steps for the MCDHF method (GRASP2018)

```
./rnucleus <<EOF
10
20
n
20.2
1.5
-0.661797
0.103
n
EOF
```

Generate nuclear data by giving:
- the atomic number Z, the mass number A
- the nuclear spin I, the nuclear dipole moment ν, the nuclear quadrupole moment Q

```
./rcsfexcitation <<EOF
0
16
1s(2,*)
1s(1,*)2s(1,*)
1s(1,*)3s(1,*)
1s(1,*)3d(1,*)
1s(1,*)4s(1,*)
1s(1,*)4d(1,*)
1s(1,*)5s(1,*)
1s(1,*)5d(1,*)
1s(1,*)5g(1,*)
1s(1,*)6s(1,*)
1s(1,*)6d(1,*)
1s(1,*)6g(1,*)
1s(1,*)7s(1,*)
1s(1,*)7d(1,*)
1s(1,*)7g(1,*)
1s(1,*)7i(1,*)
 8s, 8p, 8d, 8f, 8g, 8h  i, 8k
0,14
2
n
EOF
```

Generate the excitation input to provide the list of CSF (configuration state function) including the AS "Active Set"

```
./rcsfgenerate < excita  ndata
```

Generate a list of CSFs including only CSFs that interact with CSFs from a reference list

```
./rangular <<EOF
y
EOF
```

Perform angular integration and calculate angular coefficients

```
./rwfnestimate <<EOF
y
1
evenmr.w
*
2
*
EOF
```

Initially estimate radial wave functions (usually hydrogen orbitals, Thomas-Fermi orbitals, or orbitals taken from previous calculations)

```
./rmcdhf <<E
y
1-7
1-11
1-10
1-8
1-6
1-4
1-2
1
5
8*

100
EOF


./rci <<EOF
y
even8
y
y
1.d-6
y
n
n
y
7
1-7
1-11
1-10
1-8
1-6
1-4
1-2
1
EOF


./jj2lsj <<EOF
even8
y
y
EOF
```

Determine the mixing coefficients of the CSFs using:

- A first diagonalization of the Hamiltonian matrix
- Determine the direct and exchange potentials for a given orbital
- Perform orbital optimization repeatedly until a relativistic self-consistent field (RSCF) is obtained

Include relativistic configuration interaction RCI (relativistic effects such as QED electrodynamic corrections and Breit effect)

Transform the jj-coupling into an LSJ-coupling to facilitate the extraction of the values obtained associated with their electronic configurations

Extract values of energy levels, wavelengths, oscillator strengths, radiative transition rates and lifetimes

Study of the atomic structure of C-like (Z= 10 -22)

❖ Energy levels

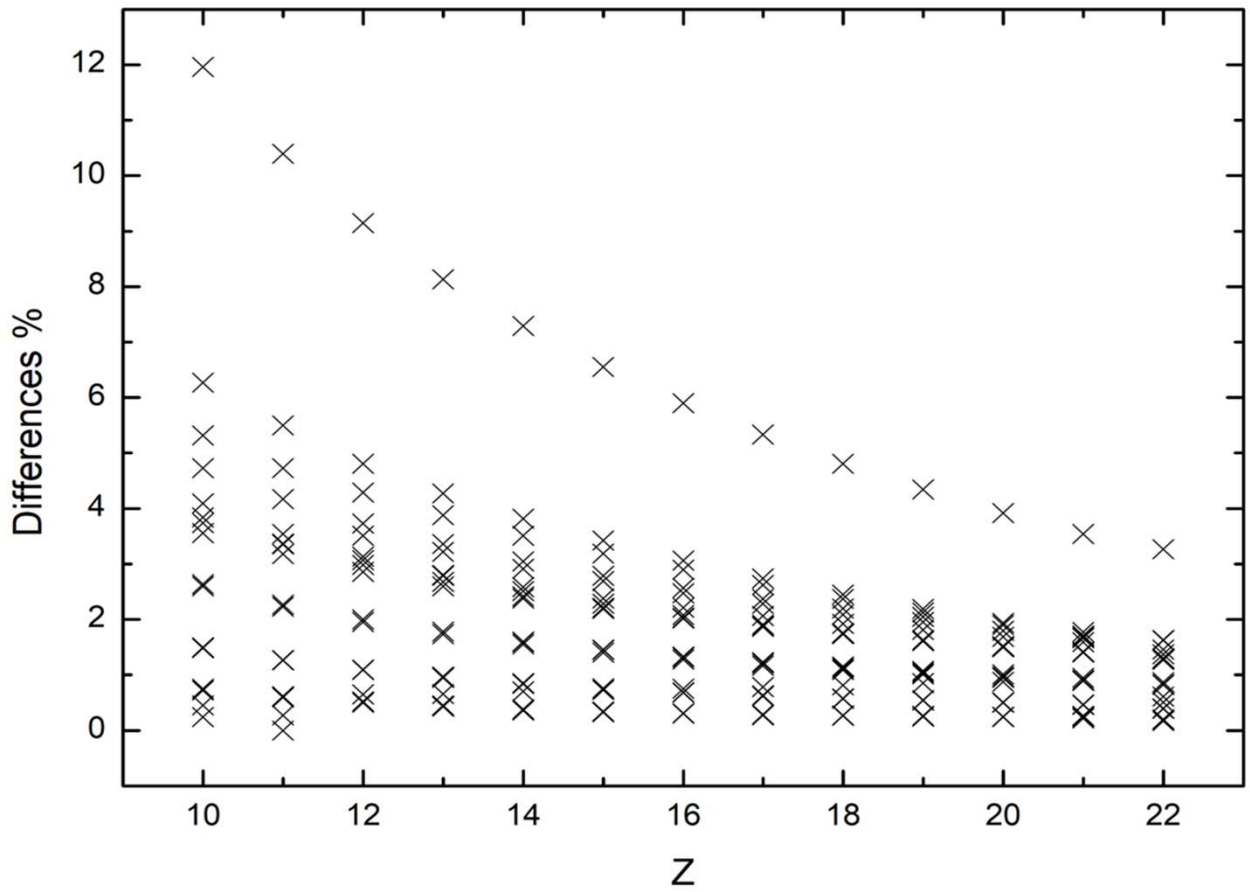

Relative deviations between the two sets of calculations of the 20 energy levels with the GRASP2018 and FAC codes

❖ Uncertainty dT

$$dT = \frac{|A_l - A_v|}{\max(A_l, A_v)}$$

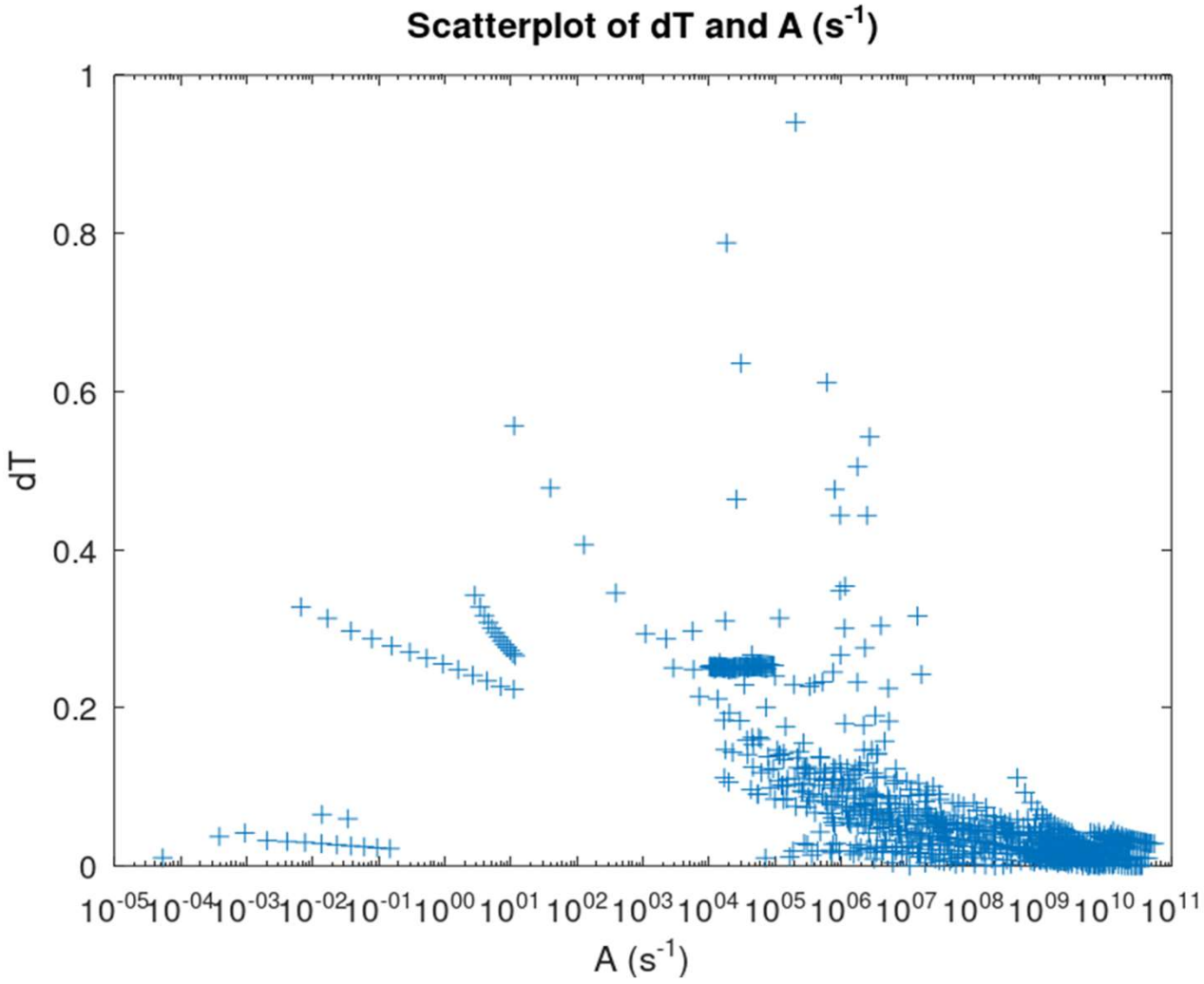

The uncertainty *dT* by the GRASP2018 code between the velocity and length forms of transitions rates as function of transitions rates A

❖ Lifetimes

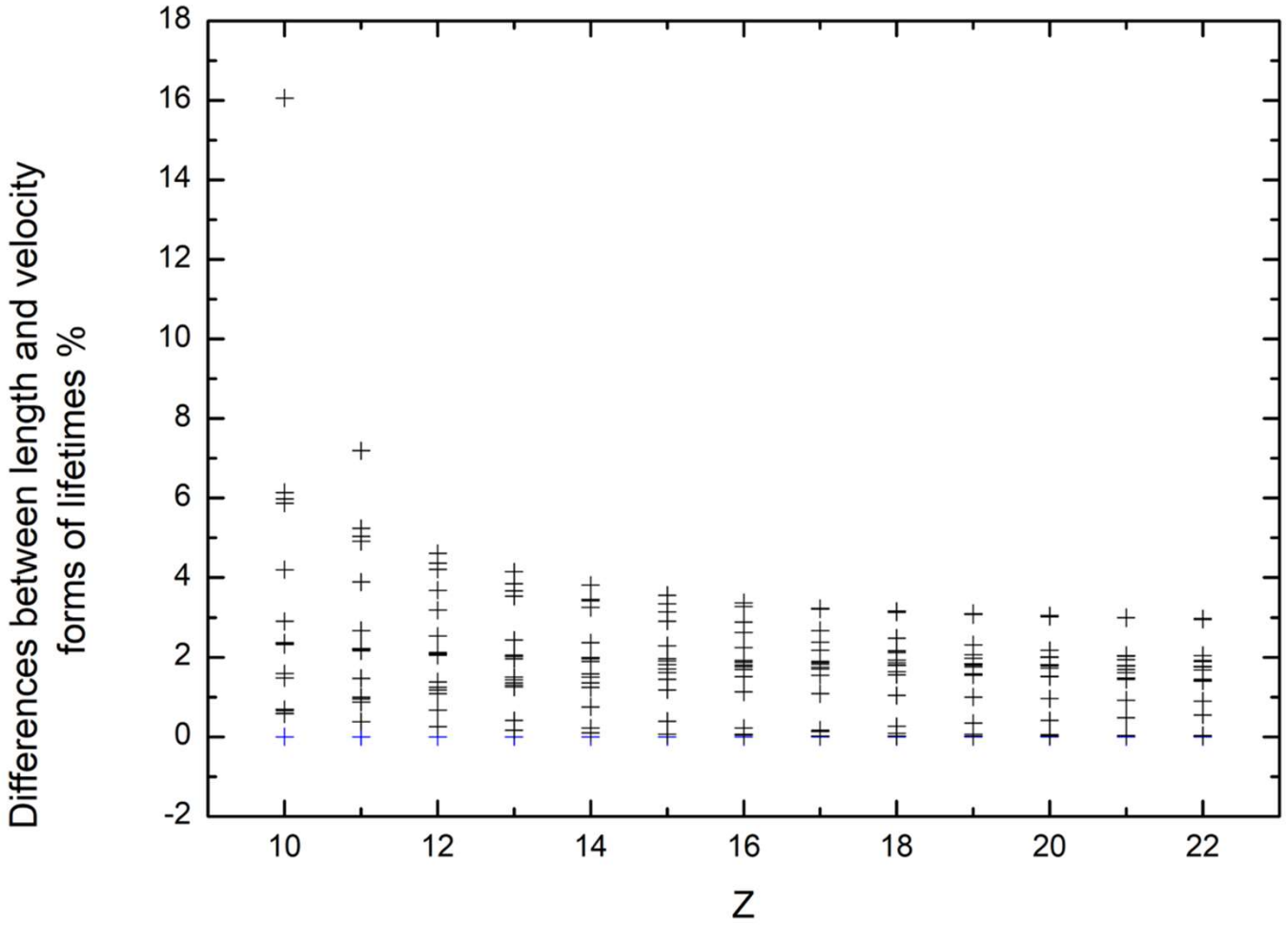

The differences between the velocity and length forms of the 19 lifetimes as function of atomic number Z

❖ Conclusion

- We have presented atomic data for calculations of energy levels and radiative rates for the iso-electronic sequence of Carbon with Z=10-22.

- The calculations were performed using two different approaches implemented in two powerful atomic codes named GRASP2018 and FAC.
- Small differences were found between the two sets of energy level values. While assessing the accuracy of transition rates and lifetimes, we discovered a few discrepancies that we intend to improve upon in our upcoming work.

- The current data are of great importance for the analysis of astrophysical and fusion plasmas and should be used in plasma diagnostics.

Poster 18


Thank You
For Your
Attention

Radiative neutron capture on $^{6\text{-}8}$Li isotopes in the cluster model

19

Sergey B. Dubovichenko[1], Nataliya A. Burkova[2], Badigul M. Yeleusheva[1,2], Alessya S. Tkachenko[1], Roman Ya. Kezerashvili[3,4]*

Total cross section of n^8Li

Band specifies the GS asymptotic constant variety in the range of C_w = 0.93 – 1.4. The results on $\sigma(E)$ obtained by Dong *et. al*. differs essentially in the whole energy range and *catch* the lower error bars limits only. Therefore, it is more reasonable to compare the MPCM and *ab initio* results by McCracken *et al*. The difference comes at the energies close to the 1st resonance $^4P_{5/2}$: the Lower set (red dash-double-dotted curve) and *ab initio* cross sections (blue dashed curve) are comparable, contrary to the Upper set application (red solid curve). Out of the resonance range $E_{c.m.}$ > 300 keV and up to 1 MeV, the Upper set and *ab initio* cross sections practically coincide and fit the second experimental point fairly well.

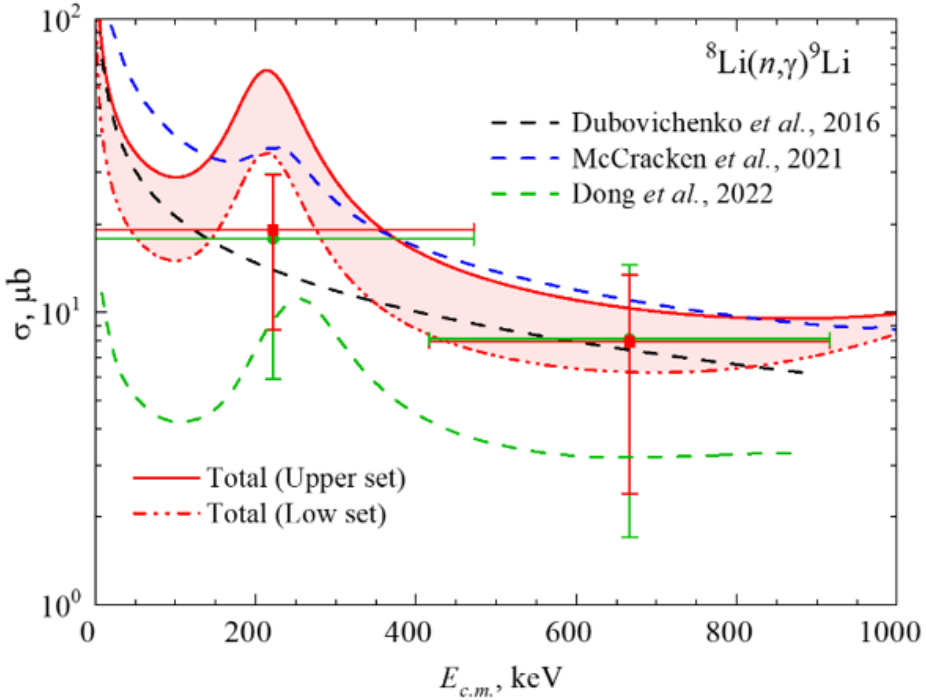

FIGURE 1 Total cross sections of radiative ^{8}Li(n,γ)^{9}Li capture to the GS and 1st ES of the ^{9}Li nucleus.

Reaction rate of n^8Li

The *ab initio* reaction rate [McCracken] (blue dashed curve) exceeds our results at low temperatures and approximately coincides in the resonance region. A noticeable decrease of $N_A\langle\sigma v\rangle_{ab\,initio}$ is observed at $T_9 > 1$. The *ab initio* cross section is calculated in the limits $E_{c.m.}$ = 20 keV – 1.6 MeV, so the energy interval extension will give rise to the reaction rate at $T_9 > 1$. The great difference between reaction rates appears at $T_9 < 1$. Both model calculations MPCM and *ab initio* contrast with [Dong] results (green dashed curve).

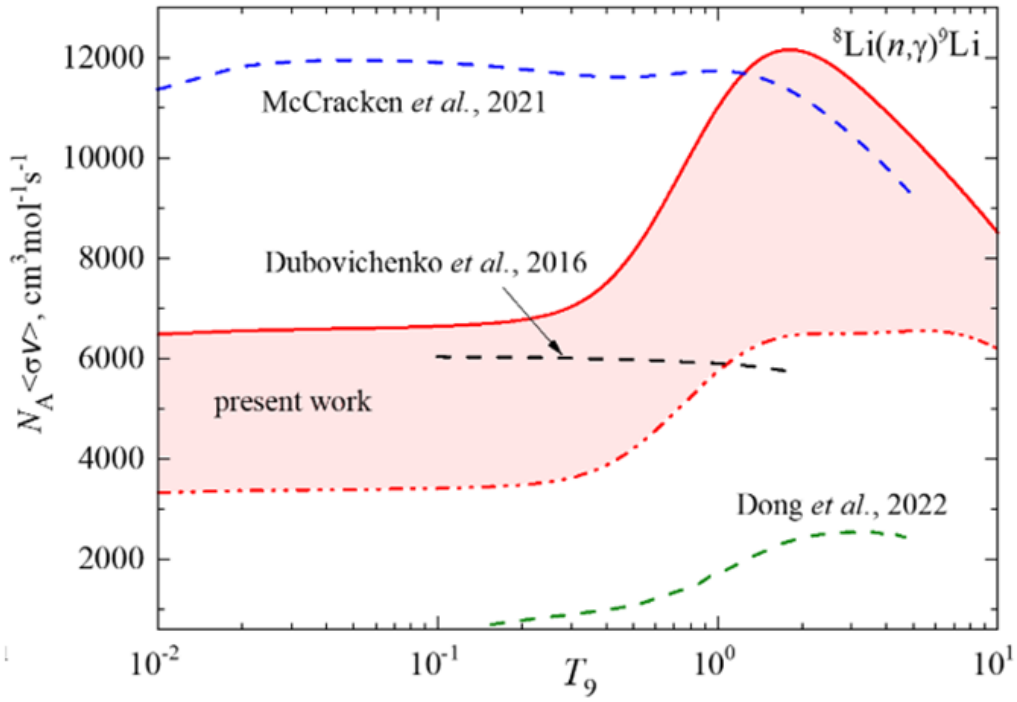

FIGURE 2 The reaction rate of radiative ^{8}Li(n,γ)^{9}Li capture to the GS and 1st ES of the ^{9}Li.

Reaction rate of n^8Li

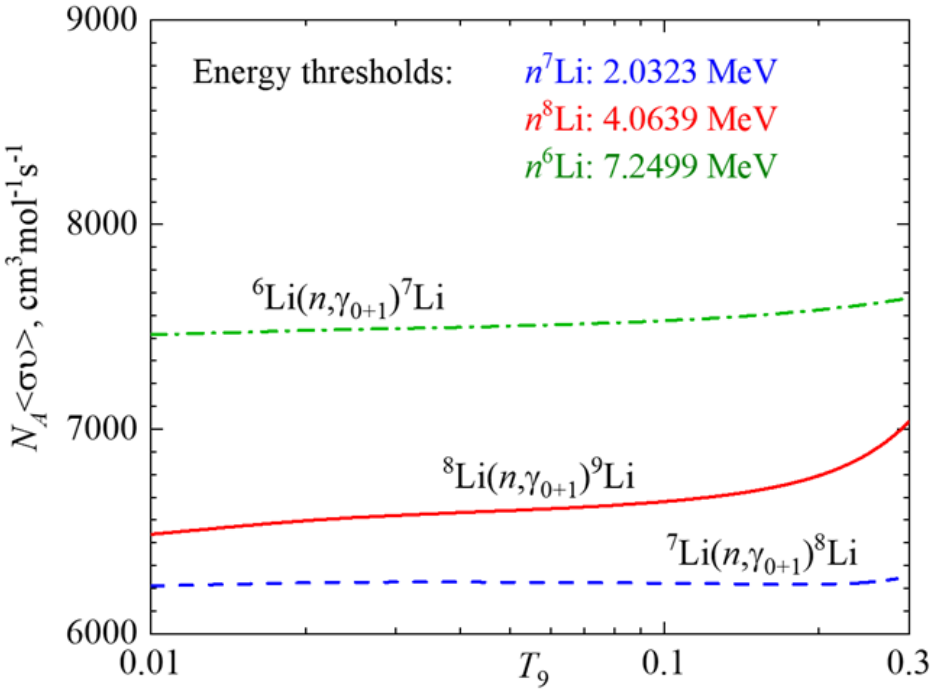

Figure 3 illustrates the reactions rates on lithium isotopes ^{6,7,8}Li calculated in the MPCM. We see that the order of $N_A\langle\sigma v\rangle$ below ~ $0.2T_9$ fit the threshold energies relation $E_{th}(n^6\text{Li}) > E_{th}(n^8\text{Li}) > E_{th}(n^7\text{Li})$ if for reaction ^{8}Li(n,γ_{0+1})^{9}Li we take the Upper set results. The reaction rates corresponding to the MPCM Lower set, as well as *ab initio* [McCracken] and data from Ref. [Dong] do not fit the discussed regularity. Note, reactions ^{6}Li(n,γ_{0+1})^{7}Li and ^{7}Li(n,γ_{0+1})^{8}Li are examined much better as they directly concern the well-known *lithium problem*.

FIGURE 3 The reaction rates of radiative neutron capture for ^{6}Li(n,γ_{0+1})^{7}Li [9], ^{7}Li(n,γ_{0+1})^{8}Li [10], and ^{8}Li(n,γ_{0+1})^{9}Li – present results for the Upper set in Figure 2.

Conclusion

Following our new results on the ^{7}Li(n,γ_{0+1})^{8}Li reaction [Burkova 2021] we reconsider the reaction ^{8}Li(n,γ_{0+1})^{9}Li. The total cross sections and reaction rates are calculated for the reaction ^{8}Li(n,γ_{0+1})^{9}Li.

The experimentally proved resonance at $E_{c.m.}$ = 0.232 MeV in the $^{4}P_{5/2}$ wave and *ab initio* predicted $^{4}P_{3/2}$ resonance at 1.32 MeV [McCracken] are considered. The intensity of $^{4}P_{5/2}$ resonance depends strongly on the range of asymptotic constants C_{w} as well the cross sections in whole, which reveals in the temperature T_9 dependence of the reaction rates.

We propose two points to constrain the declared in our study reaction rate interval. The first one concerns the values of thermal cross sections. Analysis of σ values leads us to the conclusion that the Upper set calculations giving 46.8 mb (C_{w} = 1.40) are more relevant as they conform to estimations of results of Descouvemont 1993.

The second point is related to the reaction rates of radiative neutron capture on lithium isotopes ^{6,7,8}Li. The examined correlation between the energy thresholds and order of reaction rates at low temperatures beyond the possible resonances $T_9 < 0.2$ leads to the conclusion that Upper set calculations are more reasonable.

Research Laboratory of Energy and Matter for Nuclear Sciences
National Centre for Nuclear Sciences and Technologies, Tunisia

20

Extensive and accurate energy levels, wavelengths, transition rates, line intensity ratio and plasma parameters for the Ne VIII, Fe XXIV and Kr XXXIV spectrum of Plasma interest

Prepared By: Soumaya MANAI

Atomic and Plasma Group: Prof. Dr. Haikel JELASSI and Dhia Elhak SALHI

Overview: Applications of Ne VIII, Fe XXIV and Kr XXXIV.

Lithium-like ions provide an important X-ray spectral diagnostics.

- Astrophysical
- High-temperature fusion plasmas

→ An interpretation of the observed spectra provides information on temperature, density and chemical compositions of the plasma.

Emission lines from the spectra of singly excited lithium-like ions are often observed.

→
- Spectra of solar
- Spectra of stellar
- Other astrophysical plasmas

Spectral lines of lithium-like ions are also prominent features.

→
- X-ray spectra of tokamak plasmas
- Laser-produced plasmas

Problematic

To analyze observations, atomic data are required for a variety of parameters, such as energy levels, wavelengths and radiative rates.

ITER: International Thermonuclear Experimental Reactor

➢**Tokamak :** **is an experimental machine designed to harness the energy of fusion.**

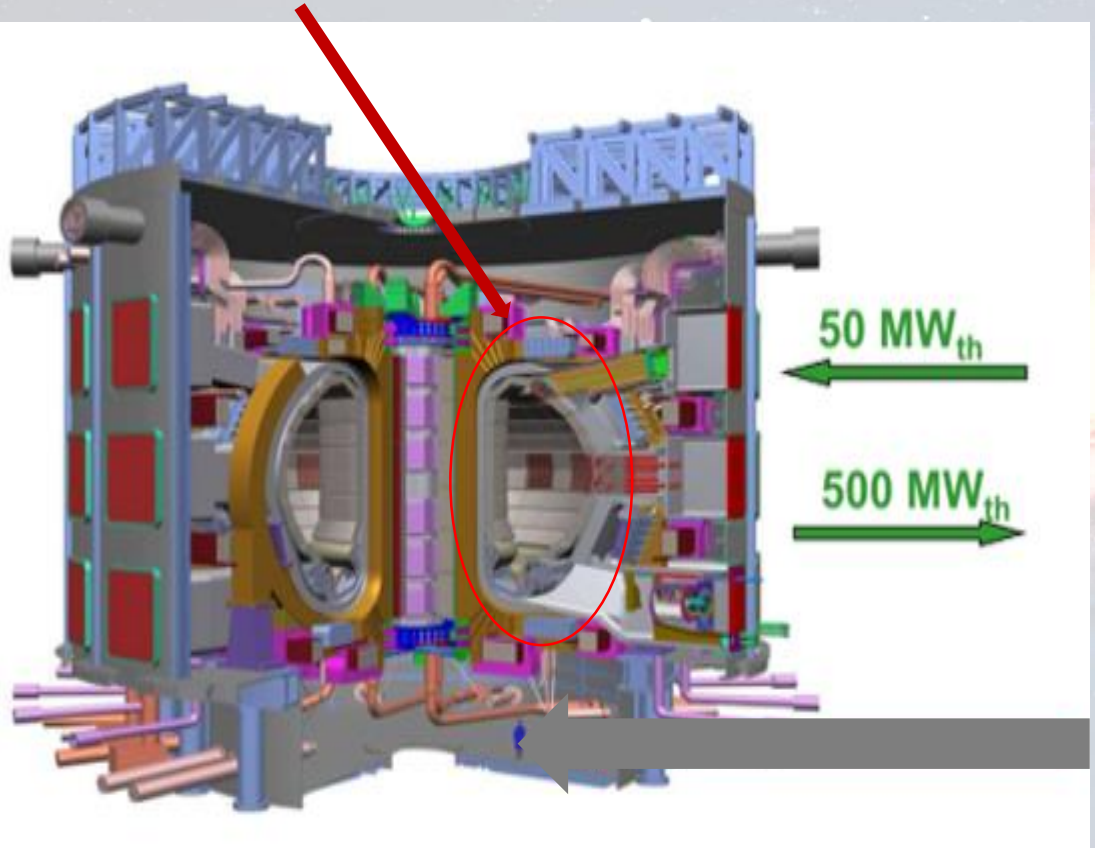

ITER

- **ITER** is an international nuclear fusion research and engineering megaproject, which will be the world's largest **magnetic confinement plasma physics experiment**. It is an experimental tokamak nuclear fusion reactor that is being built in south of France (Cadarache).

- The **ITER** fusion reactor has been designed to produce 500 megawatts of output power for several seconds while needing 50 megawatts to operate.

- The **ITER** project aims to make the long-awaited transition from experimental studies of plasma physics to full-scale electricity-producing fusion power stations.

Accumulation of impurities in Tokamak

- These impurities are essential to properly control the nuclear fusion reaction in a tokamak plasma.
- The stability of the plasma is disturbed by impurity ions. These ions constitute an important factor of energy loss by radiation.
- For the impurity ions, their injection lowers the temperature on board, and therefore limits the erosion of the tokamak wall.
- Location of each of elements studied in a tokamak to produce the nuclear fusion reaction by magnetic confinement.

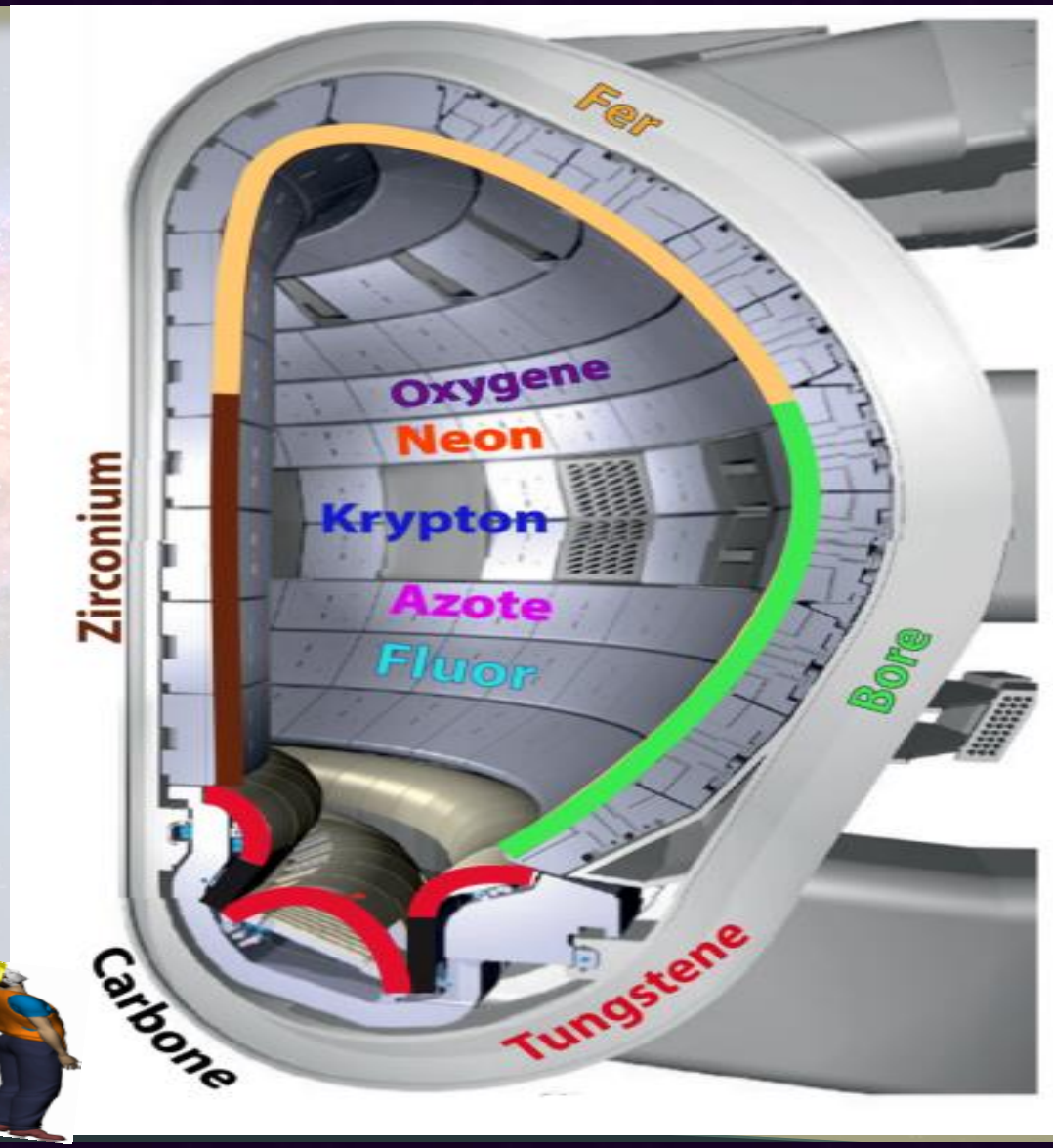

Daniel Villegas. Etude expérimentale de l'influence du gradient de température électronique sur le transport turbulent des impuretés dans un plasma de fusion. PhD thesis, Aix-Marseille 1, 2010

Our contribution consists in the study of He - like and Li - like ions

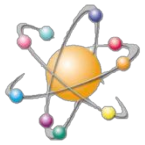

Periodic table of Elements

1	1 H Hydrogène																2 He Hélium
2	3 Li Lithium	4 Be Béryllium											5 B Bore	6 C Carbone	7 N Azote	8 O Oxygène	9 F Fluor	10 Ne Néon
3	11 Na Sodium	12 Mg Magnésium											13 Al Aluminium	14 Si Silicone	15 P Phosphore	16 S Soufre	17 Cl Chlore	18 Ar Argon
4	19 K Potassium	20 Ca Calcium	21 Sc Scandium	22 Ti Titane	23 V Vanadium	24 Cr Chrome	25 Mn Manganèse	26 Fe Fer	27 Co Cobalt	28 Ni Nickel	29 Cu Cuivre	30 Zn Zinc	31 Ga Gallium	32 Ge Germanium	33 As Arsenic	34 Se Sélénium	35 Br Brome	36 Kr Krypton
5	37 Rb Rubidium	38 Sr Strontium	39 Y Yttrium	40 Zr Zirconium	41 Nb Niobium	42 Mo Molybdène	43 Tc Technétium	44 Ru Ruthénium	45 Rh Rhodium	46 Pd Palladium	47 Ag Argent	48 Cd Cadmium	49 In Indium	50 Sn Étain	51 Sb Antimoine	52 Te Tellure	53 I Iode	54 Xe Xénon
6	55 Cs Césium	56 Ba Baryum	57-71 La.. Lanthanide	72 Hf Hafnium	73 Ta Tantale	74 W Tungstène	75 Re Rhénium	76 Os Osmium	77 Ir Iridium	78 Pt Platine	79 Au Or	80 Hg Mercure	81 Tl Thallium	82 Pb Plomb	83 Bi Bismuth	84 Po Polonium	85 At Astate	86 Rn Radon
7	87 Fr Francium	88 Ra Radium	89-103 Ac.. Actinide	104 Rf Rutherfordium	105 Db Dubnium	106 Sg Seaborgium	107 Bh Bohrium	108 Hs Hassium	109 Mt Meitnérium	110 Ds Darmstadtium	111 Rg Roentgenium	112 Uub Ununbium	113 Nh Nihonium	114 Fl Flérovium	115 Mc Moscovium	116 Lv Livermorium	117 Ts Tennessine	118 Og Oganesson

57 La Lanthane	58 Ce Cérium	59 Pr Praséodyme	60 Nd Néodyme	61 Pm Prométhium	62 Sm Samarium	63 Eu Europium	64 Gd Gadolinium	65 Tb Terbium	66 Dy Dysprosium	67 Ho Holmium	68 Er Erbium	69 Tm Thulium	70 Yb Ytterbium	71 Lu Lutécium
89 Ac Actinium	90 Th Thorium	91 Pa Protactinium	92 U Uranium	93 Np Neptunium	94 Pu Plutonium	95 Am Américium	96 Cm Curium	97 Bk Berkélium	98 Cf Californium	99 Es Einsteinium	100 Fm Fermium	101 Md Mendélévium	102 No Nobélium	103 Lr Lawrencium

Z masse
Symbole
Nom

Work objectives

Provide more complete and accurate atomic data of the lithium isoelectronic sequence for Li-like ions with Z = 10, 26 and 35.

Multiconfigurational Dirac-Hartree-Fock (MCDHF)

Energy levels, wavelength and transition rates.

Goal

Method

Program

Outcome

$\Delta E_{ji} = E_j - E_i \ (cm^{-1})$

$\lambda_{ji} = {}^{1}/_{(E_j - E_i)} \ (\text{Å})$

$A_{ji} \ (s^{-1})$

we compare our result with NIST database.

Evaluation of spectroscopic data

Relative deviation:

$$\frac{Our\ value - value\ for\ comparison}{Value\ for\ comparison} \times 100$$

Compare our values with the results published in the NIST database: https://www.nist.gov/pml/atomic-spectra-database

Compare our values with previous theoretical and experimental results.

Reference configurations up to the layer n = 6: $1s^2$2s, $1s^2$2p, $1s^2$3s, $1s^2$3p, $1s^2$3d, $1s^2$4s, $1s^2$4p, $1s^2$4d, $1s^2$4f, $1s^2$5s, $1s^2$5p, $1s^2$5d, $1s^2$5f, $1s^2$5g, $1s^2$6s, $1s^2$6p, $1s^2$6d, $1s^2$6f, $1s^2$6g and $1s^2$6h.. We obtain 35 energy levels for each Li like ion.

ASD Data — Lines Levels — Information — List of Spectra | Ground States & Ionization Energies | Bibliography | Help

NIST Atomic Spectra Database Levels Data

C V 101 Levels Found

Z = 6, He isoelectronic sequence

Data on Landé factors and level compositions are not available for this ion in ASD

Primary data source	Query NIST Bibliographic Database for C V (new window)
Engström et al. 1992	Literature on C V Energy Levels

Configuration	Term	J	Level (cm^{-1})	Uncertainty (cm^{-1})	Reference
$1s^2$	^{1}S	0	0.0		L11091
1s2s	^{3}S	1	2 411 271.2		
1s2s	^{1}S	0	2 455 025.5		
1s2p	^{3}P°	1	2 455 157.3		
		0	2 455 169.9		
		2	2 455 293.2		

S. Manai et al, Results in Physics, 37, 105487 (2022).

Energy levels and Wavelengths of Li-like neon ion: $1s^2nl\left(n \leq 6, l \leq (n-1)\right)$

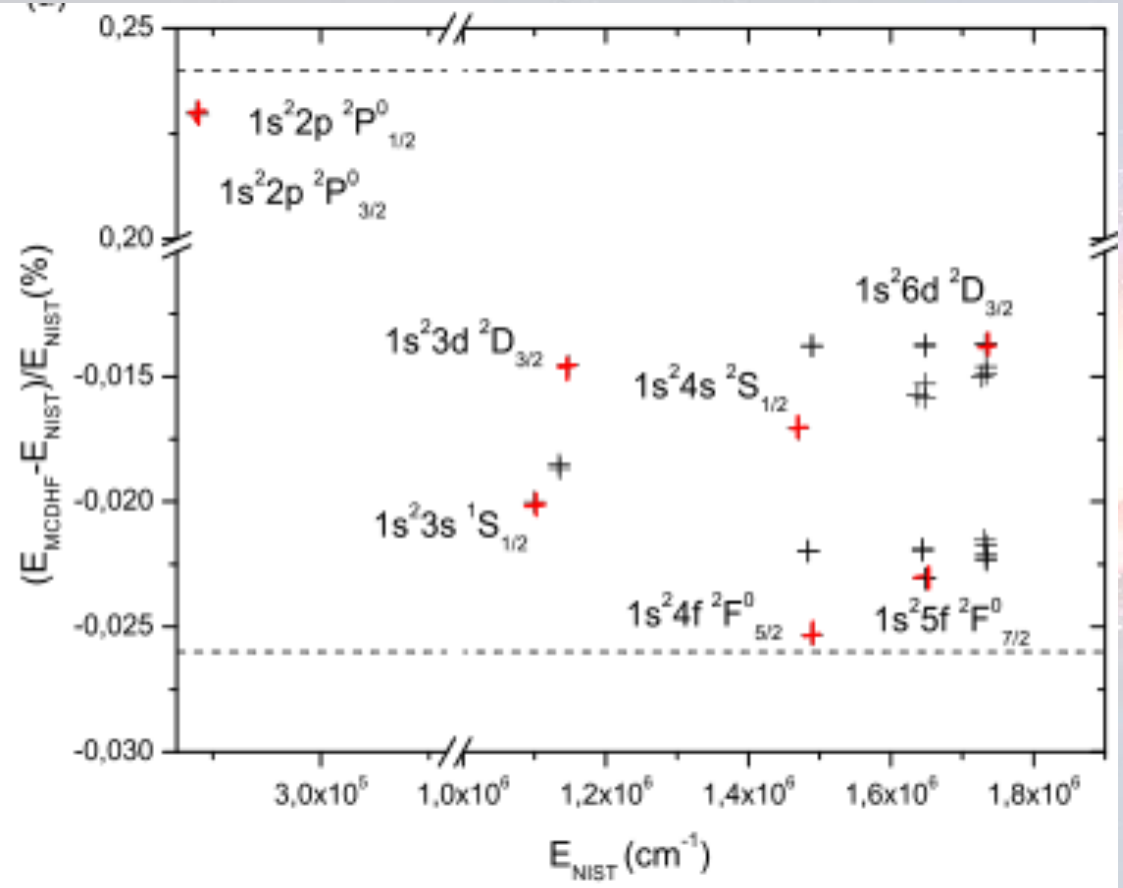

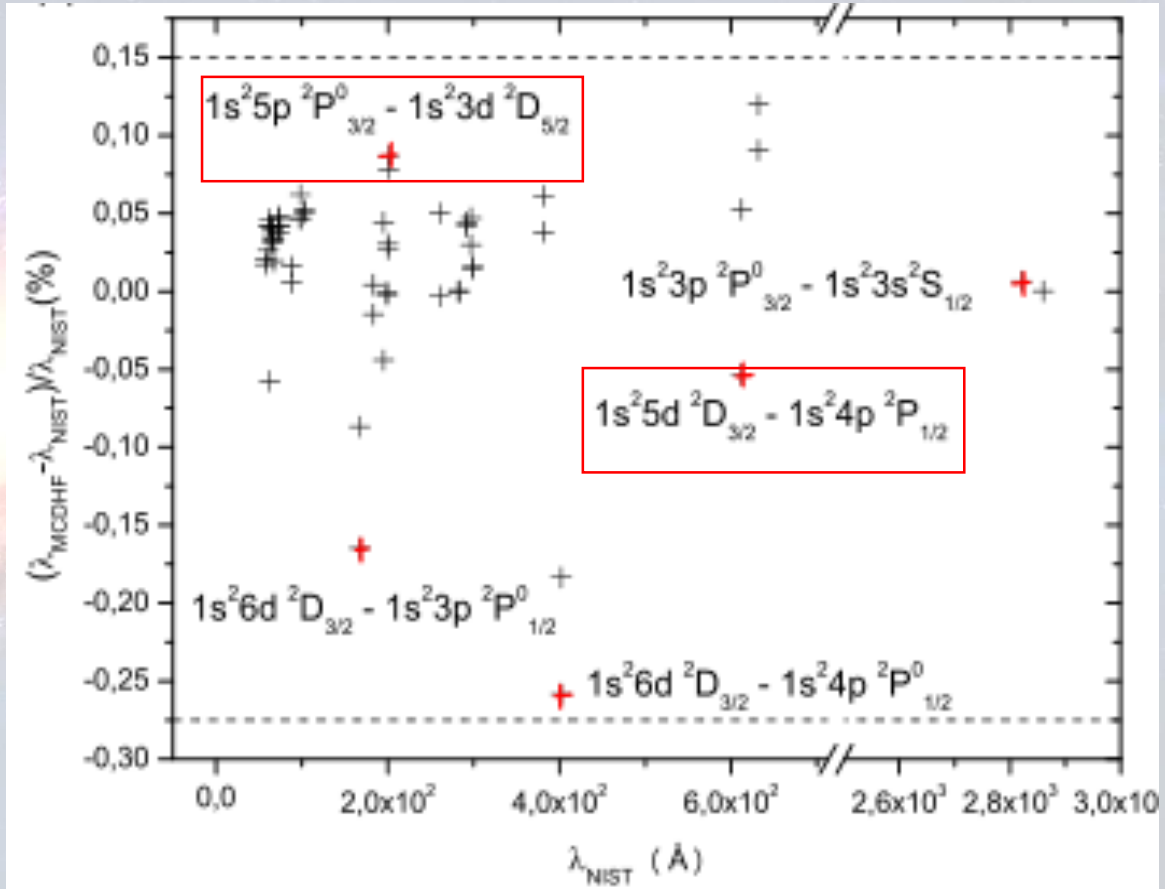

A good agreement with our MCDHF calculations performed by the GRASP2018 code and those obtained by NIST.

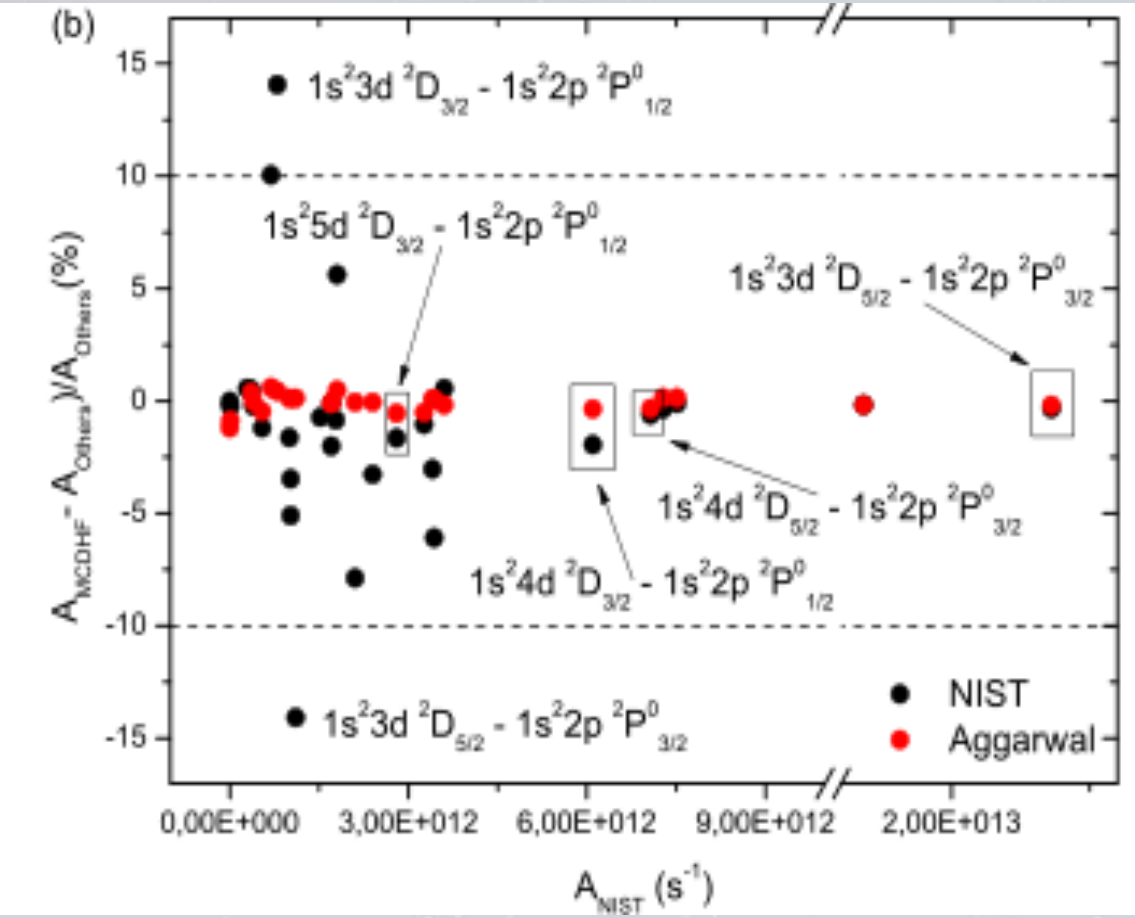

- Electron density, $n_e \geq 1.6 \times 10^{12} T^{\frac{1}{2}} (\Delta E)^3$.
- The relationship between the plasma parameter (Λ), electron density n_e and plasma temperature (T) can be expressed as follows: $\Lambda = 4\pi \times 10^{12}\ {n_e}^{-\frac{1}{2}} T^{\frac{1}{2}}$.
- The coupling parameter (Γ) and the plasma parameter (Λ) are related as follows: $\Gamma \approx \Lambda^{-2/3}$.

- By measuring these two parameters, it becomes possible to distinguish between strongly coupled and weakly coupled plasmas, as well as to determine the plasma's characteristics. Therefore, based on the condition Γ > 1, we can infer that the optically thin plasma in LTE is cold, dense, and strongly coupled

Conclusion

- Calculation of 35 energy levels and the transitions between simply excited states from the configurations $1s^2nl\left(n \leq 6, l \leq (n-1)\right)$ for the Ne VIII, Fe XXIV and Kr XXXIV

- Good agreement between our calculated energy levels using MCDHF method and the available NIST data reflects the quality of calculation of the wave-functions.

- Our analysis of the derived plasma parameters and coupling parameter suggests that the plasma investigated can be characterized as cold, dense and strongly coupled.

- The present complete and consistent results can be used to facilitate the identification of many observed spectral lines in astrophysical and contribute to the control of nuclear fusion reactions in tokamak plasmas.

The End

Thank you for your attention

21

Exact Solvable Two-Body Problem in Two-Dimensional Quantum Mechanics

Roman Kezerashvili, Jianning Luo, Claudio Malvino

Department of Physics

CUNY New York City College of Technology

Two-Dimensional Schrödinger Equation

$$\frac{d^2\phi(r)}{dr^2} + \frac{1}{r}\frac{d\phi(r)}{dr} - \frac{m^2}{r^2}\phi(r) + \frac{2\mu}{\hbar^2}[E - V(r)]\phi(r) = 0$$

$$\frac{d^2u(r)}{dr^2} - \frac{m^2 - \frac{1}{4}}{r^2}u(r) + \frac{2\mu}{\hbar^2}[E - V(r)]\phi(r) = 0$$

Two-Dimensional Schrödinger Equation

$$\frac{d^2\phi(r)}{dr^2} + \frac{1}{r}\frac{d\phi(r)}{dr} - \frac{m^2}{r^2}\phi(r) + \frac{2\mu}{\hbar^2}[E - V(r)]\phi(r) = 0$$

$$\frac{d^2u(r)}{dr^2} - \frac{m^2 - \frac{1}{4}}{r^2}u(r) + \frac{2\mu}{\hbar^2}[E - V(r)]\phi(r) = 0$$

The Nikifurov-Uvarov Method

$$\frac{d^2\phi(z)}{dz^2} + \frac{\widetilde{\tau}(z)}{\sigma(z)}\frac{d\phi(z)}{dz} + \frac{\widetilde{\sigma}(z)}{\sigma^2(z)}\phi(z) = 0$$

$$\sigma(r)\,\frac{d^2u(r)}{dr^2} + \tau(r)\,\frac{du(r)}{dr} + \lambda u(r) = 0$$

Circular Infinite Well

$$V(r) = \begin{cases} 0, & \text{if } r < R, \\ \infty, & \text{if } r \geq R. \end{cases}$$

$$u(z) = z^m e^{iz}$$

$$z\frac{d^2u(z)}{dz^2} + (1 + 2m + 2iz)\frac{du(z)}{dz} + i(2m+1)u(r) = 0$$

$$\sigma(z) = z,\ \tau(z) = 1 + 2m + 2iz, \text{ and } \lambda = i(2m+1)$$

$$\Psi(r,\varphi) = \left(\pi R^2 \left[J_m(kR) - J_{m-1}(kR)J_{m+1}(kR)\right]\right)^{-1/2}$$

$$\frac{1}{\Gamma(m+1)}\left(\frac{kr}{2}\right)^n {}_1F_1\left(m + \frac{1}{2}, 2m+1, 2ikr\right) e^{-i(kr-m)\varphi}$$

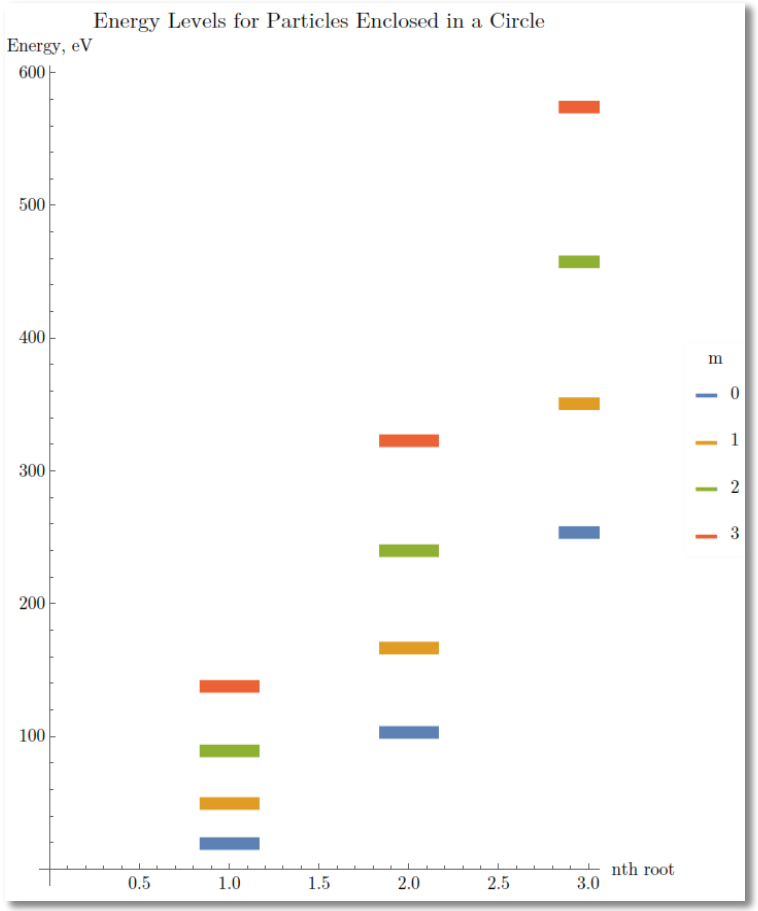

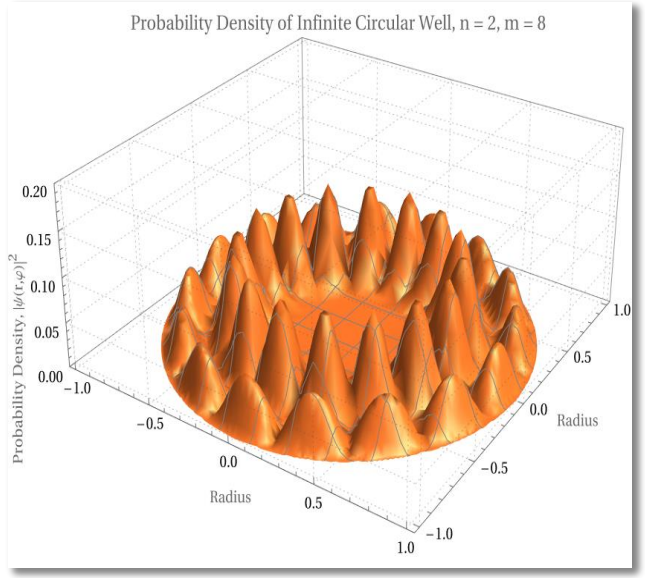

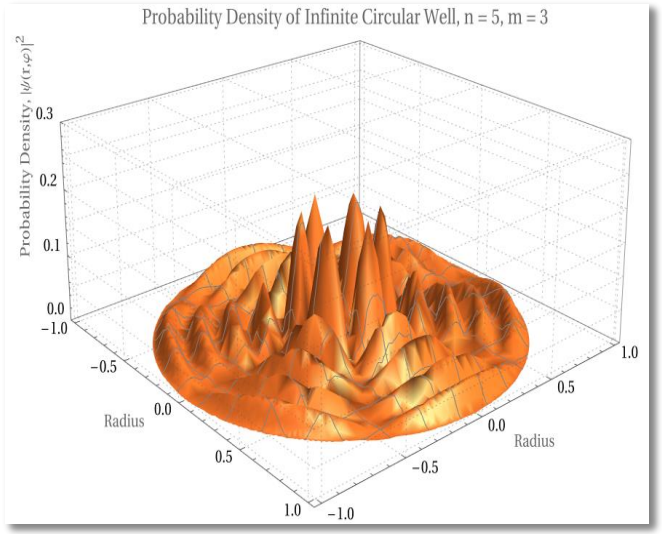

2D Harmonic Oscillator

$$V(r) = \frac{1}{2}\mu\omega^2 r^2$$

$$\phi(z) = z^{m/2} e^{-z/2} u(z)$$

$$z\frac{d^2u(z)}{dz^2} + (m+1-z)\frac{du(z)}{dz} + \frac{1}{4}\left[\frac{k^2}{\gamma} - 2(m+1)\right]u(z) = 0$$

$$\sigma(z) = z,\ \tau(z) = m+1-z,\ \lambda = \tfrac{1}{4}\left[\frac{k^2}{\gamma} - 2(m+1)\right],$$

$$\overline{\sigma} = \tfrac{1}{4}\left[\frac{k^2}{\gamma} - 2(m+1)\right] z = \lambda\sigma(z) \qquad p(z) = \frac{\tau(z)-\widetilde{\tau}(z)}{2} = \frac{m-z}{2},$$

$$\Psi(r,\varphi) = \frac{1}{m!\,(n+1)}\sqrt{\frac{\gamma\,(n+m)!}{\pi n!}}\,(\gamma r^2)^{m/2}\,e^{-\gamma r^2/2}\;{}_1F_1\left(-n, 1+m; \gamma r^2\right) e^{im\varphi}$$

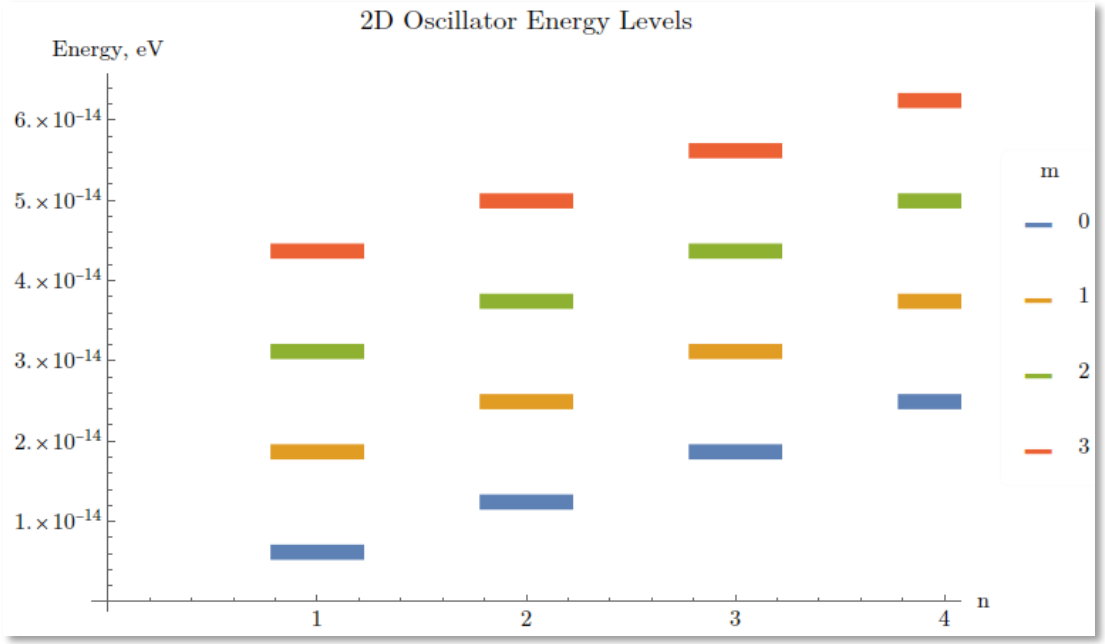

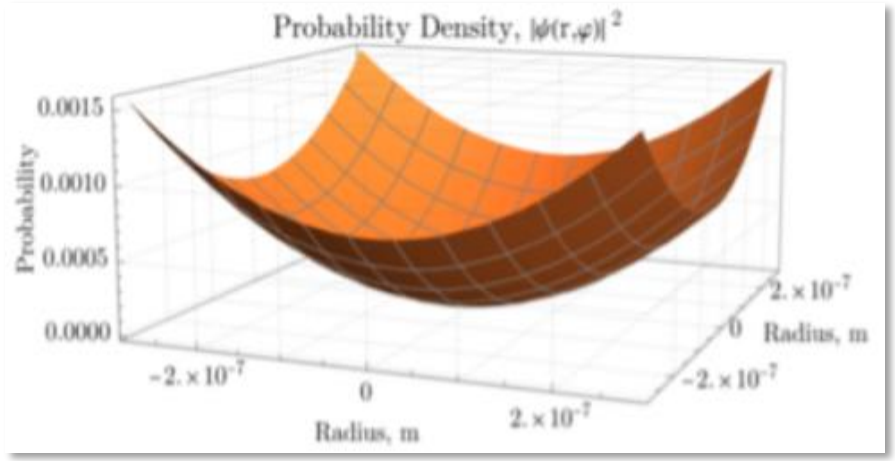

2D Coulomb

$$V(r) = -\Re\frac{e^2}{r}$$

$$\phi(r) = r^m\ e^{-kr}u(r)\ ,\ z = 2kr$$

$$z\frac{d^2u(z)}{dz^2} + (2m+1-z)\frac{du(z)}{dz} + \left(\frac{v^2}{k} - m - \frac{1}{2}\right)u(z) = 0$$

$$\sigma(z) = z,\ \tau(z) = (2m+1-z)2\gamma\ ,\ \lambda = \frac{v^2}{k} - m - \frac{1}{2}$$

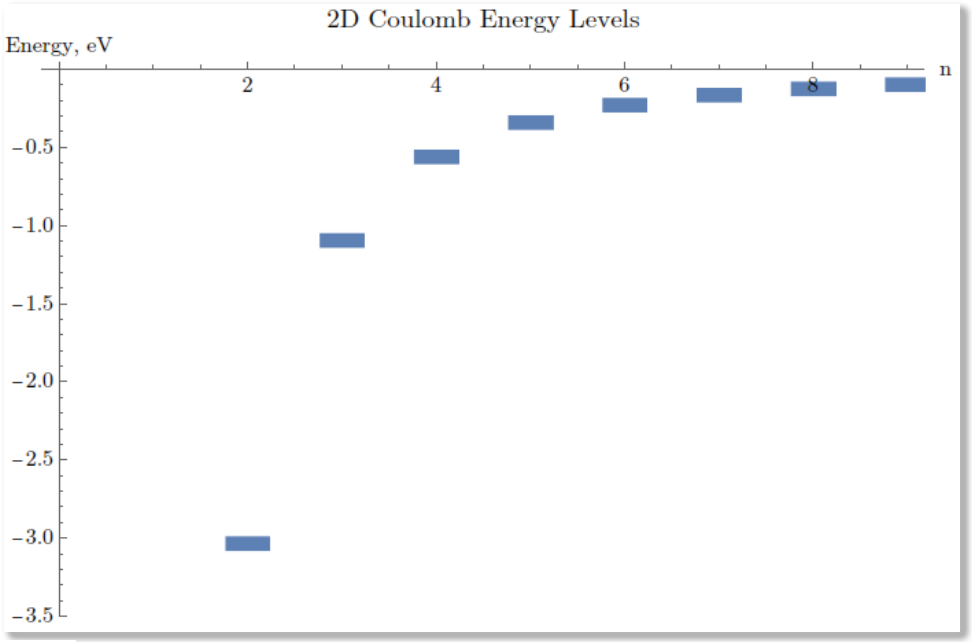

$$\Psi(r,\varphi) = \frac{(2k)^{m+1}}{(2m)!\,(n-m+1)}\sqrt{\frac{(n+m)!}{2\pi\,(2n+1)\,(n-m)!}}r^m\ e^{-kr}\ {}_1F_1\left(-n+m, 1+2m; 2kr\right)e^{im\varphi}$$

Kratzer Potential

$$V(r) = -2D_0\left(\frac{r_0}{r} - \frac{1}{2}\frac{r_0^2}{r^2}\right)$$

$$\phi(z) = z^{\alpha}e^{-\varkappa z}u(z)$$

$$z\frac{d^2u(z)}{dz^2} + (1 + 2\alpha - 2\varkappa z)\frac{du(z)}{dz} - \left(\varkappa + 2\varkappa\alpha - 2\gamma_0^2\right)u(z) = 0$$

$$\sigma(z) = z,\ \tau(z) = 1 + 2\alpha - 2\varkappa z,\ \lambda = -\left(\varkappa + 2\varkappa\alpha - 2\gamma_0^2\right)$$

$$p(z) = \frac{\tau(z) - \widetilde{\tau}(z)}{2} = \alpha - \varkappa z,\ \overline{\sigma}(z) = -\left(\varkappa + 2\varkappa\alpha - 2\gamma_0^2\right)z = \lambda\sigma(z)$$

$$\Psi(r,\varphi) = \frac{(2\varkappa)^{\alpha+1}}{r_0}\sqrt{\frac{n!}{2\pi(2n + 2\alpha + 1)\Gamma(n + 2\alpha + 1)}}\left(\frac{r}{r_0}\right)^{\alpha}e^{-\varkappa\frac{r}{r_0}}\ L_n^{2\alpha}\left(2\varkappa\frac{r}{r_0}\right)e^{im\varphi}$$

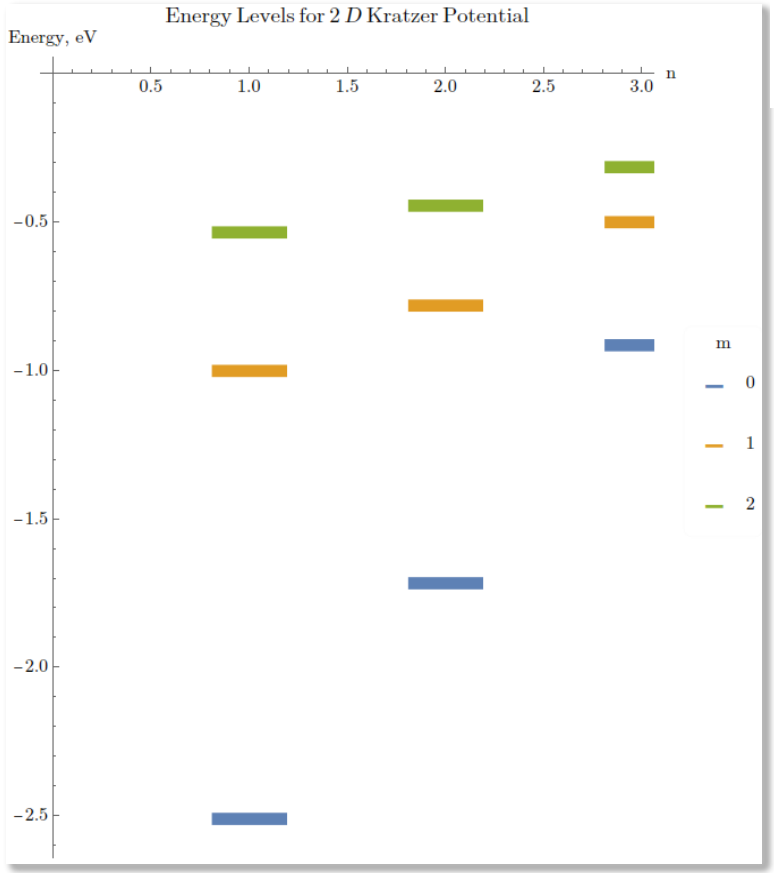

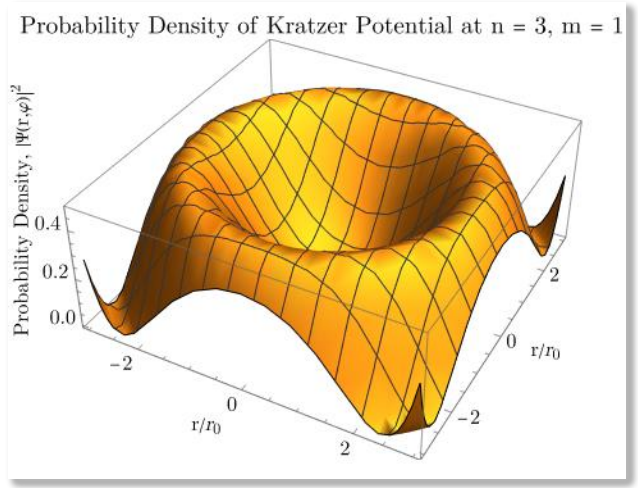

Mod. Kratzer Potential (Electron-Hole)

$$V(r) = -\mathfrak{K}\frac{e^2}{\rho}\left(\frac{r_0}{r} - g^2\,\frac{r_0^2}{r^2}\right)$$

$$\phi(z) = z^{\eta}e^{-\varkappa z}u(z)$$

$$z\frac{d^2u(z)}{dz^2} + (1 + 2\eta - 2\varkappa z)\frac{du(z)}{dz} - (\varkappa + 2\varkappa\eta - 2\delta^2)u(z) = 0$$

$$\sigma(z) = z,\ \tau(z) = 1 + 2\eta - 2\varkappa z,\ \overline{\sigma}(z) = 2\delta^2 z - 2\eta\varkappa z - \varkappa z = \lambda\sigma(z)$$

$$\Psi(r,\varphi) = \frac{(2\varkappa)^{\eta+1}}{r_0}\sqrt{\frac{n!}{(2n+2\alpha+1)\Gamma(n+2\alpha+1)}}\left(\frac{r}{r_0}\right)^{\eta} e^{-\varkappa\frac{r}{r_0}}\ L_n^{2\eta}\left(2\varkappa\frac{r}{r_0}\right)e^{im\varphi}$$

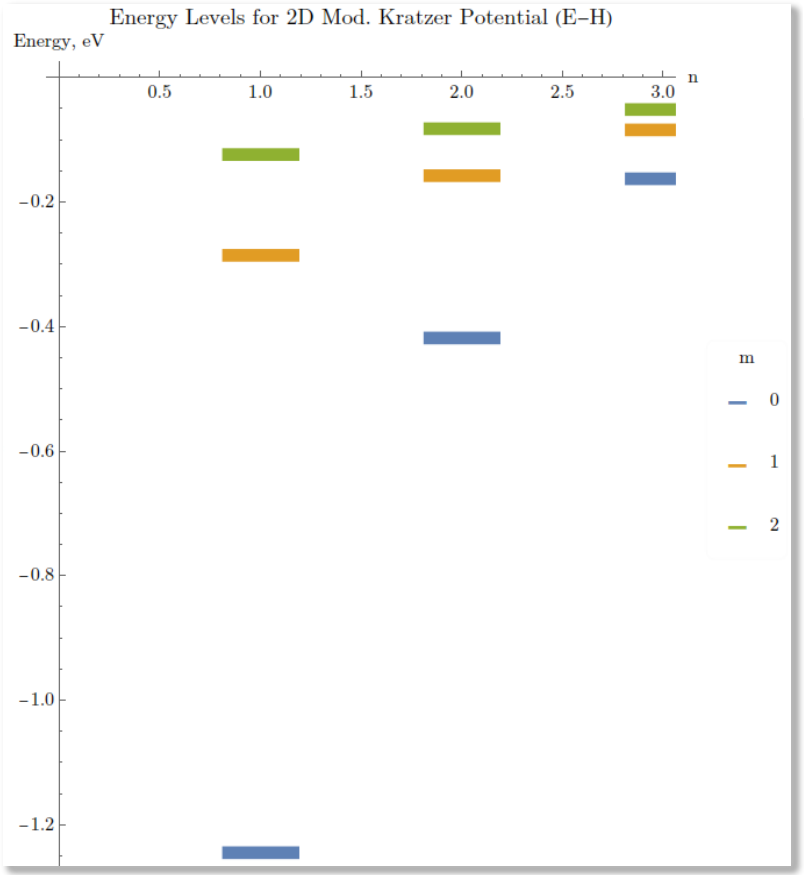

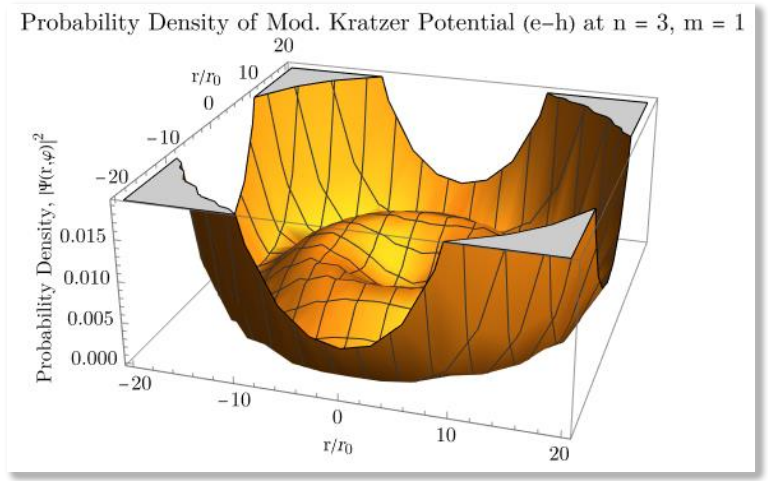

Mod. Kratzer Potential (Diatomic)

$$V(r) = D_0 \left(\frac{r - r_0}{r} \right)^2$$

$$\phi(z) = z^{\alpha} e^{-\beta z} u(z), \qquad x = 2\beta z$$

$$x \frac{d^2 u(x)}{dx^2} + (1 + 2\alpha - x) \frac{du(x)}{dx} - \left[\frac{1}{2} + \alpha - \frac{\gamma_0^2}{\beta} \right] u(x) = 0$$

$$\Psi(r, \varphi) = \frac{(2\beta)^{\alpha+1}}{r_0} \sqrt{\frac{n!}{2\pi(2n + 2\alpha + 1)\Gamma(n + 2\alpha + 1)}} \left(\frac{r}{r_0} \right)^{\alpha} \mathrm{e}^{-\beta \frac{r}{r_0}} \; L_n^{2\alpha} \left(2\beta \frac{r}{r_0} \right) e^{im\varphi}$$

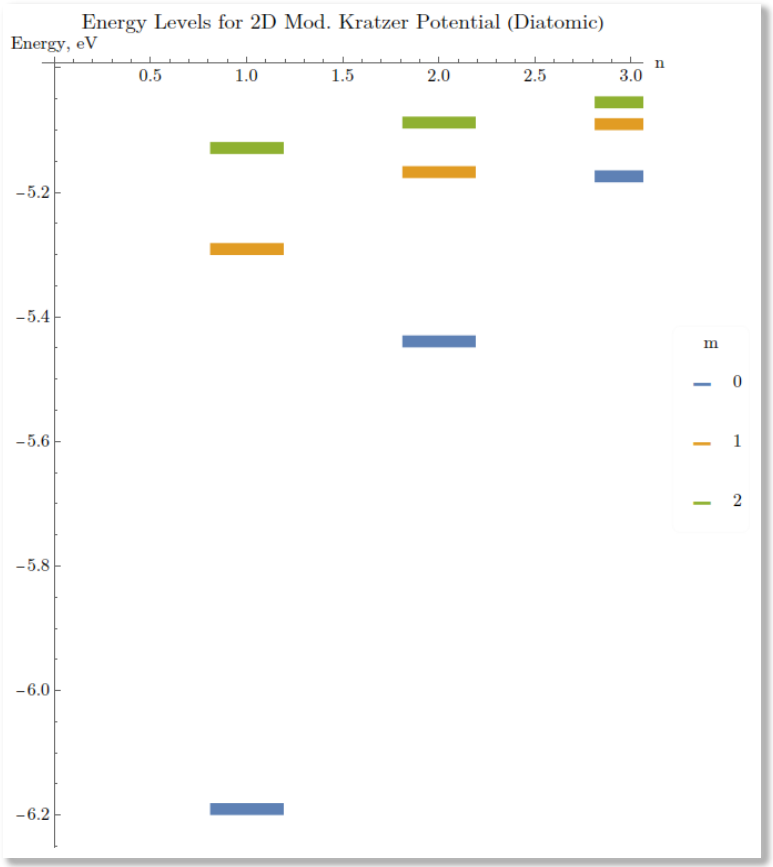

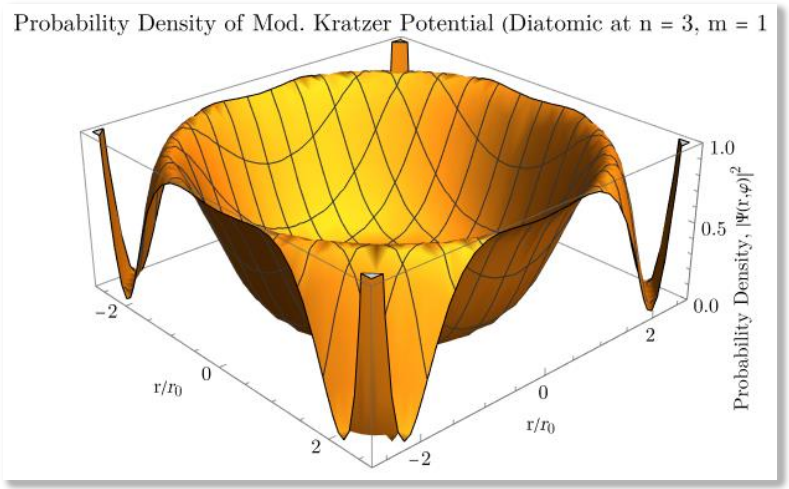

Thank You!

Danke!

2023/8/4
EFB25 Poster Session # 22

Preparation for Spin Correlation Coefficients Measurement in Polarized Deuteron-Polarized Proton Scattering Experiment

Department of Physics, Graduate School of Science, Tohoku University
Exotic Nuclear Physics Group
Yuko Saito

- **Tokyo Tech. Univ. :** K. Sekiguchi, A. Watanabe, K. Suzuki, H. Sugahara, D. Takahashi
- **Tohoku Univ. :** Y. Maruta, T. Matsui
- **RIKEN :** K. Tateishi, D. Miura, N. Sakamoto, H. Otsu, T. Uesaka, H. Sakai
- **Kyushu Univ. :** T. Wakasa, K. Nishibata, K. Hirasawa, K. Aradono, T. Kajihara, S. Sakaguchi
- **QST :** T. Wakui

1. Introduction

Study of 3*N*Fs via few-nucleon scattering experiments

- momentum, spin, isospin dependence of the 3*N*Fs

  Direct comparison between…

  - **high-precision data** in few-nucleon scattering (differential cross sections, spin observables)
  - **theoretical predictions** based on rigorous numerical calculations

- d- p scattering (E/A 70–300 MeV)

  Differential cross section
  →3NF effect observed at cross section minimum

  Spin observables
  →some data not explained by incorporating 3*N*Fs

  →defects in spin dependent parts of 3*N*Fs potentials?

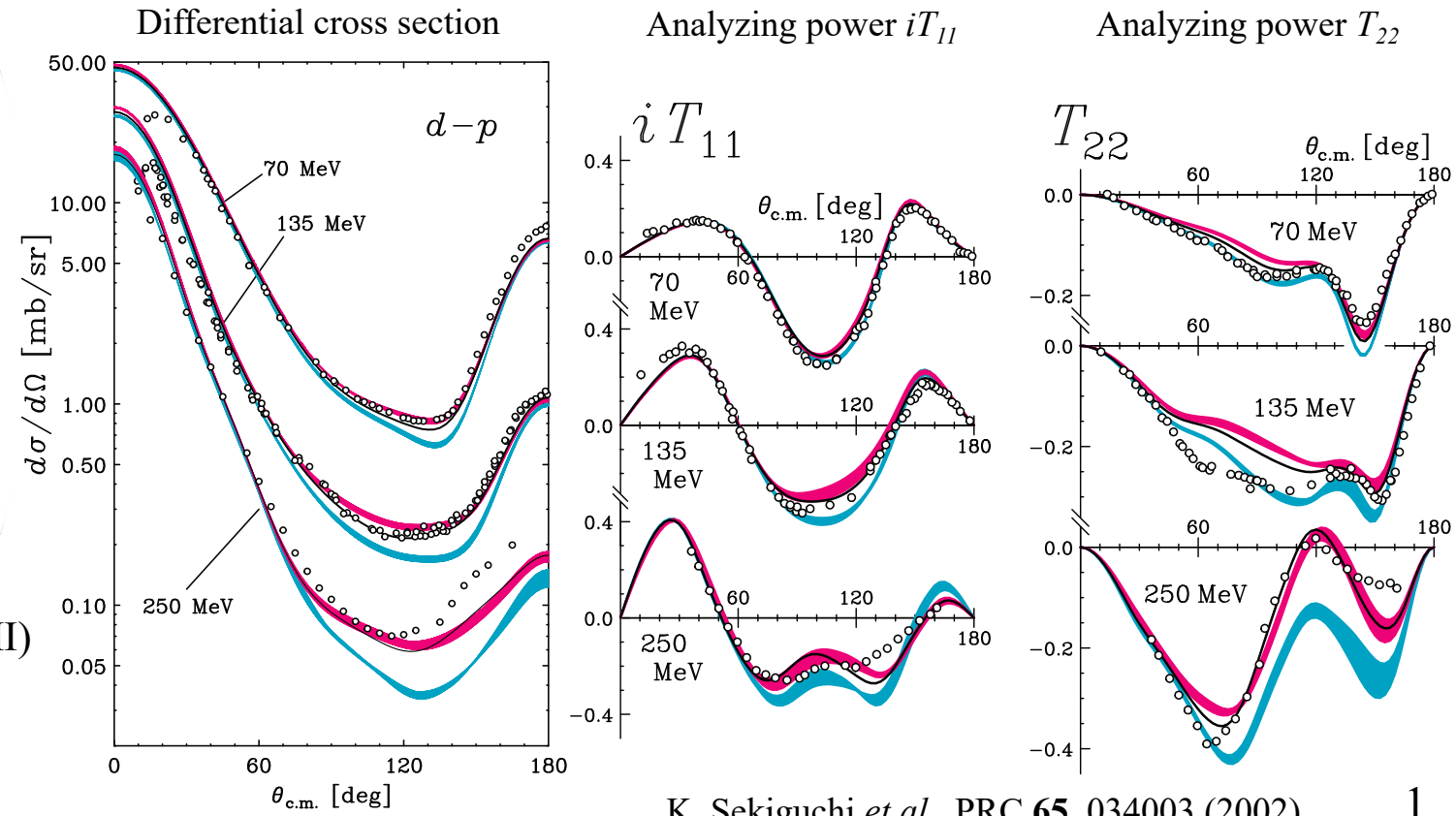

K. Sekiguchi *et al.*, PRC **65**, 034003 (2002).

Chiral Effective Theory and Three-Nucleon Force

Chiral Effective Theory

- Newly progressing theory based on low energy QCD

χEFT's 3*N* : aim to develop an accurate potential at N^{4}LO

→**low energy constants (LECs)** must be fixed from experimental data

11/13 LECs can be probed in *d-p* scattering
→ *data of spin observables crucial*

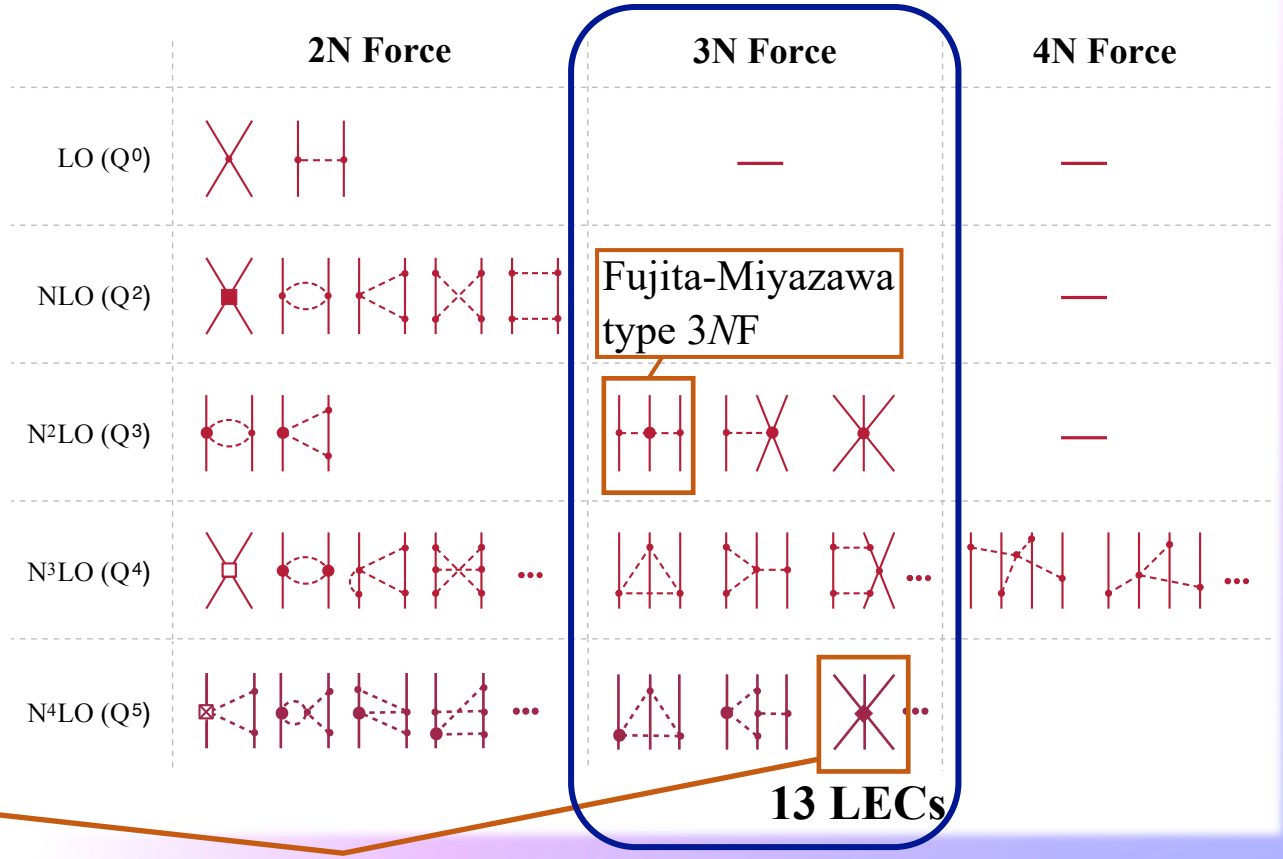

E. Epelbaum, arXiv:1908.09349 (2019).

measurement of **spin correlation coefficients** in *d* - *p* scattering
→ complete set of spin observables
→ determination of 11 LECs in N^{4}LO's 3*N*F sector

2. Experiment

Measurement of Spin Correlation Coefficients in $\vec{d}$ - $\vec{p}$ elastic scattering

- Polarized deuteron beam ($\vec{d}$) : polarized ion source @ RIKEN RIBF H. Okamura *et al.*, AIP Conf. Proc. **293**, 84 (1994).
- Polarized proton target ($\vec{p}$) : newly developed based on triplet-DNP method (2021~)

Polarized cross sections of Left, Right, Up, Down directions

$$L(\theta) = L_0(\theta)\left\{1 + \frac{3}{2}p_y\left(A_y^d(\theta) + p_y^T C_{y,y}(\theta)\right) + p_y^T A_y^p(\theta) + \frac{1}{2}p_{yy}\left(A_{yy}^d(\theta) + p_y^T C_{yy,y}(\theta)\right)\right\},$$

$$R(\theta) = R_0(\theta)\left\{1 + \frac{3}{2}p_y\left(-A_y^d(\theta) + p_y^T C_{y,y}(\theta)\right) - p_y^T A_y^p(\theta) + \frac{1}{2}p_{yy}\left(A_{yy}^d(\theta) - p_y^T C_{yy,y}(\theta)\right)\right\},$$

$$U(\theta) = U_0(\theta)\left\{1 + \frac{3}{2}p_y p_y^T C_{x,x}(\theta) + \frac{1}{2}p_{yy}A_{xx}^d(\theta)\right\},$$

$$D(\theta) = D_0(\theta)\left\{1 + \frac{3}{2}p_y p_y^T C_{x,x}(\theta) + \frac{1}{2}p_{yy}A_{xx}^d(\theta)\right\}.$$

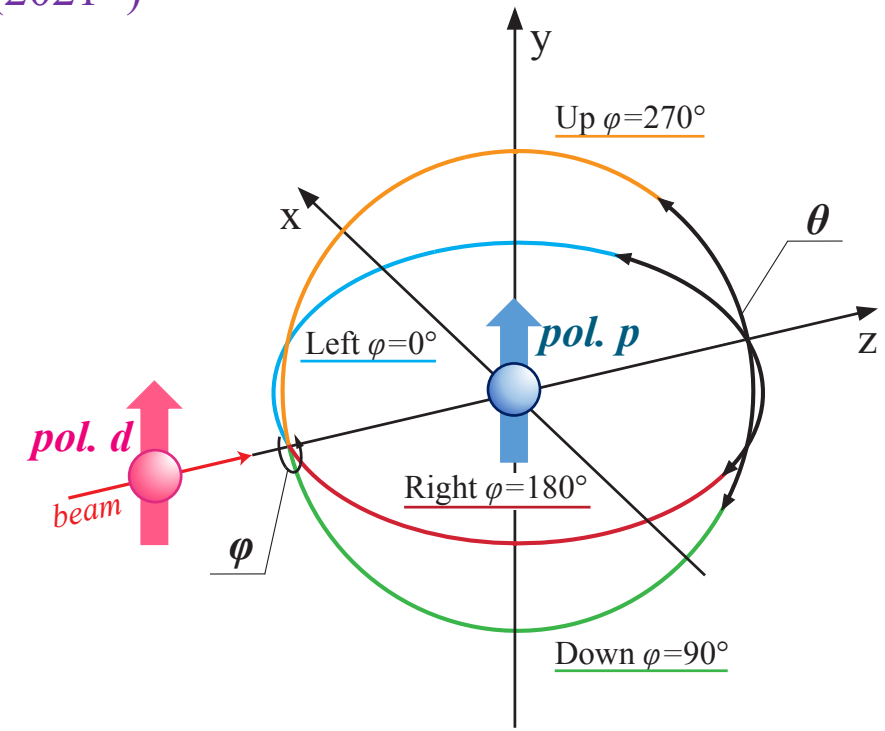

❖ **New detector system developed** for
Measurement of *L, R, U, D* at wide angular (θ) range

❖ **First beam test on the new detector system**:
→ p - $\vec{p}$ Experiment @ 200 MeV, HIMAC (2022.12.26 - 30)

Resonances of exotic helium-like systems

Jean Servais, École Polytechnique de Bruxelles, ULB

August 3rd, 2023

ULB

23

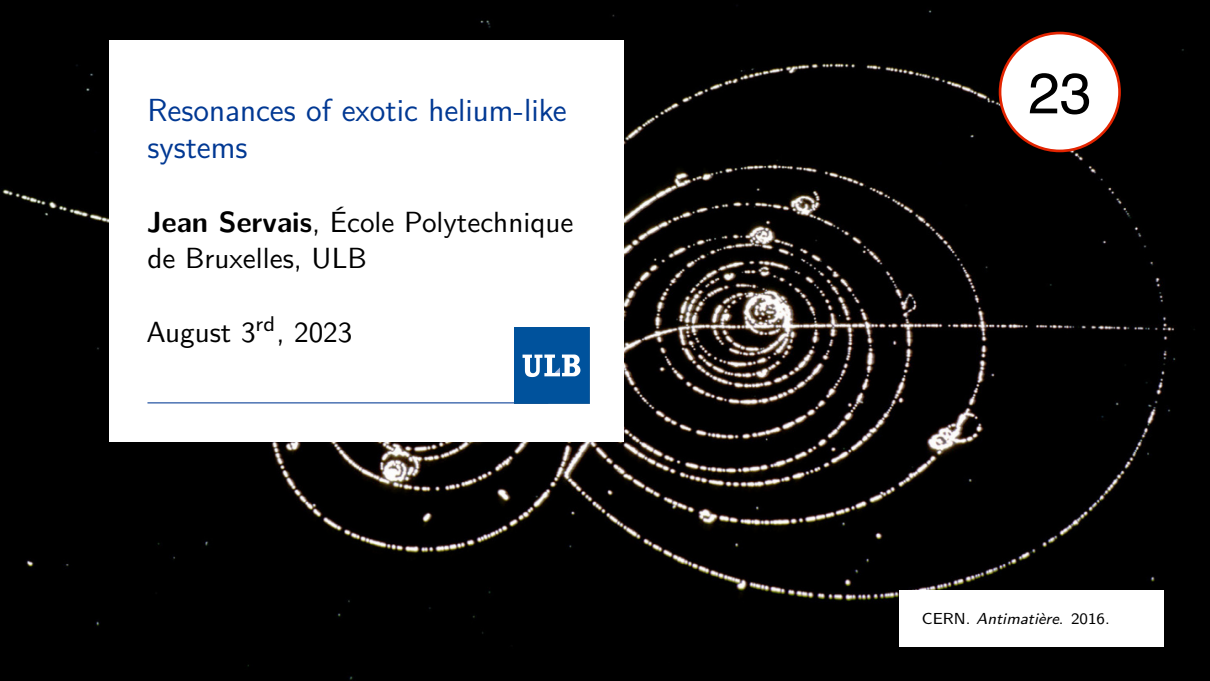

CERN. *Antimatière*. 2016.

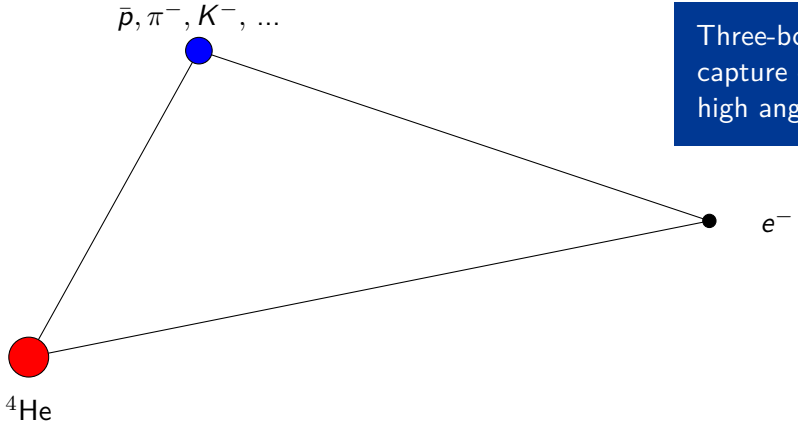

Three-body exotic systems: capture of the exotic particle at high angular momentum L

Figure: Helium-like exotic system.

Cascade process in antiprotonic helium

- Large angular momentum, $L = 30 - 40$
- Auger (e^-) emission or EM transitions
- Spectroscopy to obtain the antiproton mass [Hori, 2006]

Objective:
Compute the Auger widths using the **Kohn variational method** and Lagrange-mesh method

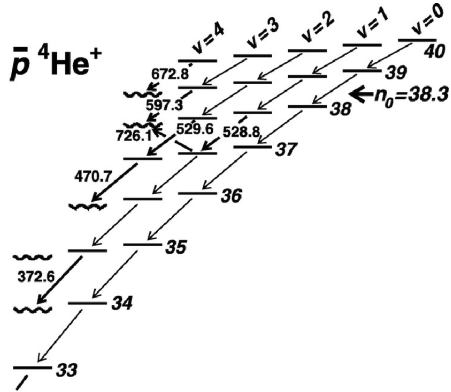

Figure: Extracted from [Hori, 2011]

[Hori, 2006] M. Hori et al., Phys. Rev. Lett. 96, 243401 (2006).
[Hori, 2011] M. Hori, Can. Jour. Phys. 89.1 (2011).

Results for antiprotonic helium

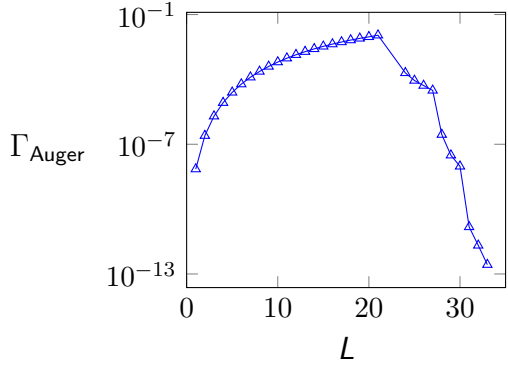

Perspectives: Study the Auger widths for other exotic systems
Compute the EM transitions and the relativistic corrections

Cluster Effective Field Theory calculation of electromagnetic breakup reactions with Lorentz Integral Transform method

24

Ylenia Capitani [1]
Elena Filandri [2] Chen Ji [3] Giuseppina Orlandini [1] Winfried Leidemann [1]

UNIVERSITÀ DI TRENTO

[1]Università di Trento and INFN-TIFPA, Trento, Italy
[2]Università del Salento and INFN, Lecce, Italy
[3]Central China Normal University, Wuhan, China

TIFPA Trento Institute for Fundamental Physics and Applications

25th European Conference on Few-Body Problems in Physics
Mainz, 3 August 2023

25 EFB

$$\gamma + {}^9\mathrm{Be} \rightarrow \alpha + \alpha + n$$

Study of the reaction in the **low-energy regime**:

- ^{9}Be 3-body ($\alpha\alpha n$) binding energy
- Cross section

$$\gamma + {}^9\mathrm{Be} \to \alpha + \alpha + n$$

Model

- Effective particles: **nucleons** and α-**particles**
- Interaction: potential models from **Effective Field Theory** (EFT)
  (2-body and 3-body potentials)
  [Hammer *et al.* (2017)]

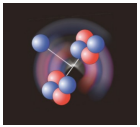

P. Mueller/Argonne National Lab

EFT approach: why?

^{9}Be binding $B_3 \approx 1.573$ MeV $<<$ α binding (≈ 20 MeV)
↓
shallow binding

$\Rightarrow$ ^{9}Be is a 3-body *effective* clustering system

$\Rightarrow$ Separation of scales $\to$ EFT approach

$$\gamma + {}^9\mathrm{Be} \to \alpha + \alpha + n$$

Method

- Bound-state problem:
  the variational method with a **Non-Symmetrized Hyperspherical Harmonics** (NSHH) basis
  [Deflorian *et al.* (2013)]

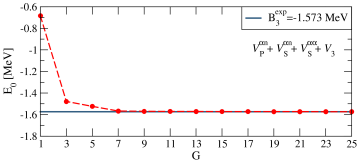

- Continuum problem:
  the **Lorentz Integral Transform** (LIT) method
  [Efros *et al.* (2007)]

$\gamma + {}^9\mathrm{Be} \to \alpha + \alpha + n$ $\quad \gamma : \hat{\epsilon}_{\boldsymbol{q},\lambda},\ \omega = |\boldsymbol{q}|$

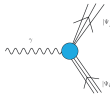

Bacca *et al* (2014)

Results

$$\sigma_\gamma \propto \mathcal{R}_\gamma(\omega) \sim \langle \Psi_f | \hat{\epsilon}_{\boldsymbol{q},\lambda} \cdot \boldsymbol{J}(\boldsymbol{q}) | \Psi_0 \rangle \leftarrow \text{Nuclear Current m.e.}$$

$$\boldsymbol{J} = \boldsymbol{J}_{\text{1-body}} + \boldsymbol{J}_{\text{2-body}} + \dots$$

We make two types of calculations (E1 contribution):

1. we use the **one-body current** $\boldsymbol{J}_{\text{1-body}}$ [Filandri (2022)]
2. we calculate the **dipole operator m.e.** $\langle \Psi_f | \boldsymbol{D} | \Psi_0 \rangle$

Why? The *Siegert theorem*, at low energy, ensures that the dipole operator contains the contribution of the 1-body current and beyond

$\Rightarrow$ inclusion of $\boldsymbol{J}_{\text{2-body}}$ and $\boldsymbol{J}_{\text{3-body}}$ contribution to σ_γ

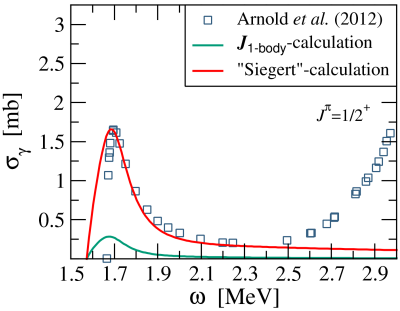

$\gamma + {}^9\mathrm{Be} \to \alpha + \alpha + n$ $\gamma : \hat{\epsilon}_{\boldsymbol{q},\lambda},\ \omega = |\boldsymbol{q}|$

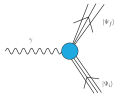

Bacca *et al* (2014)

Results

$$\sigma_\gamma \propto \mathcal{R}_\gamma(\omega) \sim \langle \Psi_f | \hat{\epsilon}_{\boldsymbol{q},\lambda} \cdot \boldsymbol{J}(\boldsymbol{q}) | \Psi_0 \rangle \leftarrow \text{Nuclear Current m.e.}$$

$$\boldsymbol{J} = \boldsymbol{J}_{\text{1-body}} + \boldsymbol{J}_{\text{2-body}} + \dots$$

We make two types of calculations (E1 contribution):

1. we use the **one-body current** $\boldsymbol{J}_{\text{1-body}}$ [Filandri (2022)]
2. we calculate the **dipole operator m.e.** $\langle \Psi_f | \boldsymbol{D} | \Psi_0 \rangle$

Why? The *Siegert theorem*, at low energy, ensures that the dipole operator contains the contribution of the 1-body current and beyond

$\Rightarrow$ inclusion of $\boldsymbol{J}_{\text{2-body}}$ and $\boldsymbol{J}_{\text{3-body}}$ contribution to σ_γ

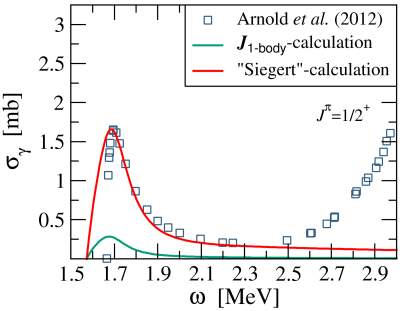

Thank You!

TRIUMF

Standard Model corrections to Fermi transitions in light nuclei

Michael Gennari

TRIUMF and University of Victoria

Research supervisor: Petr Navrátil

Academic supervisor: Robert Kowalewski

Collaborators: Mehdi Drissi, Mack Atkinson, Chien-Yeah Seng, Misha Gorchtein

University of Victoria

FRIB

JOHANNES GUTENBERG UNIVERSITÄT MAINZ

Discovery, accelerated

Beta decay in the Standard Model

$$\mathcal{L}_{\mathrm{CC}} = -\frac{G_F}{\sqrt{2}} \begin{pmatrix} \bar{u}_L & \bar{c}_L & \bar{t}_L \end{pmatrix} \gamma^\mu W_\mu^+ V_{\mathrm{CKM}} \begin{pmatrix} d_L \\ s_L \\ b_L \end{pmatrix} + \mathrm{h.c.}$$

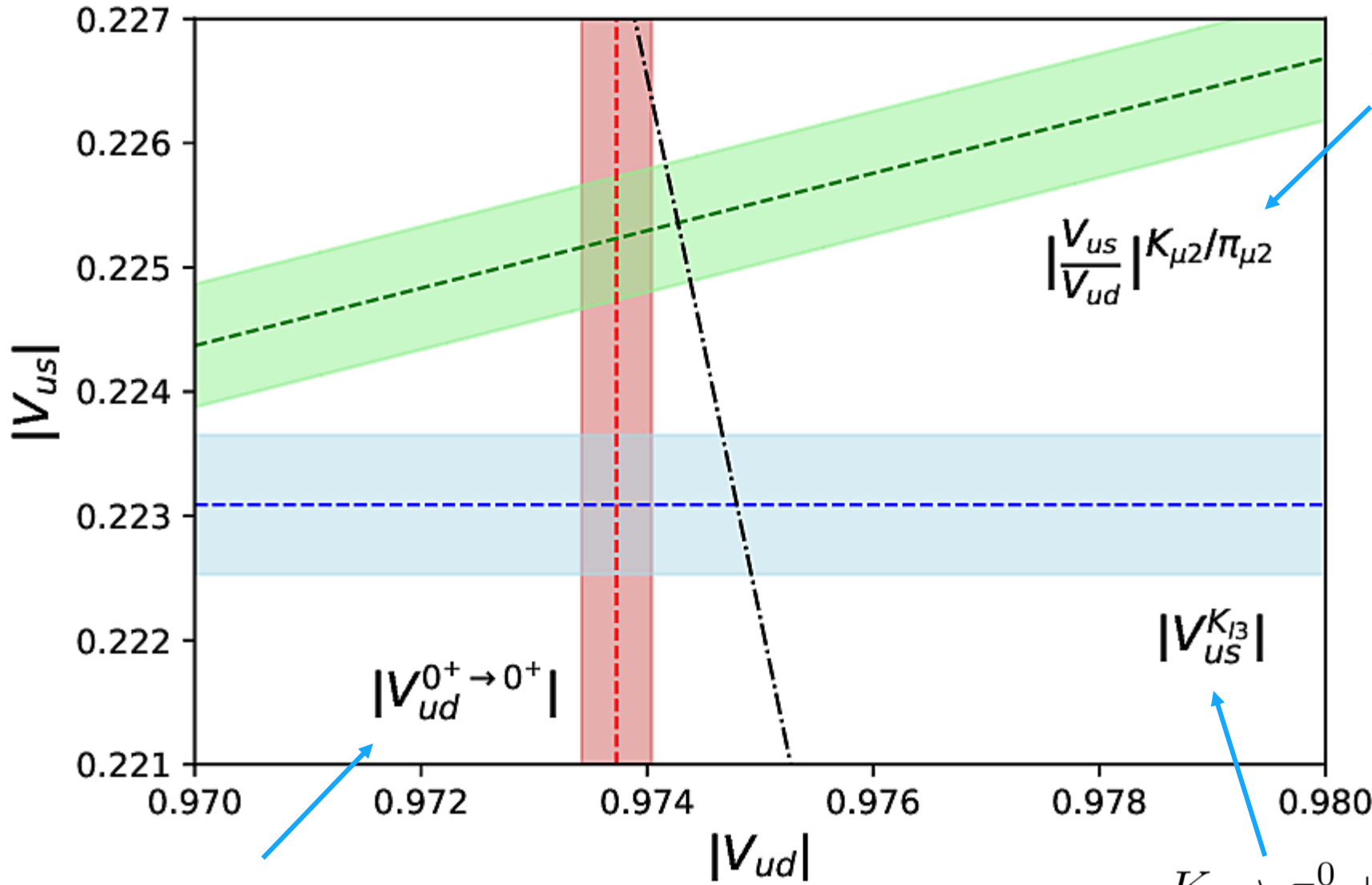

$K \to \mu^+ + \nu_\mu$

$\pi^+ \to \mu^+ + \nu_\mu$ 3

$|0^+\rangle \to |0^+\rangle$

$K \to \pi^0 + e^+ + \nu_e$

$K \to \pi^0 + \mu^+ + \nu_\mu$

Seng (2022) and references therein.

V_{ud} element of CKM matrix

	$\lvert V_{ud}\rvert$
superallowed	0.97373(31)[19]
n	0.97377(90)[20]
nuclear mirror	0.9739(10)[21]
π_{e3}	0.9740(28)[22]

	$\lvert V_{us}\rvert$
$K_{\ell 3}$	0.22309(56)[23]
τ	0.2221(13)[24]
Hyperon	0.2250(27)[25]

	$\lvert V_{us}/V_{ud}\rvert$
$K_{\mu 2}/\pi_{\mu 2}$	0.23131(51)[23]
$K_{\ell 3}/\pi_{e3}$	0.22908(87)[23]

$$|0^+\rangle \rightarrow |0^+\rangle$$

$$n \rightarrow p e^- \bar{\nu}_e$$

$$\pi^+ \rightarrow \pi^0 e^+ \nu_e(\gamma)$$

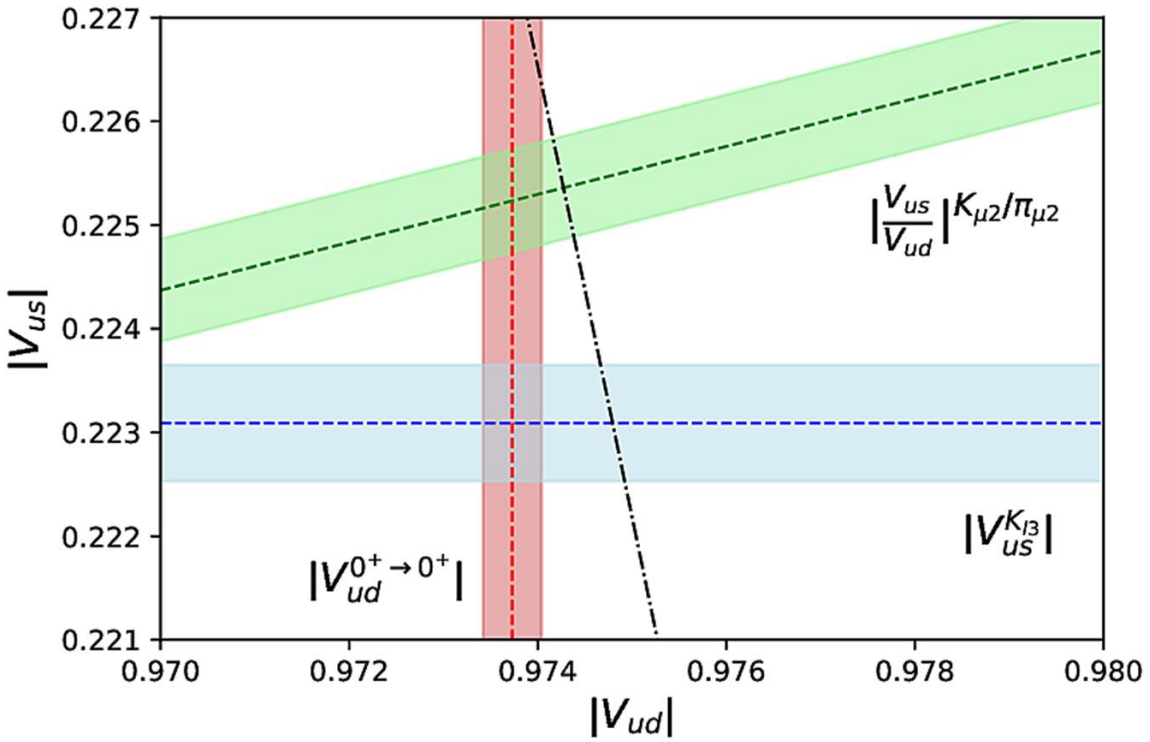

Beta decay in the Standard Model

$$\mathcal{L}_{\mathrm{CC}} = -\frac{G_F}{\sqrt{2}} \begin{pmatrix} \bar{u}_L & \bar{c}_L & \bar{t}_L \end{pmatrix} \gamma^\mu W_\mu^+ V_{\mathrm{CKM}} \begin{pmatrix} d_L \\ s_L \\ b_L \end{pmatrix} + \mathrm{h.c.}$$

$$|V_{ud}|^2 = \frac{\hbar^7}{G_F^2 m_e^5 c^4} \frac{\pi^3 \ln(2)}{\mathcal{F}t(1+\Delta_R^V)}$$

$$\left|0^+\right\rangle \rightarrow \left|0^+\right\rangle$$

$G_F \equiv$ Fermi coupling constant
determined from muon β decay

Zyla et al. (2020)

V_{ud} element of CKM matrix

$$|V_{ud}|^2 = \frac{\hbar^7}{G_F^2 m_e^5 c^4} \frac{\pi^3 \ln(2)}{\mathcal{F}t(1+\Delta_R^V)}$$

- hadronic matrix elements modified by nuclear environment
- Fermi matrix element renormalized by isospin non-conserving forces

$$\mathcal{F}t = ft(1+\delta'_R)(1-\delta_C+\delta_{NS}) \qquad \mathcal{F}t = \frac{K}{G_V^2 |M_{F0}|^2 (1+\Delta_R^V)}$$

Zyla et al. (2020)

Standard Model

Chiral Effective Field Theory

Entem et al. (2017)
Somà et al. (2020)

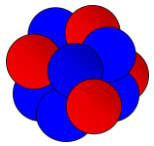

$$H\left|\Psi_A^{J^\pi T}\right\rangle = E^{J^\pi T}\left|\Psi_A^{J^\pi T}\right\rangle$$

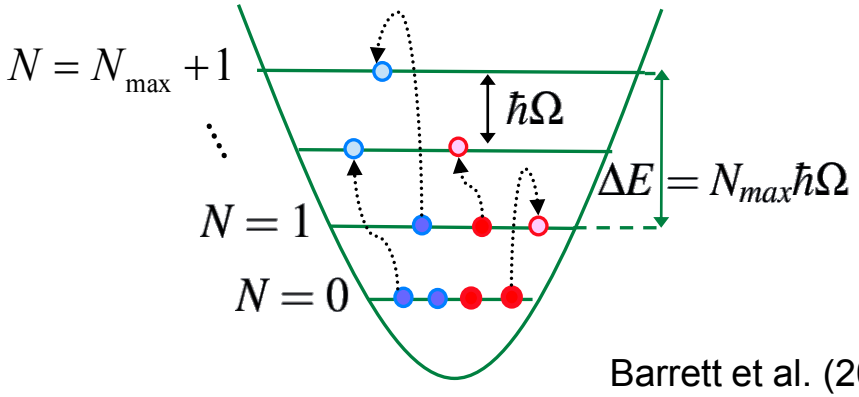

Barrett et al. (2013)
Haydock (1974)

E

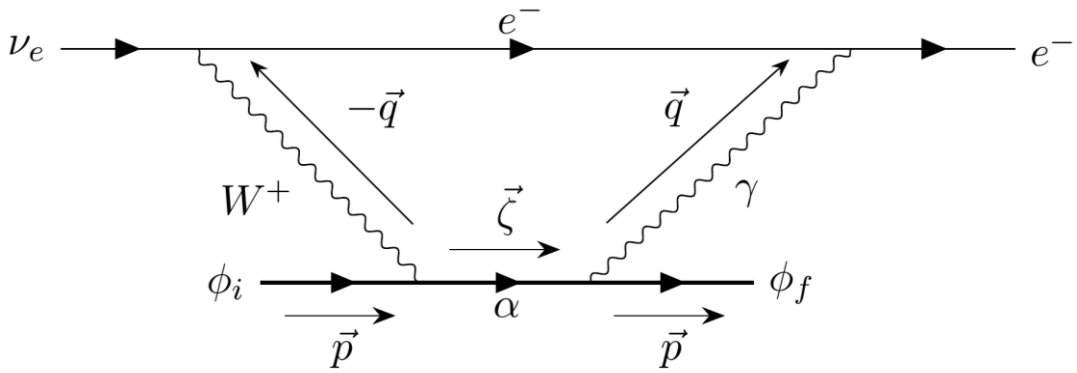

- **Goal**: Non-relativistic currents
- Generalized multipole expansion

Haxton et al. (2007)
Seng et al. (2023)

M. Gorshteyn, Private Communication.
Hardy et al. (2020)

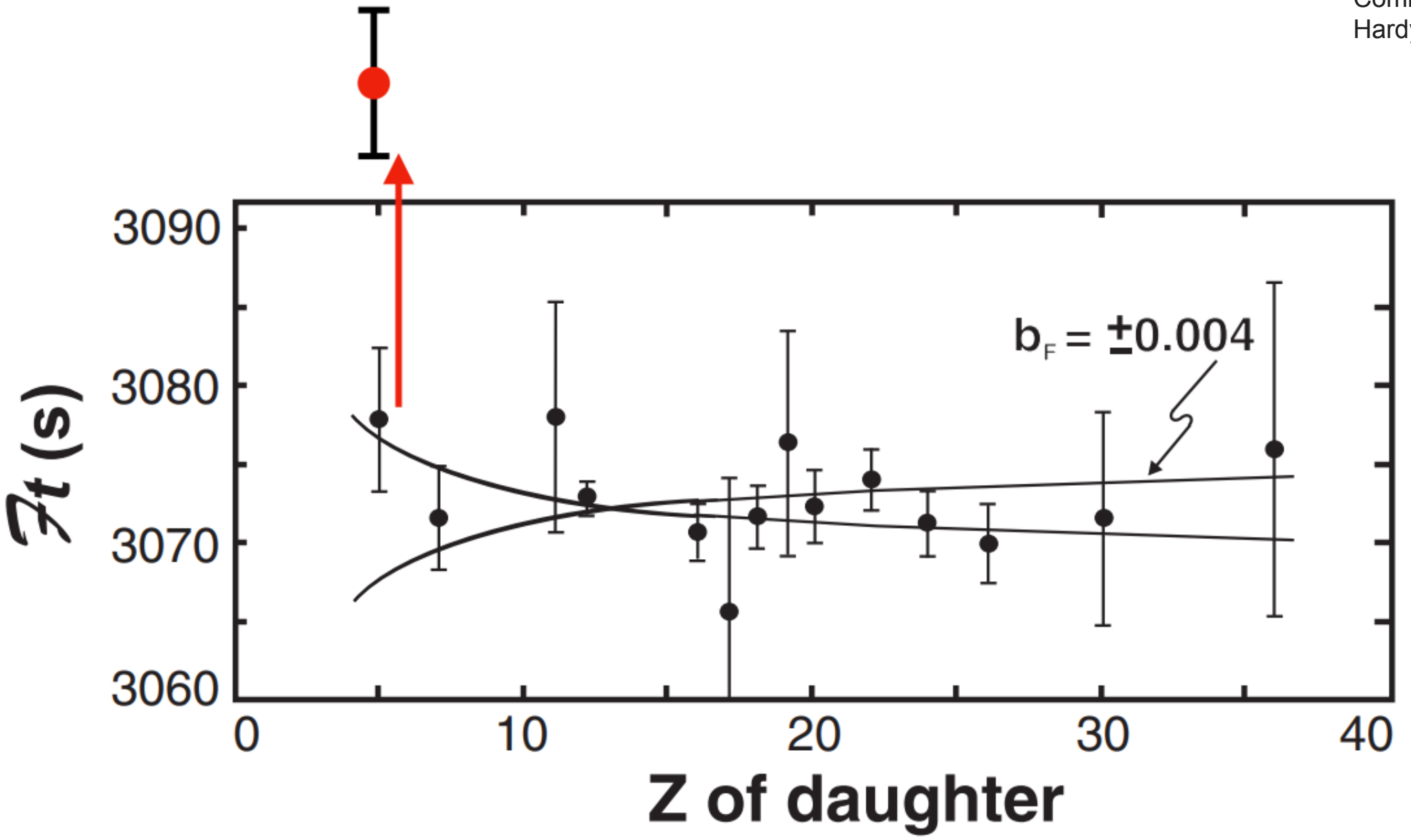

TRIUMF

Thank you
Merci

www.triumf.ca

Follow us **@TRIUMFLab**

Discovery, accelerated

Five-body calculations of s-wave n-^{4}He scattering at NLO with $\not\pi$EFT

Mirko Bagnarol

Hebrew University of Jerusalem
Racah Institute of Physics

3rd August 2023

$\not\pi$EFT interaction

	2-body	3-body	4-body	5-body
LO	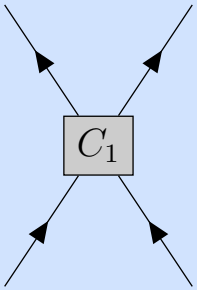	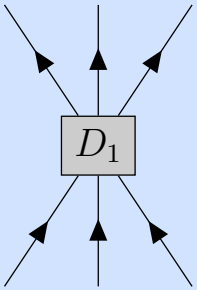	–	–
NLO	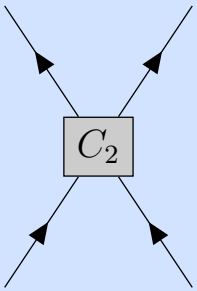	–	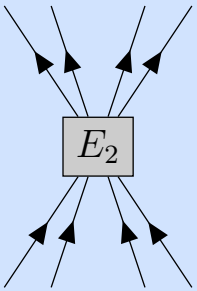	–
N^{2}LO	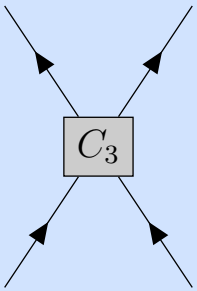	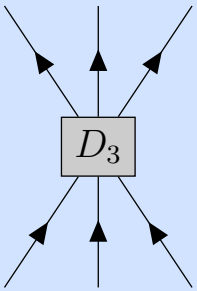	?	?

Application to ^{4}He+n scattering

- We applied our interaction to ^{4}He+n scattering in the $^2S_{\frac{1}{2}^+}$ channel
- We confined our system in an harmonic potential and used the Busch formula to extract the scattering parameters, a_0 and r_{eff}
- We solved the Schrödinger equation with the Stochastic Variational Method (SVM)

Phase shifts

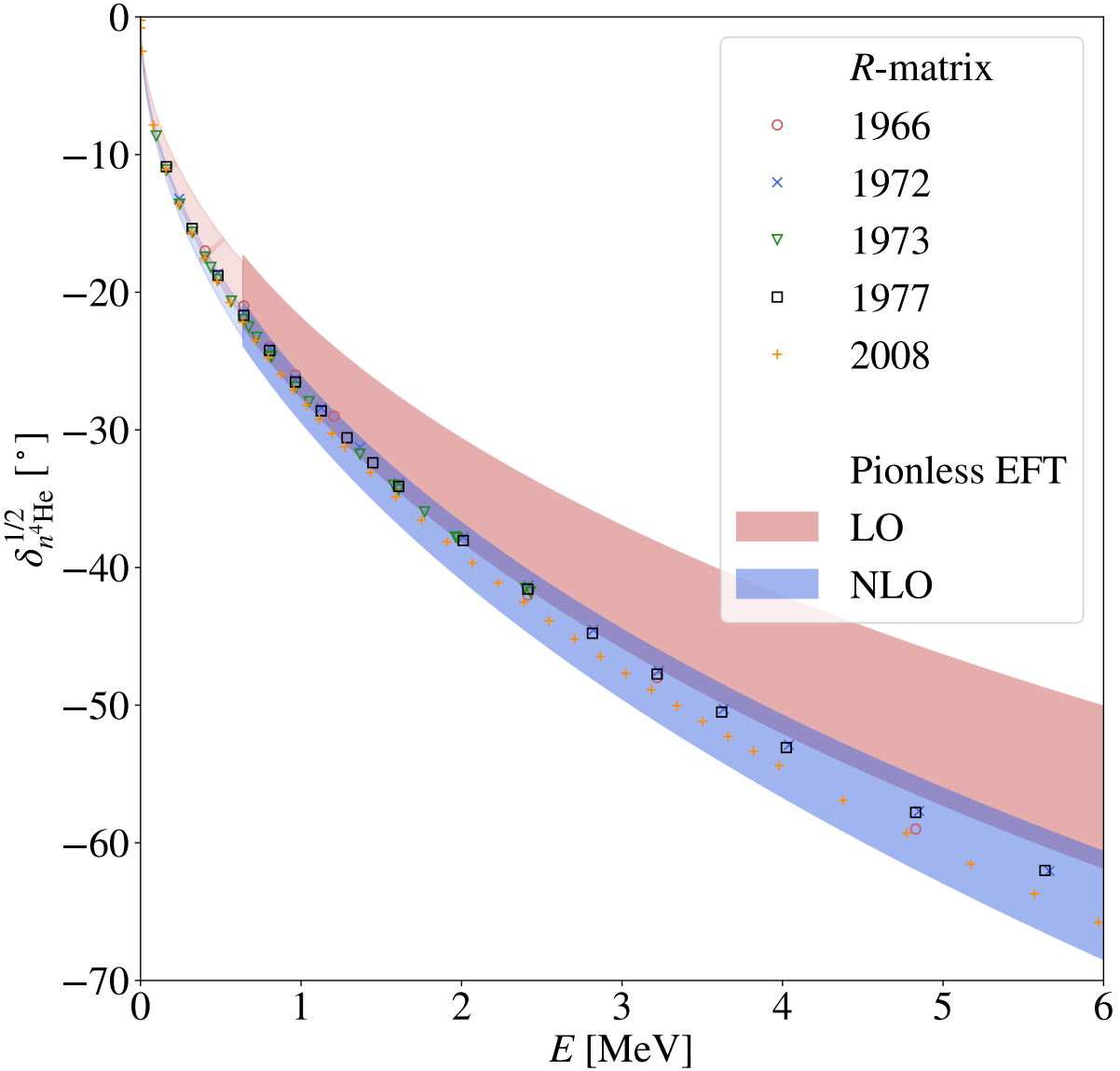

Scattering parameters

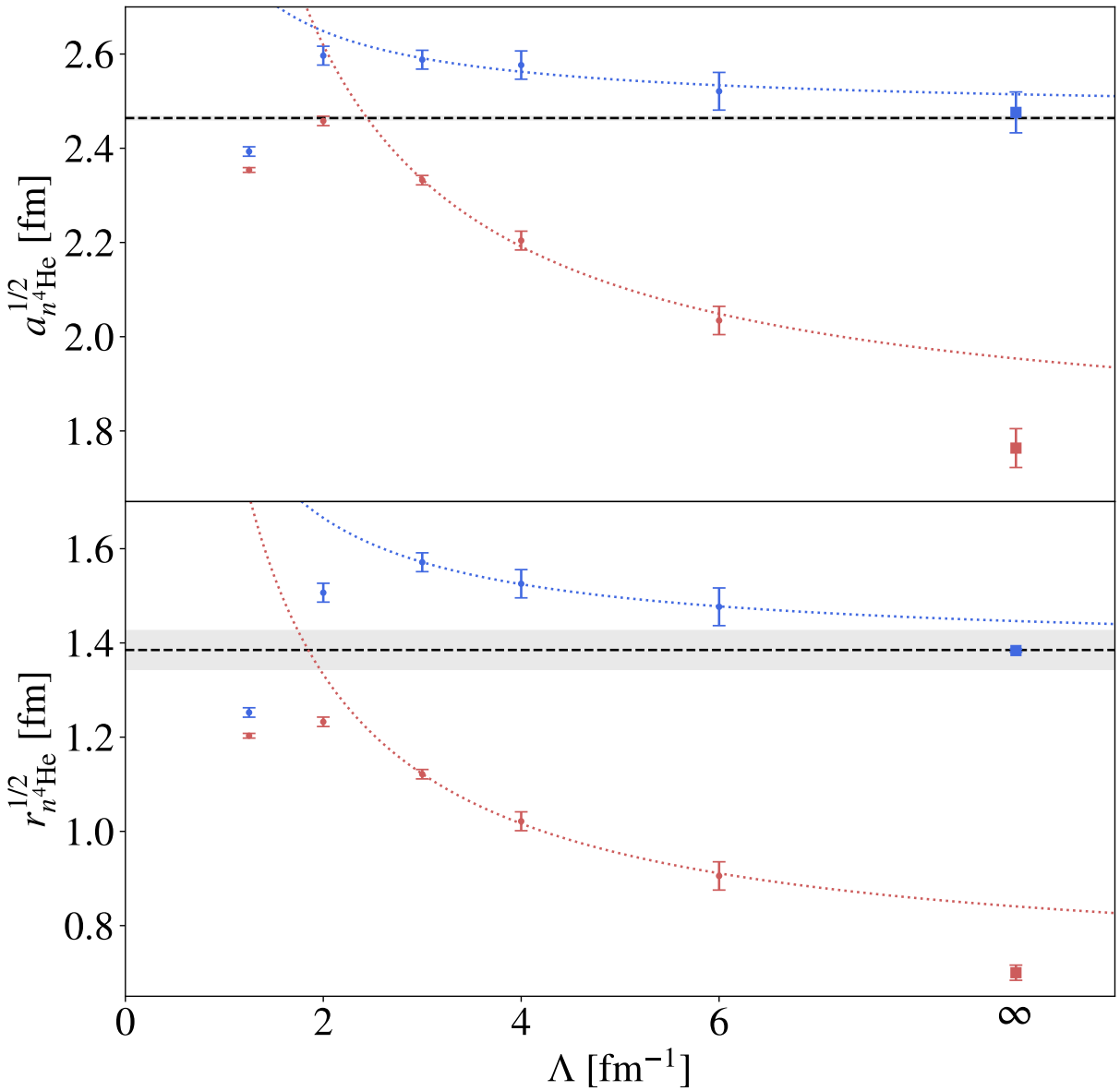

a_0 in the literature

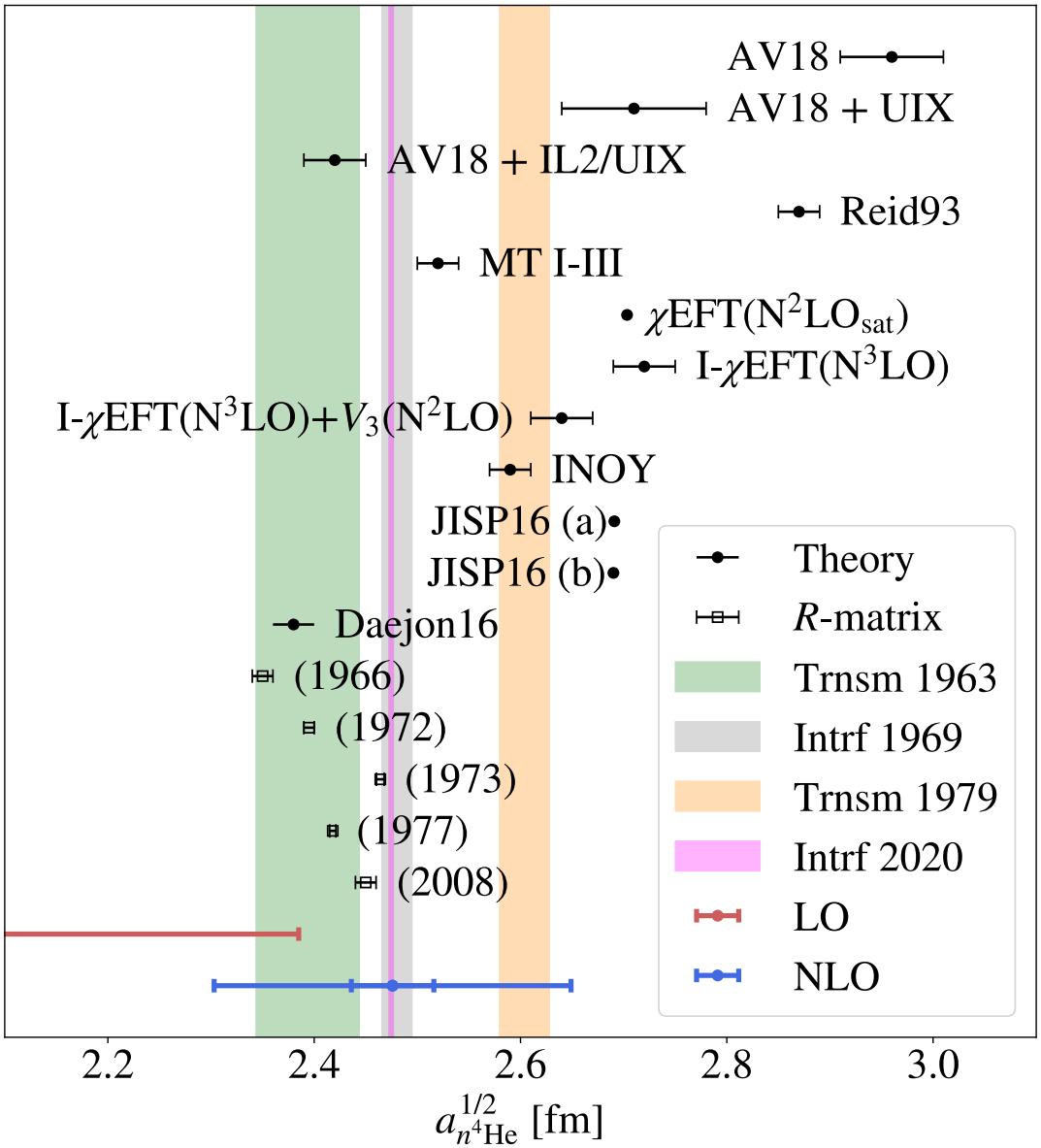

Come by to the poster to know more!

האוניברסיטה העברית בירושלים
THE HEBREW UNIVERSITY OF JERUSALEM

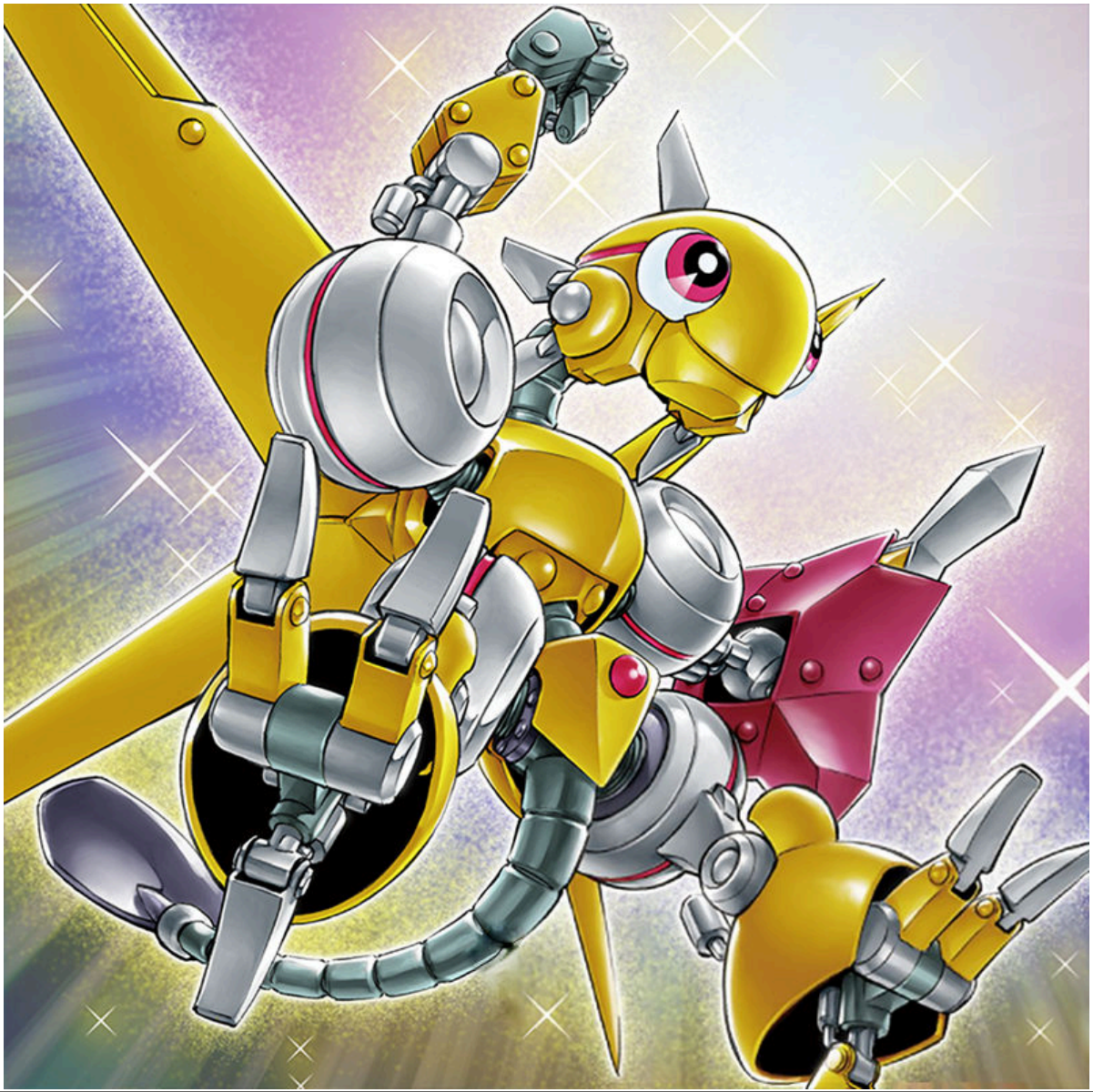

Entanglement in few-particle scattering

TECHNISCHE UNIVERSITÄT DARMSTADT

Poster 27

Tanja Kirchner

https://scienceexchange.caltech.edu/topics/quantum-science-explained/entanglement

Examples

product state $=$ no entanglement

$$|\psi_0\rangle = \frac{1}{4}(|\uparrow\rangle \otimes |\uparrow\rangle + |\uparrow\rangle \otimes |\downarrow\rangle + |\downarrow\rangle \otimes |\uparrow\rangle + |\downarrow\rangle \otimes |\downarrow\rangle)$$

Examples

product state $=$ no entanglement

$$|\psi_0\rangle = \frac{1}{4}(|\uparrow\rangle \otimes |\uparrow\rangle + |\uparrow\rangle \otimes |\downarrow\rangle + |\downarrow\rangle \otimes |\uparrow\rangle + |\downarrow\rangle \otimes |\downarrow\rangle)$$
$$= \frac{1}{2}(|\uparrow\rangle + |\downarrow\rangle) \otimes \frac{1}{2}(|\uparrow\rangle + |\downarrow\rangle)$$

Examples

product state = no entanglement

$$|\psi_0\rangle = \frac{1}{4}(|\uparrow\rangle \otimes |\uparrow\rangle + |\uparrow\rangle \otimes |\downarrow\rangle + |\downarrow\rangle \otimes |\uparrow\rangle + |\downarrow\rangle \otimes |\downarrow\rangle)$$
$$= \frac{1}{2}(|\uparrow\rangle + |\downarrow\rangle) \otimes \frac{1}{2}(|\uparrow\rangle + |\downarrow\rangle)$$

maximally entangled state

$$|\psi_{\max}\rangle = \frac{1}{2}(|\uparrow\rangle \otimes |\downarrow\rangle + |\downarrow\rangle \otimes |\uparrow\rangle)$$

Examples

product state = no entanglement

$$|\psi_0\rangle = \frac{1}{4}(|\uparrow\rangle \otimes |\uparrow\rangle + |\uparrow\rangle \otimes |\downarrow\rangle + |\downarrow\rangle \otimes |\uparrow\rangle + |\downarrow\rangle \otimes |\downarrow\rangle)$$
$$= \frac{1}{2}(|\uparrow\rangle + |\downarrow\rangle) \otimes \frac{1}{2}(|\uparrow\rangle + |\downarrow\rangle)$$

maximally entangled state

$$|\psi_{\text{max}}\rangle = \frac{1}{2}(|\uparrow\rangle \otimes |\downarrow\rangle + |\downarrow\rangle \otimes |\uparrow\rangle)$$
$$\neq |\psi_1\rangle \otimes |\psi_2\rangle$$

Outlook

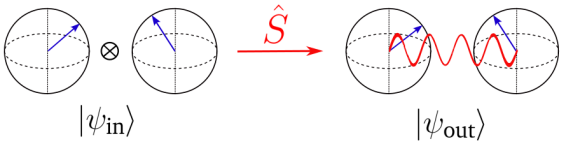

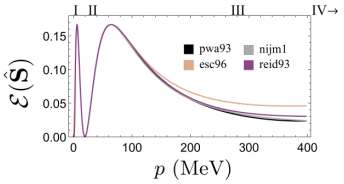

[Beane *et al.* PRL 122, 102001 (2019)]

- Beane *et al.* investigated **entanglement power** for *p*-*n* scattering [PRL 122, 102001 (2019)]
- Extensions:
  - different entropies
  - analysis of Taylor expansions
  - spin $\frac{1}{2}$ and spin **1** in the nucleon regime
  - investigation of Coulomb interaction

Thank you for your attention!

See you at my poster No. 27!

28

האוניברסיטה העברית בירושלים
THE HEBREW UNIVERSITY OF JERUSALEM

Boosting of the Generalized Contact Formalism

NITZAN GOLDBERG

The GCF

Describing short range correlations.

$$\psi \rightarrow \phi(p_{12}) \cdot A(P_{12}, p_3 \dots)$$

Universal Function

The Contact $C = AA^{\dagger}$

High Momentum Electron Scattering

Inclusive CS

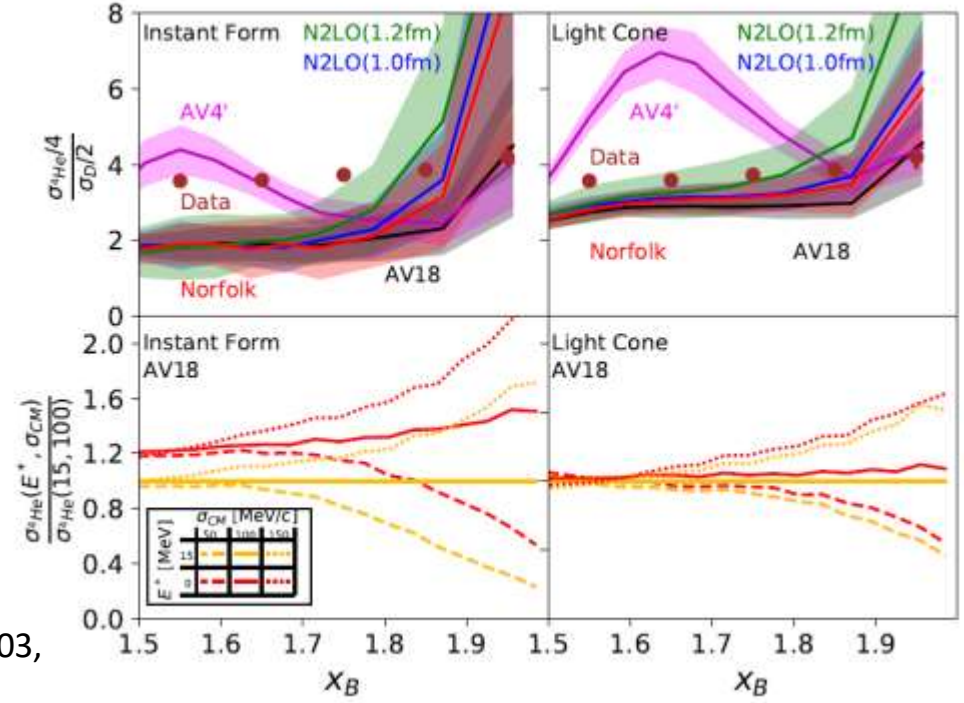

R. Weiss et al. Phys. Rev. C 103, (2021).

Exclusive CS

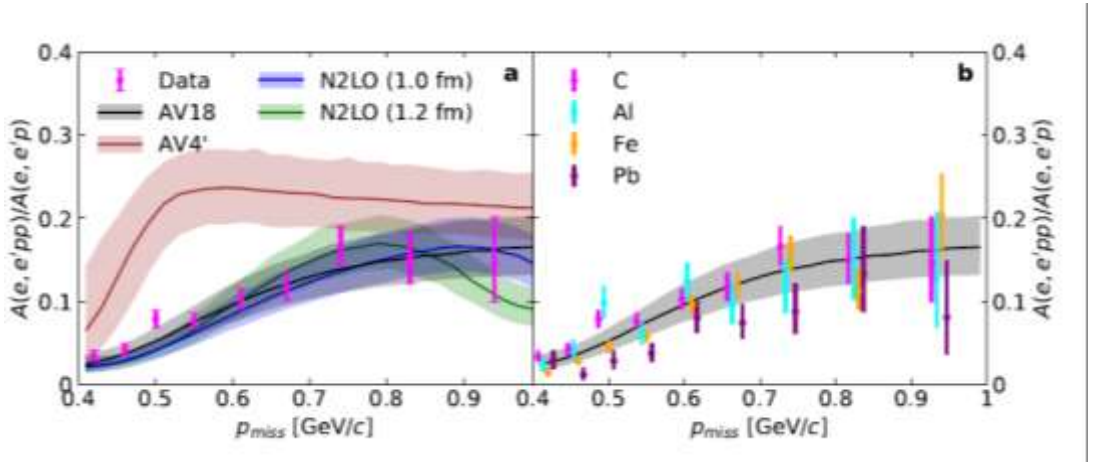

A. Schmidt et al. (CLAS), Nature 578, 540 (2020).

How sensitive is the SF to Lorentz boost?

Within the GCF the spectral function takes the form

$$S(E, p_1) = \int d^3 p_2 \delta\big(f(p_2)\big) \phi(p_{12}) n(P_{12})$$

Using Lorentz boost: $p_1^\nu \to \Lambda_\mu^\nu p_1^\mu,\ p_2^\nu \to \Lambda_\mu^\nu p_2^\mu,\ P_{nucleus}^\nu \to \Lambda_\mu^\nu P_{nucleus}^\mu$ we calculated the spectral function in different reference frames.

Boost Results